Fairfield University
DigitalCommons@Fairfield

Physics Faculty Publications | Physics Department

1-1-2006

Differential cross sections for γ+p→K++Y for Λ and Σ0 hyperons

R. Bradford

Angela Biselli
Fairfield University, abiselli@fairfield.edu

CLAS Collaboration

Follow this and additional works at: https://digitalcommons.fairfield.edu/physics-facultypubs

Copyright American Physical Society Publisher final version available at http://prc.aps.org/pdf/PRC/v73/i3/e035202

Peer Reviewed

Repository Citation

Bradford, R.; Biselli, Angela; and CLAS Collaboration, "Differential cross sections for γ+p→K++Y for Λ and Σ0 hyperons" (2006). *Physics Faculty Publications*. 81.
https://digitalcommons.fairfield.edu/physics-facultypubs/81

Published Citation

R. Bradford et al. [CLAS Collaboration], "Differential cross sections for γ+p→K++Y for Λ and Σ0 hyperons", Physical Review C 73.3 (2006) DOI: 10.1103/PhysRevC.73.035202

This item has been accepted for inclusion in DigitalCommons@Fairfield by an authorized administrator of DigitalCommons@Fairfield. It is brought to you by DigitalCommons@Fairfield with permission from the rights-holder(s) and is protected by copyright and/or related rights. **You are free to use this item in any way that is permitted by the copyright and related rights legislation that applies to your use. For other uses, you need to obtain permission from the rights-holder(s) directly, unless additional rights are indicated by a Creative Commons license in the record and/or on the work itself.** For more information, please contact digitalcommons@fairfield.edu.

Differential cross sections for $\gamma + p \rightarrow K^+ + Y$ for Λ and Σ^0 hyperons

R. Bradford,[1,*] R. A. Schumacher,[1] J. W. C. McNabb,[1] L. Todor,[1] G. Adams,[29] P. Ambrozewicz,[10] E. Anciant,[5] M. Anghinolfi,[16] B. Asavapibhop,[22] G. Asryan,[38] G. Audit,[5] H. Avakian,[15,33] H. Bagdasaryan,[27] N. Baillie,[37] J. P. Ball,[2] N. A. Baltzell,[32] S. Barrow,[11] V. Batourine,[20] M. Battaglieri,[16] K. Beard,[19] I. Bedlinskiy,[18] M. Bektasoglu,[27,†] M. Bellis,[1] N. Benmouna,[12] B. L. Berman,[12] N. Bianchi,[15] A. S. Biselli,[1,29] B. E. Bonner,[30] S. Bouchigny,[17,33] S. Boiarinov,[18,33] D. Branford,[9] W. J. Briscoe,[12] W. K. Brooks,[33] S. Bültmann,[27] V. D. Burkert,[33] C. Butuceanu,[37] J. R. Calarco,[24] S. L. Careccia,[27] D. S. Carman,[26] B. Carnahan,[4] S. Chen,[11] P. L. Cole,[14,33] A. Coleman,[37] P. Coltharp,[11] P. Corvisiero,[16] D. Crabb,[36] H. Crannell,[4] J. P. Cummings,[29] R. DeVita,[16] E. De Sanctis,[15] P. V. Degtyarenko,[33] H. Denizli,[28] L. Dennis,[11] A. Deur,[33] K. V. Dharmawardane,[27] K. S. Dhuga,[12] C. Djalali,[32] G. E. Dodge,[27] J. Donnelly,[13] D. Doughty,[6,33] P. Dragovitsch,[11] M. Dugger,[2] S. Dytman,[28] O. P. Dzyubak,[32] H. Egiyan,[33,37] K. S. Egiyan,[38] L. Elouadrhiri,[6,33] A. Empl,[29] P. Eugenio,[11] R. Fatemi,[36] G. Fedotov,[23] G. Feldman,[12] R. J. Feuerbach,[1] T. A. Forest,[27] H. Funsten,[37] M. Garçon,[5] G. Gavalian,[27,38] G. P. Gilfoyle,[31] K. L. Giovanetti,[19] F. X. Girod,[5] J. T. Goetz,[3] E. Golovatch,[16] A. Gonenc,[10] R. W. Gothe,[32] K. A. Griffioen,[37] M. Guidal,[17] M. Guillo,[32] N. Guler,[27] L. Guo,[33] V. Gyurjyan,[33] C. Hadjidakis,[17] R. S. Hakobyan,[4] J. Hardie,[6,33] D. Heddle,[6,33] F. W. Hersman,[24] K. Hicks,[26] I. Hleiqawi,[26] M. Holtrop,[24] J. Hu,[29] M. Huertas,[32] C. E. Hyde-Wright,[27] Y. Ilieva,[12] D. G. Ireland,[13] B. S. Ishkhanov,[23] M. M. Ito,[33] D. Jenkins,[35] H. S. Jo,[17] K. Joo,[7,36] H. G. Juengst,[27] J. D. Kellie,[13] M. Khandaker,[25] K. Y. Kim,[28] K. Kim,[20] W. Kim,[20] A. Klein,[27] F. J. Klein,[4,33] A. V. Klimenko,[27] M. Klusman,[29] M. Kossov,[18] L. H. Kramer,[10,33] V. Kubarovsky,[29] J. Kuhn,[1] S. E. Kuhn,[27] S. V. Kuleshov,[18] J. Lachniet,[1] J. M. Laget,[5,33] J. Langheinrich,[32] D. Lawrence,[22] A. C. S. Lima,[12] K. Livingston,[13] K. Lukashin,[33] J. J. Manak,[33] C. Marchand,[5] S. McAleer,[11] B. McKinnon,[13] B. A. Mecking,[33] M. D. Mestayer,[33] C. A. Meyer,[1] T. Mibe,[26] K. Mikhailov,[18] R. Minehart,[36] M. Mirazita,[15] R. Miskimen,[22] V. Mokeev,[23] S. A. Morrow,[5,17] V. Muccifora,[15] J. Mueller,[28] G. S. Mutchler,[30] P. Nadel-Turonski,[12] J. Napolitano,[29] R. Nasseripour,[32] S. Niccolai,[12,17] G. Niculescu,[19,26] I. Niculescu,[12,19] B. B. Niczyporuk,[33] R. A. Niyazov,[27,33] M. Nozar,[33] G. V. O'Rielly,[12] M. Osipenko,[16,23] A. I. Ostrovidov,[11] K. Park,[20] E. Pasyuk,[2] C. Paterson,[13] S. A. Philips,[12] J. Pierce,[36] N. Pivnyuk,[18] D. Pocanic,[36] O. Pogorelko,[18] E. Polli,[15] I. Popa,[12] S. Pozdniakov,[18] B. M. Preedom,[32] J. W. Price,[3] Y. Prok,[36] D. Protopopescu,[13] L. M. Qin,[27] B. P. Quinn,[1] B. A. Raue,[10,33] G. Riccardi,[11] G. Ricco,[16] M. Ripani,[16] B. G. Ritchie,[2] F. Ronchetti,[15] G. Rosner,[13] P. Rossi,[15] D. Rowntree,[21] P. D. Rubin,[31] F. Sabatié,[5,27] C. Salgado,[25] J. P. Santoro,[33,35] V. Sapunenko,[16,33] V. S. Serov,[18] A. Shafi,[12] Y. G. Sharabian,[33,38] J. Shaw,[22] S. Simionatto,[12] A. V. Skabelin,[21] E. S. Smith,[33] L. C. Smith,[36] D. I. Sober,[4] M. Spraker,[8] A. Stavinsky,[18] S. S. Stepanyan,[20] S. Stepanyan,[33,38] B. E. Stokes,[11] P. Stoler,[29] I. I. Strakovsky,[12] S. Strauch,[12] R. Suleiman,[21] M. Taiuti,[16] S. Taylor,[30] D. J. Tedeschi,[32] U. Thoma,[33] R. Thompson,[28] A. Tkabladze,[26] S. Tkachenko,[27] C. Tur,[32] M. Ungaro,[7,29] M. F. Vineyard,[31,34] A. V. Vlassov,[18] K. Wang,[36] L. B. Weinstein,[27] H. Weller,[8] D. P. Weygand,[33] M. Williams,[1] E. Wolin,[33] M. H. Wood,[32] A. Yegneswaran,[33] J. Yun,[27] L. Zana,[24] J. Zhang,[27] and B. Zhao[7]

(CLAS Collaboration)

[1]*Carnegie Mellon University, Pittsburgh, Pennsylvania 15213, USA*
[2]*Arizona State University, Tempe, Arizona 85287-1504, USA*
[3]*University of California at Los Angeles, Los Angeles, California 90095-1547, USA*
[4]*Catholic University of America, Washington, DC 20064, USA*
[5]*CEA-Saclay, Service de Physique Nucléaire, F-91191 Gif-sur-Yvette, Cedex, France*
[6]*Christopher Newport University, Newport News, Virginia 23606, USA*
[7]*University of Connecticut, Storrs, Connecticut 06269, USA*
[8]*Duke University, Durham, North Carolina 27708-0305, USA*
[9]*Edinburgh University, Edinburgh EH9 3JZ, United Kingdom*
[10]*Florida International University, Miami, Florida 33199, USA*
[11]*Florida State University, Tallahassee, Florida 32306, USA*
[12]*The George Washington University, Washington, DC 20052, USA*
[13]*University of Glasgow, Glasgow G12 8QQ, United Kingdom*
[14]*Idaho State University, Pocatello, Idaho 83209, USA*
[15]*INFN, Laboratori Nazionali di Frascati, Frascati, Italy*
[16]*INFN, Sezione di Genova, I-16146 Genova, Italy*
[17]*Institut de Physique Nucleaire ORSAY, Orsay, France*
[18]*Institute of Theoretical and Experimental Physics, Moscow, RU-117259, Russia*
[19]*James Madison University, Harrisonburg, Virginia 22807, USA*
[20]*Kyungpook National University, Daegu 702-701, South Korea*
[21]*Massachusetts Institute of Technology, Cambridge, Massachusetts 02139-4307, USA*
[22]*University of Massachusetts, Amherst, Massachusetts 01003, USA*
[23]*Moscow State University, General Nuclear Physics Institute, RU-119899 Moscow, Russia*
[24]*University of New Hampshire, Durham, New Hampshire 03824-3568, USA*
[25]*Norfolk State University, Norfolk, Virginia 23504, USA*

 ©2006 The American Physical Society

[26]*Ohio University, Athens, Ohio 45701, USA*
[27]*Old Dominion University, Norfolk, Virginia 23529, USA*
[28]*University of Pittsburgh, Pittsburgh, Pennsylvania 15260, USA*
[29]*Rensselaer Polytechnic Institute, Troy, New York 12180-3590, USA*
[30]*Rice University, Houston, Texas 77005-1892, USA*
[31]*University of Richmond, Richmond, Virginia 23173, USA*
[32]*University of South Carolina, Columbia, South Carolina 29208, USA*
[33]*Thomas Jefferson National Accelerator Facility, Newport News, Virginia 23606, USA*
[34]*Union College, Schenectady, New York 12308, USA*
[35]*Virginia Polytechnic Institute and State University, Blacksburg, Virginia 24061-0435, USA*
[36]*University of Virginia, Charlottesville, Virginia 22901, USA*
[37]*College of William and Mary, Williamsburg, Virginia 23187-8795, USA*
[38]*Yerevan Physics Institute, 375036 Yerevan, Armenia*
(Received 24 September 2005; published 7 March 2006)

High-statistics cross sections for the reactions $\gamma + p \to K^+ + \Lambda$ and $\gamma + p \to K^+ + \Sigma^0$ have been measured using CLAS at Jefferson Lab for center-of-mass energies W between 1.6 and 2.53 GeV, and for $-0.85 < \cos\theta_{K^+}^{\text{c.m.}} < +0.95$. In the $K^+\Lambda$ channel we confirm a resonance-like structure near $W = 1.9$ GeV at backward kaon angles. The position and width of this structure change with angle, indicating that more than one resonance is likely playing a role. The $K^+\Lambda$ channel at forward angles and all energies is well described by a t-channel scaling characteristic of Regge exchange, whereas the same scaling applied to the $K^+\Sigma^0$ channel is less successful. Several existing theoretical models are compared to the data, but none provide a good representation of the results.

DOI: 10.1103/PhysRevC.73.035202 PACS number(s): 25.20.Lj, 13.40.−f, 13.60.Le, 14.20.Gk

I. INTRODUCTION

We report on measurements of the photoproduction from the proton of two ground-state hyperons, namely the reactions $\gamma + p \to K^+ + \Lambda$ and $\gamma + p \to K^+ + \Sigma^0$. Intermediate baryonic states in these reactions can be the N^* resonances in the case of Λ production, and N^* or Δ resonances in the case of Σ^0 production. In either case one expects strange meson exchange in the t channel and hyperon exchange in the u channel. This is illustrated in Fig. 1. To unravel the production mechanism in these reactions, highly detailed measurements of as many observables as possible are needed.

In this paper we present results for the differential cross sections $d\sigma/d\cos(\theta_{K^+}^{\text{c.m.}})$, obtained with the CLAS system in Hall B at Jefferson Lab. Following our previous publication [1], these results are based on additional data accumulated by CLAS and use a different analysis technique. In another forthcoming paper we will present results for the beam-recoil double polarization observables C_x and C_z for the same reactions obtained from the same data set.

The main motivation for this work was to provide data to investigate the spectrum of nonstrange (N^* and Δ) baryon resonances above the strangeness-production threshold at $W = \sqrt{s} = 1.6$ GeV. Between this threshold and the upper limit of our data set, at $W = 2.53$ GeV, many baryon resonances are predicted by quark models [2], but relatively few are clearly established [3]. These resonances are broad and overlapping, making partial wave analysis challenging, but it is also possible that some dynamical aspect of hadronic structure may act to restrict the quark models' spectrum of states to something closer to what has already been established [4]. This is the so-called missing resonance problem. Although the branching fractions of most high-mass resonances to KY final states are expected to be small (cross sections $\sim 1\,\mu$65b) compared to those of three-body modes such as $\pi\pi N$ ($\sim 100\,\mu$b), the study of these decays do have advantages. First, two-body final states are often easier to analyze than three-body final states. Second, couplings of nucleon resonances to KY final states will differ from coupling to πN, ηN, or $\pi\pi N$ final states [2]. Thus, one can hope that this alternative light cast on the baryon resonance spectrum may emphasize resonances not otherwise revealed. Some "missing" resonances may only be "hidden" when sought in more well-studied reaction channels.

The Λ and Σ^0 hyperons have isospin 0 and 1, respectively, and so intermediate baryonic states leading to the production of Λ's can only have isospin 1/2 (N^* only), whereas for the Σ^0's, intermediate states with both isospin 1/2 and 3/2 (N^* or Δ) can contribute. Thus, simultaneous study of these reactions provides a kind of isospin selectivity of the sort used in comparing η and π photoproduction reactions. To date, however, the PDG compilation [3] gives poorly known $K\Lambda$ couplings for only five well-established resonances and no $K\Sigma$ couplings for any resonances. The most widely available model calculation of the $K\Lambda$ photoproduction, the KAON-MAID code [5], includes a mere three well-established N^* states: The $S_{11}(1650)$, the $P_{11}(1710)$, and the $P_{13}(1720)$. Thus, it is timely and interesting to have additional good-quality photoproduction data of these channels to see what additional resonance formation and decay information can be obtained.

Section II of this paper discusses briefly the reaction models that will be compared with the present data. Section III discusses the experimental setup of the CLAS system for this experiment. The steps taken to obtain the cross sections from

*Current address: University of Rochester, New York 14627, USA.
†Current address: University of Sakarya, Turkey.

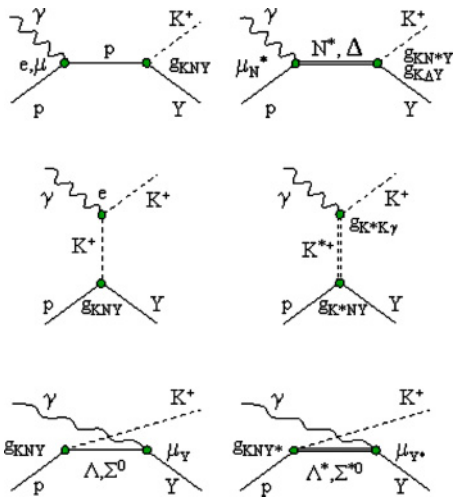

FIG. 1. (Color online) Representative tree-level diagrams illustrating s- (top), t- (middle), and u-channel (bottom) exchanges. Born terms (left column), baryon resonance excitations (top right), and other exchanges (right middle, bottom) lead to production of K^+Y. Models differ in their electromagnetic transition moments (μ's), the strong couplings (g_{MBB}'s), and form factors, as well as the effects of channel couplings.

the raw data are discussed in Sec. IV. Section V presents the results for the measured angular distributions and W dependence of the cross sections. In Sec. VI we discuss the results in light of previous measurements and in relation to several previously published reaction models. We also show how the data can be parametrized in terms of t-channel scaling using a simple Regge-based picture and in terms of simple Legendre polynomials. In Sec. VII we recapitulate the main results.

II. THEORETICAL MODELS

The results in this experiment will be compared to model calculations that fall into two classes: Tree-level effective Lagrangian models and Reggeized meson exchange models. Effective Lagrangian models evaluate tree-level Feynman diagrams as in Fig. 1, including resonant and nonresonant exchanges of baryons and mesons. A complete description of the physics processes will require taking into account all possible channels that could couple to the one being measured, but the advantages of the tree-level approach are to limit complexity and to identify the dominant trends. In the one-channel tree-level approach, some tens of parameters (in particular, the couplings of the nonstrange baryon resonances to the hyperon-kaon systems) must be fixed by fitting to data, since they are poorly known from other sources. An alternative approach is to use no baryon resonance terms and instead model the cross sections in a Reggeized meson exchange picture. Although this is not expected to reproduce the results in detail, it will show where the high-energy phenomenology of t-channel dominance blends into the nucleon-resonance-region picture.

For $K^+\Lambda$ production, the model of Mart and Bennhold [6] has four baryon resonance contributions. Near threshold, the steep rise of the cross section is accounted for with the N^* states $S_{11}(1650)$, the $P_{11}(1710)$, and $P_{13}(1720)$. To explain the broad cross-section bump in the mass range above these resonances, they introduced the $D_{13}(1895)$ resonance, which was predicted in the relativized quark models of Capstick and Roberts [2] and Löring, Metsch, and Petry [7] to have especially strong coupling to the $K^+\Lambda$ channel. In addition, the higher mass region has contributions, in this model, from the exchange of vector $K^*(892)$ and pseudovector $K_1(1270)$ mesons. The hadronic form factors, cutoff masses, and the prescription for enforcing gauge invariance were elements of the model for which specific choices were made. The content of this model is embedded in the KAON-MAID code [5], which was used for the comparisons in this paper. This model was tuned to results from the experiment at Bonn/SAPHIR [8] and offers a fair description of those results.

In contrast, analysis by Saghai and co-workers [9] using the same data set showed that, by tuning the background processes involved, the need for the extra resonance was removed. Janssen *et al.* [10,11] showed that the same data set was not complete enough to make firm statements since models with and without the presence of a hypothesized $N^*(1895)D_{13}$ resulted in equally good fits to data. A subsequent analysis [12], which also fitted calculations to photon beam asymmetry measurements from SPring-8 [13] and electroproduction data measured at Jefferson Lab [14], indicated weak evidence for one or more of S_{11}, P_{11}, P_{13}, or $D_{13}(1895)$, with the P_{11} solution giving the best fit. The conclusion was that a more comprehensive data set would be required to make further progress.

More elaborate model calculations have been undertaken in which channel coupling is considered, in addition to the tree-level approaches just mentioned. Penner and Mosel [15] found fair agreement for the $K^+\Lambda$ data without invoking a new D_{13} structure. Chiang and co-workers [16] showed that coupled channel effects are significant at the 20% level in the total cross sections when including pionic final states. Shklyar, Lenske, and Mosel [17] used a unitary coupled-channel effective Lagrangian model applied to π- and γ-induced reactions to find dominant resonant contributions from $S_{11}(1650)$, $P_{13}(1720)$, and $P_{13}(1895)$ states, but not from $P_{11}(1710)$ or $D_{13}(1895)$. This conclusion was true despite the discrepancies between previous data from CLAS [1] and SAPHIR [18]. Recently, Sarantsev *et al.* [19] did a phenomenological multichannel fit for $K\Lambda$, $K\Sigma$, as well as π and η photoproduction data. They found fairly strong evidence for a P_{11} at 1840 MeV and two D_{13} states at 1870 and 2170 MeV. Even better quality KY data such as we are presenting here are needed to solidify these conclusions. We will not compare the present results to those models in this paper, however.

Although it is to be expected that s-channel resonance structure is a significant component of the $K^+\Lambda$ and $K^+\Sigma^0$ reaction mechanisms, it is instructive to compare to a model that has no such content at all. The model of Guidal, Laget, and Vanderhaeghen [20,21] is such a model; in it the exchanges are restricted to two linear Regge trajectories corresponding to the vector K^* and the pseudovector K_1. The model was fit to higher energy photoproduction data where there is little doubt of the dominance of these exchanges. In this paper, we extend that model into the resonance region to make a critical comparison.

III. EXPERIMENTAL SETUP

Differential cross section data were obtained with the CLAS system in Hall B at the Thomas Jefferson National Accelerator Facility. Electron beam energies of 2.4 and 3.1 GeV contributed to the data set, each of typically 10-nA current. Real photons were produced via bremsstrahlung from a 1×10^{-4} radiation length gold radiator and "tagged" using the recoiling electrons analyzed in a dipole magnet and scintillator hodoscopes [22]. The energy tagging range was from 20% to 95% of the beam endpoint energy, and the integrated rate of tagged photons was typically 5×10^6 /s. Using the tagger and the accelerator RF signal, photon timing at the physics target was defined with an rms precision of 180 ps. The useful energy range for this experiment was from the strangeness-production threshold at $E_\gamma = 0.911$ GeV ($W = 1.61$ GeV) up to 2.95 GeV ($W = 2.53$ GeV). In this range, the tagger resolution was typically 5 MeV, set by the size of the hodoscope elements, but the data were analyzed in bins of 25 MeV photon energy to be commensurate with any energy-dependent structure expected in the hadronic cross sections. The centroids of these bins were adjusted in the analysis by between -6 and $+5$ MeV to compensate for mechanical sag of the hodoscope array measured by kinematically fitting $p(\gamma, p\pi^+\pi^-)$ data; hence our final results are given in unequal energy steps.

The physics target consisted of a 17.9-cm-long liquid-hydrogen cell of diameter 4.0 cm. Temperature and pressure were monitored continuously to determine the density to 0.3% precision. The target cell was surrounded by a set of six 3-mm-thick scintillators to help define the starting time for particle tracks leaving the target, though actually the timing given by the photon tagger was used to define the event times.

The CLAS system, described in detail elsewhere [23], consisted of a toroidal magnetic field, with drift chamber tracking of charged particles. The overall geometry was sixfold symmetric viewed along the beam line. Particles could be tracked from 8° to 140° in laboratory polar angle, and over about 80% of 2π in the azimuthal direction. Outside the magnetic field region a set of 288 scintillators was used for triggering and for later particle identification using the time-of-flight (TOF) technique. The momentum resolution of the system was ≈0.5%, with variations resulting from multiple scattering and tracking resolution considerations. The low-momentum cutoff was set in the analysis at 200 MeV/c. Other components of the CLAS system, such as the electromagnetic calorimeter and the Cerenkov counters, were not used for these measurements.

The event trigger required an electron signal from the photon tagger and at least one charged-track coincidence between the TOF "Start" counters near the target and the TOF "Stop" counters surrounding the drift chambers. The photon tagger signal consisted of the OR of coincidences among hits in a two-plane hodoscope, which had 61 timing scintillators in coincidence with their matching energy-defining scintillators. The charged-track trigger in CLAS was a coincidence of six OR'd start counter elements and the OR of the outer TOF scintillators. Events were accumulated at the rate of ∼2500 hadronic events per second, though only a subpercent fraction of these events contained the kaons and hyperons of interest for the present analysis.

IV. DATA ANALYSIS

A. Data and event selection

The data used in this experiment were obtained in late 1999 as part of the CLAS "g1c" data-taking period. Since the electronic trigger was loose, data for several photoproduction studies were contained in the data set. Offline calibration was performed to align the timing spectra of the elements of the photon tagger, the six elements of the start counter, and the 288 elements of the TOF counters. Drift-time calibrations were made for the 18 drift chamber packages. Pulse-height calibrations and timing-walk corrections were made for the TOF counters. The raw data were then processed to reconstruct tracks in the drift chambers and to associate them with hits in the TOF counters.

B. Particle identification

Kaon, proton, and pion tracks were separated using momentum and TOF measurements. The momentum $\vec{p}$ of each track was measured directly via track reconstruction through the CLAS magnetic field; this measurement also gave the path length d from the reaction vertex to the TOF counter hit by the track. The starting time of the track was determined by projecting the tagger signal time, synchronized with the accelerator RF timing, to the reaction vertex inside the hydrogen target. The stopping time was determined by the element hit in the array of TOF scintillators. The difference T between these two times was the measured time of flight, which in CLAS could range between about 4 and 100 ns. From T the speed β could be obtained as $\beta = d/(cT)$. The mass m_x was then computed according to $m_x = \sqrt{1-\beta^2} \times pT/d$. In CLAS, the dominant mass uncertainty in this situation came from the TOF resolution δT, which was independent of particle momentum, so particle selection based on TOF was largely independent of momentum as well. For kaon identification we used the TOF difference technique, where the measured time T of the track was compared to the expected time T_h for a hadron of mass m_h and momentum p. For a hypothesized value of m_h we can define $\Delta\,\mathrm{tof} = T - T_h$ and write

$$\Delta\,\mathrm{tof} = T\left(1 - \sqrt{\frac{(m_h c)^2 + p^2}{(m_x c)^2 + p^2}}\right). \tag{1}$$

Figure 2 shows an example of such a time difference spectrum when we took m_h to be the kaon mass. The candidate kaon tracks were selected using a ±1-ns cut centered at zero. Pion and proton bands are well separated from the kaons up to 1 and 2 GeV, respectively. A crossing band caused by a badly calibrated detector element is shown for illustration; such tracks were later rejected by removing the detector element and/or by the kinematic cuts and fits applied later. Above 1 GeV some pions leak into the set of candidate kaon tracks. These were rejected by subsequent event reconstruction cuts and by background rejection fitting. Protons were identified using a similar Δ tof correlation but with looser cuts owing to the straggling effects that broadened the distribution.

Photons matching the hadronic tracks in CLAS were selected using the time difference between the hadronic track

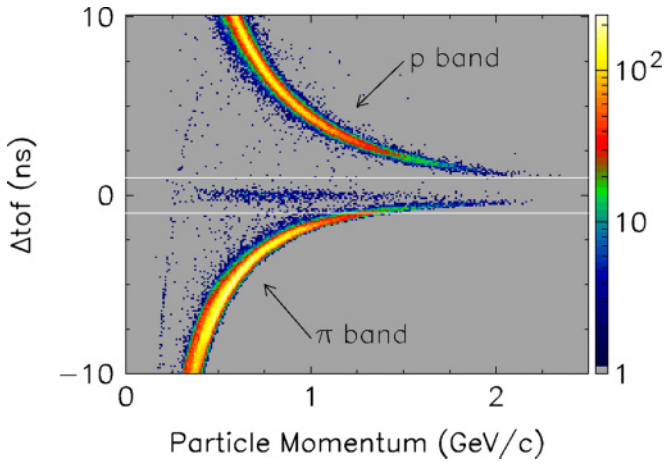

FIG. 2. (Color online) Time-of-flight difference spectrum for a sample of tracks, assuming the mass of the particle is that of a kaon. White lines indicate the cut limits for selecting kaons in a time window of ±1.0 ns. Note the logarithmic scale on the intensity axis.

projected back to the event vertex and the photon tagger time projected forward to the event vertex. Figure 3 shows such a spectrum, which illustrates the presence of random coincidences between the photons and the hadronic tracks. The 2-ns RF time structure of the accelerator is clearly seen. A ±1.0-ns cut was used to reject out-of-time combinations. In-time accidentals under the central peak were treated as potentially correct photons, and such particle-photon combinations were retained in the analysis. Since ambiguous photons were generally widely separated in energy, the (γ, K^+) missing mass for incorrect combinations fell into the broad background under the hyperons and were then rejected at the peak-fitting stage of the analysis discussed in the following.

In this analysis we demanded detection of positive kaons and protons. Negative pions from Λ decay or photons from Σ^0

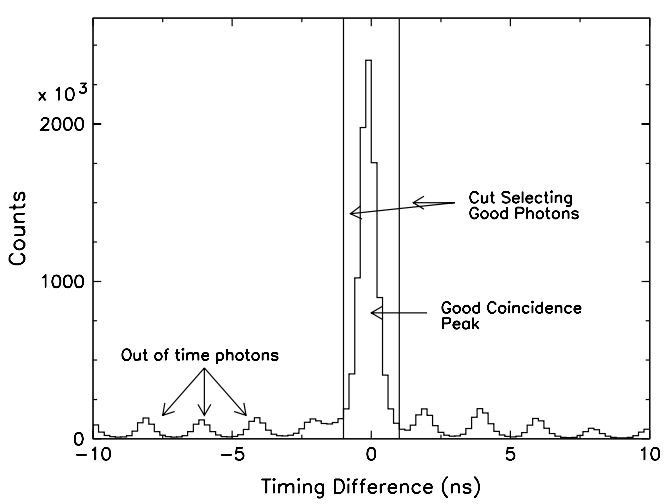

FIG. 3. Time difference between photon tagger time and target start counter time showing the peak at zero of good matches between the photons and the hadrons at the event vertex in CLAS. Coincidences from hadrons mismatched to random photons in the tagger show the 2-ns bunch structure of CEBAF.

decay were not required. Fiducial cuts were applied in track angle and momentum to restrict events to the well-described portions of the detector. This included removal of 9 out of 288 TOF elements owing to poor timing properties. Corrections were applied for the mean energy losses of kaons and protons as they passed through the production target, target walls, beam pipe, and air. The nominal CLAS momentum reconstruction algorithms were found to provide sufficient hyperon mass resolution (see the following) that no higher order momentum corrections were applied.

A missing-mass cut was applied to $p(\gamma, K^+p)\pi^-(\gamma)$ to select events consistent with a missing pion and (for the Σ^0) a missing photon. The losses incurred by this cut owing to multiple scattering effects on the part of the kaons and protons were studied in the real data and in Monte Carlo. The estimated residual uncertainty from the cut and its compensation via the acceptance calculation was 1%–2%.

C. Yield of hyperons

The extraction of kaon yields in each bin of photon energy and kaon angle depended on fits to the missing-mass spectrum given by $p(\gamma, K^+)Y$. When integrated over all of our 3.1-GeV data, for all energies and angles, the resulting missing-mass spectrum is shown in Fig. 4. This figure illustrates that the overall missing-mass resolution of the system was $\sigma = 8.9$ MeV for the Λ and $\sigma = 8.2$ MeV for the Σ^0. The overall resolution averaged 6.3 MeV in the 2.4-GeV data set, where all the average momenta were lower. However, the width of the peaks and the extent of the background to be removed from under the peaks via fitting varied substantially across the measured range of energy and angle, so a careful fitting procedure was needed to obtain well-controlled hyperon yields.

The main source of background in the hyperon mass spectra was due to events where the kaons were actually misidentified pions. The yields of Λ and Σ^0 hyperons were obtained using line-shape fits to missing-mass spectra in each of over 1450 kinematic bins of photon energy and kaon angle. The data were binned in 25-MeV steps in E_γ and in 18 bins of

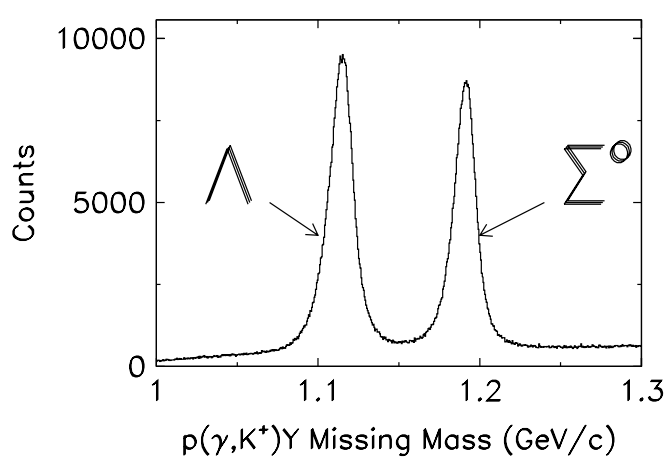

FIG. 4. Hyperon spectrum via missing mass using the photon and detected kaon, integrated over all kaon angles and photon energies using a 3.1-GeV endpoint energy.

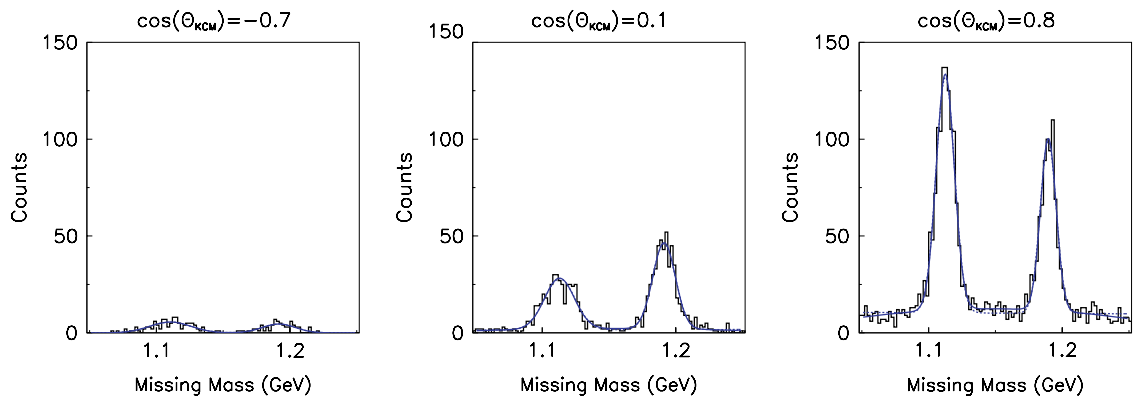

FIG. 5. (Color online) Sample missing mass fits used for the determination of hyperon yields at $E_\gamma = 1.825$ GeV and for three representative K^+ angles: $\cos(\theta_{K^+}^{\text{c.m.}}) = -0.7, +0.1, +0.8$. The fits to different orders of polynomial background (solid lines for quadratic and dashed lines for linear) are nearly indistinguishable.

kaon center-of-mass (c.m.) angle, $\cos(\theta_{K^+}^{\text{c.m.}})$, centered in steps of 0.1 between -0.8 and $+0.9$.

Typical hyperon yield fits of $p(\gamma, K^+)Y$ for the middle of the photon energy range are shown in Fig. 5. The fits were performed in two passes. In the first pass, events for all kaon c.m. angles were summed together. These first fits served to determine and fix the centroids and widths of the Gaussian peaks for the two hyperons. These were seven- to nine-parameter fits, depending on the background model employed. A log-likelihood fitting algorithm was used. The background was modeled as polynomials of order up to 2 (quadratic). In the second pass, fits were made with three to five parameters for the yields in each kaon angle bin, allowing only the integrated counts of the peaks to vary in addition to the background parameters. The two-pass method was used to stabilize fits of low-yield bins at low photon energy and backward kaon angle. Acceptable fits all had χ^2 per degree of freedom of less than 2.0.

Background parametrizations that were a simple constant or a sloped line were sufficient to yield good fits over most of the kinematic range. At more forward kaon angles the effect of background from misidentified pions increased and the quadratic fits generally gave the best results. Above $E_\gamma = 2.3$ GeV the momentum resolution of CLAS broadened to the degree that the forward-angle quadratic fits became less stable, so the linear fits were preferred. This led to an extra estimated systematic uncertainty of 10% on both the forward-angle differential and total cross sections above this energy. In some low-yield back-angle bins, where no good fits were obtained, side-band subtraction was used to determine the yield.

The final cross sections were based on the following numbers of fully reconstructed events: From the 2.4- and the 3.1-GeV data sets we had 236,260 and 325,792 $K^+\Lambda$ events, respectively, and 169,796 and 269,216 $K^+\Sigma^0$ events, respectively.

D. Acceptance calculation

The acceptance and efficiency were modeled using a CLAS-standard GEANT-based simulation code (GSIM). Events were initially modeled using a phase-space distribution for $\gamma + p \to K^+ + Y$. The GSIM code simulated the events in the CLAS detector at the level of analog to digital converter (ADC) and time to digital converter (TDC) hits in the scintillators and drift-time information in the tracking chambers. The events were further fine-tuned such that the time distributions in the TDCs accurately matched the actual data using another well-tested CLAS software package (GPP). These simulated events were then processed through the same analysis codes as the real data, and thus the acceptance was computed in each kinematic bin. Dead regions of the drift chambers were removed both from the real data and from the simulated data during track reconstruction (A1C). Detector efficiency was simultaneously accounted for through the simulation: Sources of inefficiency included track reconstruction failures and TOF paddle removals. The only particle background in this physics Monte Carlo was due to particle decays, especially the kaons, and multiple scattering effects. Thus, we relied on the yield extractions discussed earlier to remove background from misidentified pions or protons. Roughly half of all kaons decayed before fully traversing the detector; the effect this had on event reconstruction efficiency was modeled by GSIM, as was hadronic absorption in the target and detector material.

The effect of using a phase-space event generator to compute the acceptance $\eta_{\text{P.S.}}$ was studied by using the fits to the angular distributions presented in Sec. V A to regenerate the acceptance η_{Data} with an improved representation of the reactions. Since these cross sections vary quite slowly with angle, and since the kinematic bins were each small on the scale of these variations, no large effects were to be expected. We found agreement between the two acceptance models at the level of 0.25% rms over essentially the whole of the kinematic space, consistent with the statistical variations of the simulations. The exception was in the forward-most angle bin ($0.85 < \cos(\theta_{K^+}^{\text{c.m.}}) < 0.95$) for both hyperons. There, because of the extrapolation of the analysis into CLAS's forward acceptance hole, the ratio of acceptances $\eta_{\text{Data}}/\eta_{\text{P.S.}}$ dropped from 1.0 to 0.85 over the range $E_\gamma \sim 1.75$ GeV to $E_\gamma \sim 2.90$ GeV. Theoretical models of the behavior of the cross section in the very forward direction differ strongly, as shown later, so it was not known whether a "flat" or a "forward-peaked" or a "forward-dipped" acceptance model was more accurate. Thus, the forward-most angle results at

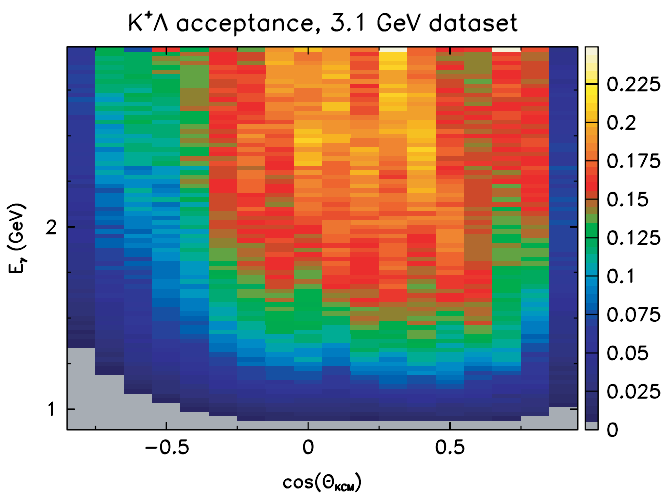

FIG. 6. (Color online) Computed CLAS acceptance for the $E_\gamma = 3.1$ GeV data set for the $\gamma + p \to K^+ + \Lambda$ reaction. The scale on the right gives the value of the acceptance for each kinematic bin.

$\cos(\theta_{K^+}^{\text{c.m.}}) = +.9$ have an additional systematic uncertainty on the cross section, which is, on the average, $\pm 8\%$.

A sample of the acceptances computed for CLAS for these reactions is shown in Fig. 6. It was largest at mid to forward kaon angles and at higher photon energies. The maximum acceptance was about 22% for $K^+\Lambda$ and 23% for $K^+\Sigma^0$. A lower cutoff was applied, such that the smallest allowed acceptance in the experiment was 0.5%. For each hyperon, 10 million events were generated at each beam endpoint energy. Nonuniformities in the distribution arise from the effects of detector element removals and track reconstruction efficiencies. Since the kinematics of the two hyperon reactions are very similar, the acceptance function for the Σ^0 looked very similar, apart from the higher production threshold.

E. Photon flux

The number of photons striking the target was computed from the measured rate of electrons detected at the tagger hodoscope. TDC spectra of the tagger elements recorded the hits of electrons in a 150-ns time range around each event. This flux was scaled and integrated in 10-s intervals. After statistical corrections for multiple hits and electronic live time, the flux was summed over whole runs. The fine granularity of the tagging system was grouped into bins of 25 MeV in photon energy.

Photon losses in the beam line resulting from tagger acceptance, beam collimation, and thin windows were determined using a separate total-absorption counter downstream of CLAS. This low-rate lead glass detector was periodically put in the beam line to monitor the tagging efficiency. For the 2.4-GeV data set the average efficiency for tagging photons was 78%, and the stability of this efficiency, which was measured periodically throughout the data-taking period, was $\pm 0.5\%$.

By taking data at 2.4- and 3.1-GeV endpoint energies it was possible to test the flux normalization of many elements of the tagging system, as discussed in the next section. At energies above $E_\gamma = 2.325$ GeV the two data sets no longer overlapped, however, and defective electronics in a few channels of the tagger led to a gap in our final spectra. Bins at $E_\gamma = 2.375$ and 2.400 GeV were removed because of this.

F. Systematic uncertainties

The 2.4- and 3.1-GeV photon beam endpoint data sets were compared to investigate variations in the photon tagger efficiency. The photon-normalized yield of particles at any given energy had to be independent of bremsstrahlung endpoint energy, so consistency of this quantity tested stability of the electronics. Localized regions of tagger inefficiency "moved" in photon energy when the endpoint energy changed. We took the higher normalized yield between the two data sets as the correct one. Localized regions of high inefficiency were found in the 3.1-GeV data set at 1.1, 1.4, and 1.8 GeV; in those regions we made corrections of up to 50% in one data set to compensate for tagger efficiency losses in the other. Much smaller corrections ($\sim$3%) were made at other energies. The absolute uncertainty on these corrections was estimated to be $\pm 3\%$.

As a check on our results, the $p(\gamma, \pi^+)n$ cross section was measured using the same analysis chain, as far as possible, as the $p(\gamma, K^+)Y$ data. The same procedure was also used to generate the acceptance for the $p(\gamma, \pi^+)n$ cross sections used to check the whole analysis process, except that the SAID code was used to generate the initial events. Figure 7 shows the pion cross section measured in this analysis as a function of W for a mid-range c.m. pion angle. The CLAS pion cross section was found to be in fair agreement with the SAID [24] parametrization of the world's data between $W = 1.6$ and 2.1 GeV, albeit lower by an average scale factor of 0.95. As a function of pion c.m. angle, the CLAS to SAID ratio was $\sim$1.0 at back angles and $\sim$0.92 at forward angles.

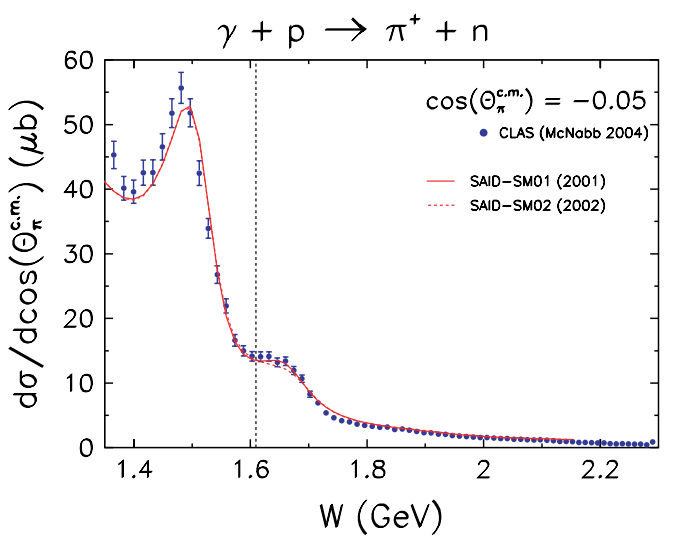

FIG. 7. (Color online) CLAS differential cross section as a function of W for $\gamma + p \to \pi^+ + n$. Shown for comparison are two versions of the SAID parametrization of world pion data. They are distinguishable only near 1.65 GeV. The vertical dotted line is the strangeness production threshold.

Thus the pion results indicate a possible systematic error in the acceptance calculation at the level of ±3%, apart from the average scale factor. The absolute accuracy of the pion cross sections, as parametrized by SAID over the range of comparison we used, is similar to this. Therefore, we chose not to make a renormalization of our results to the average pion cross sections. The results presented in this paper are on an absolute scale. The kaon analysis was not identical to the pion analysis, since the kaon decay corrections are much larger in the former case, and since the final kaon analysis included detection of the proton from the hyperon decays. Hence, it was difficult to translate the systematic trends in our pion results compared to SAID to the kaon results presented here. However, based on the comparison to the pion data analysis, we estimated the overall systematic uncertainty in our kaon cross section to be less than ±7%. This was the largest single contribution to our cross section systematic uncertainty.

The analysis of this experiment was done twice, in largely independent ways. The first analysis [1,25] computed cross sections based on detection of the kaon alone, or $p(\gamma, K^+)Y$. Starting from the same data set, the second analysis [26] detected the kaon and the proton for each event, or $p(\gamma, K^+p)\pi^-(\gamma)$, where the π^- (and the possible γ from Σ^0 decay) were ignored. Particle identification and acceptances were developed independently. For the results presented here, the first analysis was revised to take into account more advanced modeling of the CLAS detector in the acceptance; both analyses used the standard CLAS GEANT package for computing acceptances. The same flux-normalization procedures were used. The first analysis used only data from the 2.4-GeV endpoint data set, whereas the second analysis also included data from 3.1-GeV endpoint. Consistency checks were then made between the two analyses. Results for the final cross sections from the two studies were in very good agreement across the full range of energies and angles where they overlapped. Isolated differences of ∼5% in small ranges of angle were attributed to details of the acceptance modeling. By comparing the acceptances developed over the course of the $p(\gamma, K^+)Y$ studies, we estimated that average systematic uncertainty across the kinematics of the experiment was ±3%, arising from variations in the implementation of the detector model and the track-reconstruction algorithms.

On the energy axis, our results are precise to ±2 MeV. This systematic uncertainty arises from an energy-bin-centering correction that was applied to each data point owing to the calibration of the photon tagger. In an independent study, kinematic fitting to the reaction $p(\gamma, p\pi^+\pi^-)$ showed that the CLAS tagger and the photon beam were mismatched by up to ±10 MeV because of mechanical effects in the structure of the tagger. The correction shifted the centroids of each energy bin by an amount estimated to be precise as previously stated. The indirect effect that this centroid shift had on the acceptance of CLAS was considered negligible, since the cross sections vary slowly in energy and the energy bins for the results are 25 MeV wide.

These estimated systematic uncertainties were combined with contributions from particle yield extraction (3.6%), photon attenuation in the beam line (0.2%), target density uncertainty (0.2%), and target length uncertainty (0.3%). This led to an estimate of the global scale uncertainty of ±8%. Because additional systematic uncertainty about extrapolation of the data to zero degrees, the forward-most angle bin above $E_\gamma = 1.75$ GeV has an overall uncertainty of ±11%.

V. RESULTS

A. Angular distributions

Since the differential cross sections in this measurement are symmetric in the azimuthal angle ϕ, we present the results in the partially integrated form

$$\frac{d\sigma}{d(\cos\theta_{K^+}^{\text{c.m.}})} = 2\pi\frac{d\sigma}{d\Omega}; \tag{2}$$

this also puts the values on a convenient scale of order 1 μb.

The angular distribution results for the reaction $\gamma + p \to K^+ + \Lambda$ are shown in Fig. 8. The results are shown as a function of $\cos(\theta_{K^+}^{\text{c.m.}})$ for 79 bins in W. The step sizes in W were determined by the 25-MeV step size in the nominal photon energy E_γ, at which the cross sections were extracted, together with a few-MeV correction for tagger recalibration. There are 18 bins in $\cos(\theta_{K^+}^{\text{c.m.}})$, each of width 0.1, centered from −0.80 to +0.90. The cross sections are the averages within each angle bin, with no bin centering. The results are the weighted means of the 2.4- and 3.1-GeV beam energy data sets. The error bars are dominated by the statistical uncertainties of the hyperon yield extraction fits but also include the statistics from the Monte Carlo acceptances. The overall systematic uncertainty, as discussed previously, is ±8%, except in the forward-most bin where above $E_\gamma = 1.75$ GeV it is ±11%. There are 1377 data points in the $K^+\Lambda$ set.

The curves in Fig. 8 arise from fits intended to capture the main features of the decay amplitudes contributing to the angular distributions. The form is

$$\frac{d\sigma}{d\cos(\theta_{K^+}^{\text{c.m.}})} = \frac{q}{k}\left\{\sum_{i=0}^{4} a_i P_i\left(\cos\theta_{K^+}^{\text{c.m.}}\right)\right\}^2, \tag{3}$$

where the P_i are the Legendre polynomials of order i, and the a_i are the fit coefficients that represent the $L = 0, 1, 2, 3, 4 \equiv S, P, D, F, G$ wave amplitudes for the decay distributions. The factor q/k is the phase-space ratio of the reaction, where k and q are the c.m. frame momenta of the initial and final states, respectively. The value of this ratio ranges from zero at threshold up to 0.86 at our highest energy.

Qualitatively, the cross section is flat as a function of $\cos(\theta_{K^+}^{\text{c.m.}})$ near threshold, as would be expected for S-wave behavior. As the energy rises to about 1.8 GeV the cross section develops a significant forward peaking consistent either with t-channel contributions or with s-channel interference effects between even and odd waves. As the energy rises further the cross section develops a tendency toward a slower rise in the extreme forward direction and also a rise in the backward direction. Above about 2.3 GeV the cross section is dominantly forward peaked, consistent with t-channel exchange dominance, though on a logarithmic scale (see discussion in Sec. VI C) the falloff is not exponential all the way to back angles.

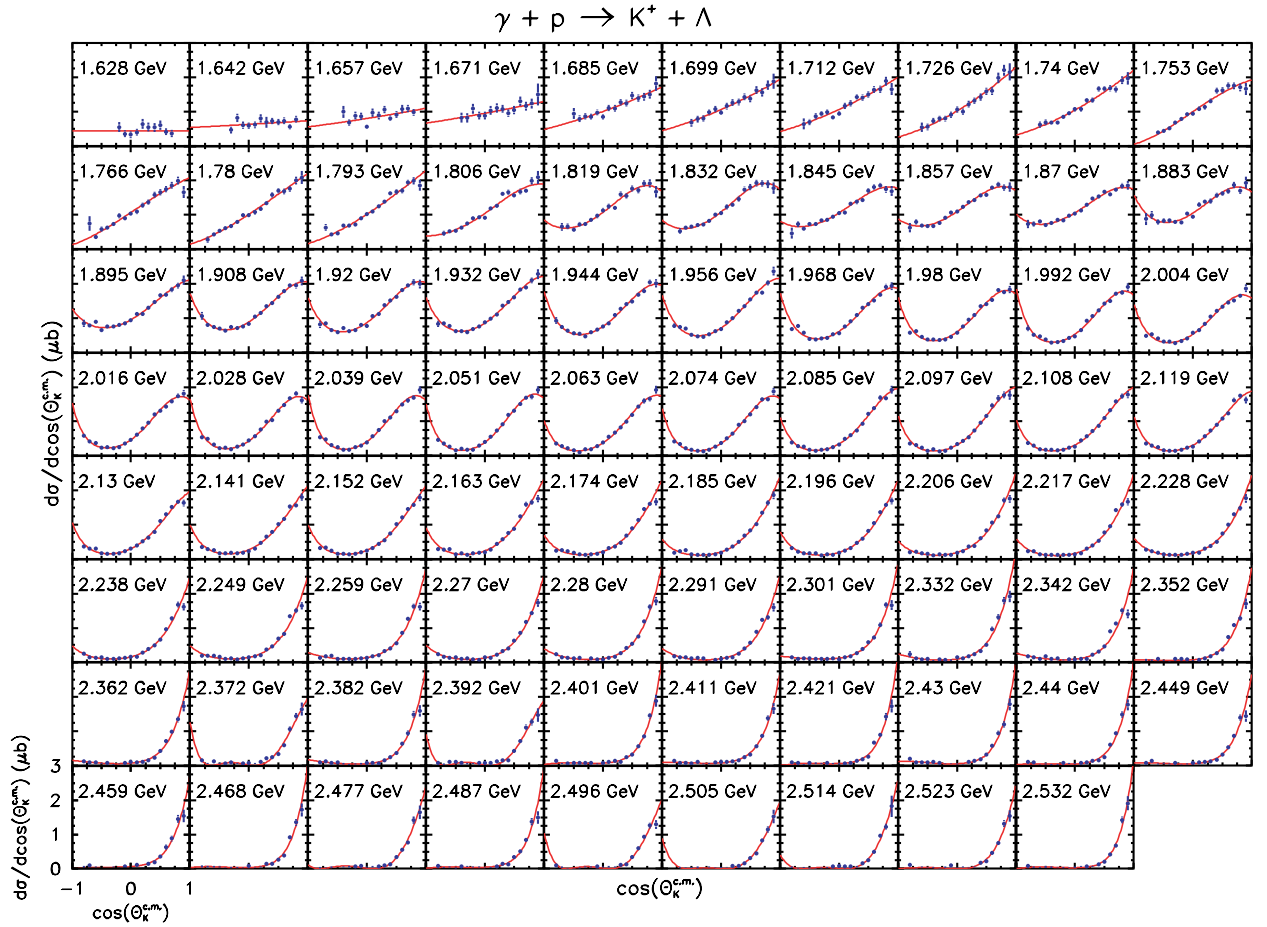

FIG. 8. (Color online) Differential cross sections for $\gamma + p \rightarrow K^+ + \Lambda$. The number in each panel designates W ($= \sqrt{s}$). The solid lines are results of the amplitude fits [Eq. (3)] discussed in the text.

The parameters of the fit may be used to gain some insight into the reaction mechanism, unraveling effects from interference among partial waves. Figure 9 shows the coefficients from the fit using Eq. (3). The a_i were taken to be purely real numbers. The range over which each parameter is plotted depended upon its significance, as estimated by the statistical F test. Mostly, the higher partial waves are not significant near threshold, but our angular coverage is also less complete

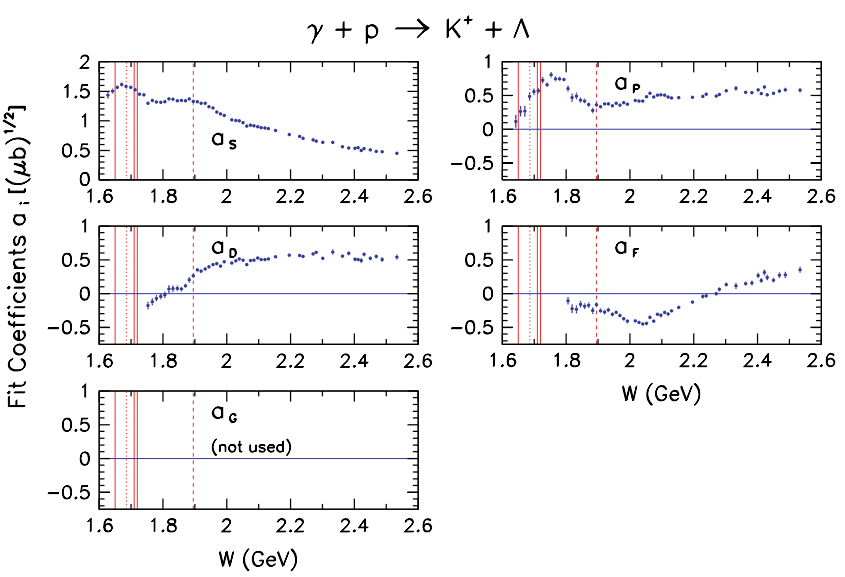

FIG. 9. (Color online) Amplitude fit to the differential cross sections for $\gamma + p \rightarrow K^+ + \Lambda$. The coefficients are defined in Eq. (3). The solid vertical lines mark the well-known N^* resonances $S_{11}(1650)$, $P_{11}(1710)$, and $P_{13}(1720)$. The dotted line marks the Σ^0 threshold, and the dashed line marks the $D_{13}(1895)$ position.

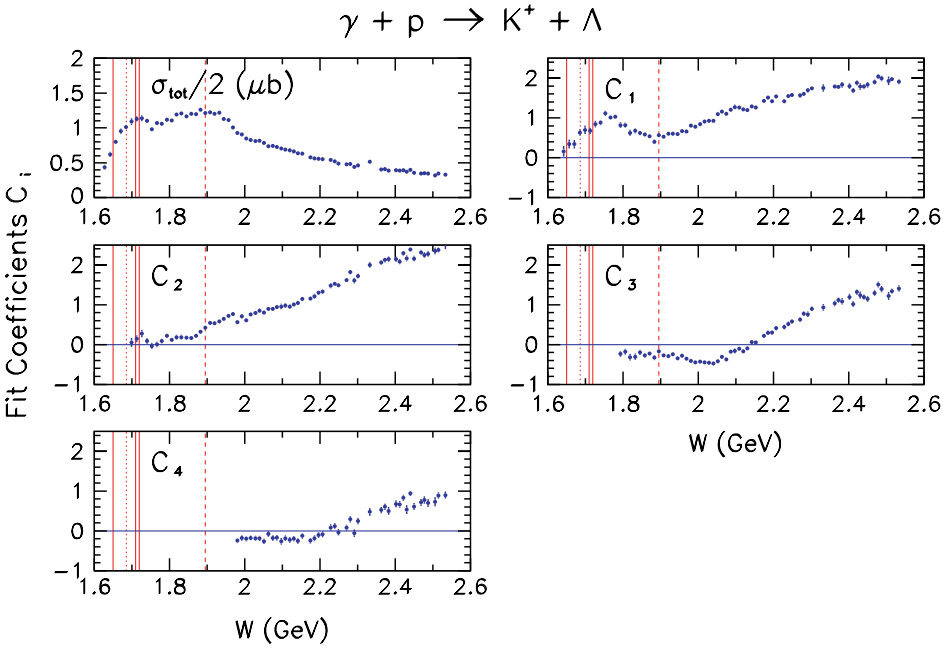

FIG. 10. (Color online) Fit to the magnitude of the differential cross sections for $\gamma + p \rightarrow K^+ + \Lambda$. The coefficients are defined in Eq. (4). The solid vertical lines mark the well-known N^* resonances $S_{11}(1650)$, $P_{11}(1710)$, and $P_{13}(1720)$. The dotted line marks the Σ^0 threshold, and the dashed line marks the $D_{13}(1895)$ position.

near threshold, disallowing higher order fits. One may note a prominent bump in the P-wave amplitude between threshold and 1.9 GeV, centered near 1.7 GeV. The D-wave amplitude turns on quite strongly near 1.9 GeV, and the F-wave amplitude has a broad dip centered at 2.05 GeV. In the $K^+\Lambda$ case, the G wave was not significant at any energy.

An alternative fitting procedure was performed that decomposes the angular distribution magnitudes directly into Legendre coefficients, rather than amplitude-level partial wave Legendre coefficients. The fits were of the form

$$\frac{d\sigma}{d\cos\left(\theta_{K^+}^{\text{c.m.}}\right)} = \frac{\sigma_{\text{tot}}}{2}\left\{1 + \sum_{i=1}^{4} C_i P_i\left(\cos\theta_{K^+}^{\text{c.m.}}\right)\right\} \qquad (4)$$

and are shown in Fig. 10. The total cross section σ_{tot} was used as a parameter to obtain a proper estimate of its uncertainty, which, because of parameter covariances, is more difficult with the fits using Eq. (3). The coefficients C_i are dimensionless ratios of the ith moments of the angular distribution to the total cross section. This fit procedure, to magnitudes rather than amplitudes of the distributions, is less useful in revealing interference effects. Nevertheless, some structure is visible. The C_1 parameter shows a bump below 1.9 GeV, which arises either from S-P or higher wave interference, and the C_3 parameter has a change in slope near 2.05 GeV. Overall, the increasingly forward-peaked cross section with increasing energy forces all the C_i's to rise with W.

The differential cross sections for the Λ can be compared to the angular distributions for Σ^0 production shown in Fig. 11. The bins in W are the same as before, allowing direct comparison of the panels in Figs. 8 and 11. Results for both hyperons were extracted together, using identical procedures discussed previously. There are 1280 data points in the $K^+\Sigma^0$ angular distributions.

Besides the higher reaction threshold, the most significant qualitative difference is that the Σ^0 cross section is not forward peaked in the energy range below 2 GeV. At $W = 1.85$ GeV, for example, the cross section peaks near $\cos(\theta_{K^+}^{\text{c.m.}}) = 0.35$, or 70° in the c.m. frame. This is consistent with a reaction mechanism for Σ^0 production that is less influenced by t-channel exchanges and is more s-channel-resonance dominated than Λ production. The back-angle cross section is less prominent than for the Λ case in this energy range as well. Above the nucleon-resonance region (above about 2.4 GeV), however, the two channels look quite similar, with characteristic t-channel forward peaking.

The coefficients of the amplitude-level fit in Eq. (3) for the Σ^0 angular distributions are shown in Fig. 12. Comparing the Λ to the Σ^0 shows that in the Σ^0 case the D wave amplitude plays a more important role, falling and rising with a centroid near 1.85 GeV. The P wave shows no strong bump in the Σ^0, unlike the Λ. In this case, the G-wave coefficient is statistically significant but shows little structure. For completeness, we also show the magnitude-level fit according to Eq. (4) in Fig. 13. The coefficient C_1 shows some structure, again owing to S-P or higher wave interference. The coefficient C_2 clearly falls and rises, which can be due to P-wave activity or interferences between S and D waves, for example.

Figures 14 and 15 show selected differential cross sections from this experiment compared to previous data and with three published model calculations. The selected panels show about one-sixth of our data, in increments of $\Delta W \approx 80$ MeV to show the trends in the cross sections and the calculations; the exact W values were chosen to emphasize available comparison data.

The results for the angular distributions of photoproduction of Σ^0 are shown in Figs. 16 and 17. Again, the panels are selected to increase in steps of about 80 MeV in W, also to allow comparison to previous data.

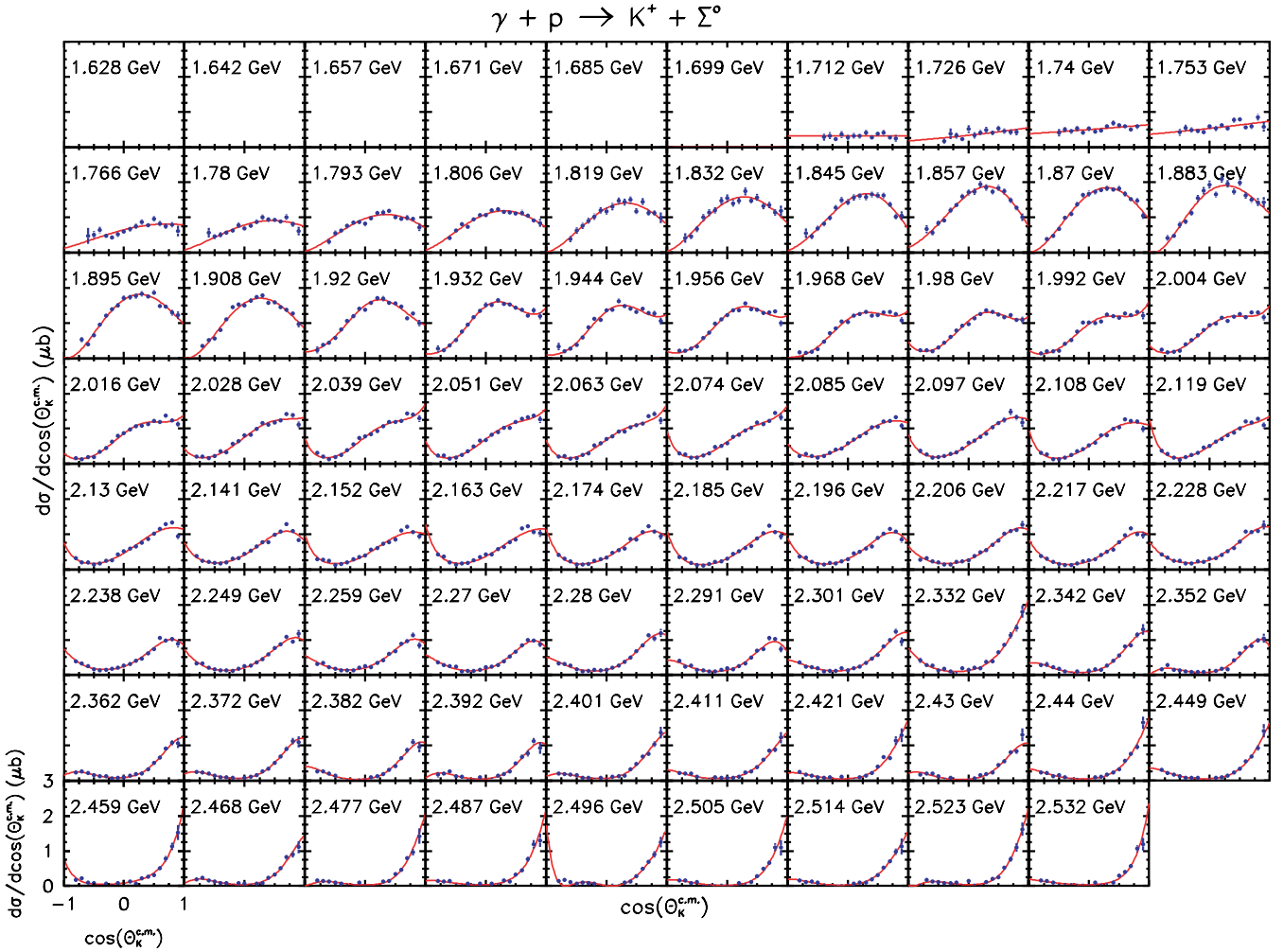

FIG. 11. (Color online) Differential cross sections for $\gamma + p \rightarrow K^+ + \Sigma^0$. The number in each panel designates W ($= \sqrt{s}$). The solid lines are results of the amplitude fits [Eq. (3)] discussed in the text.

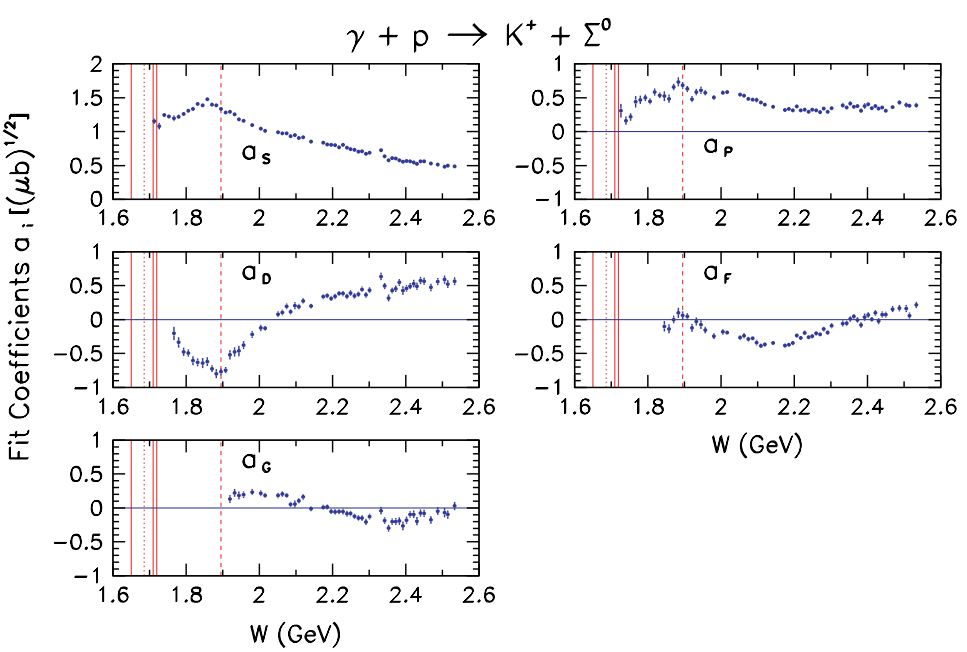

FIG. 12. (Color online) Amplitude fit to the differential cross sections for $\gamma + p \rightarrow K^+ + \Sigma^0$. The coefficients are defined in Eq. (3). The solid vertical lines mark the well-known N^* resonances $S_{11}(1650)$, $P_{11}(1710)$, and $P_{13}(1720)$. The dotted line marks the Σ^0 threshold, and the dashed line marks the $D_{13}(1895)$ position.

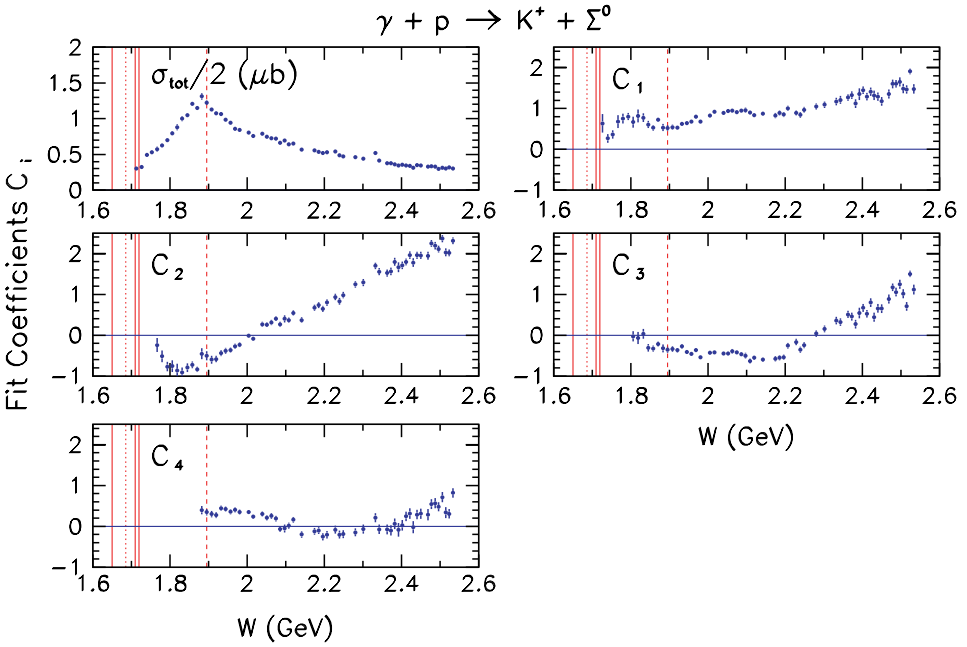

FIG. 13. (Color online) Fit to the magnitude of the differential cross sections for $\gamma + p \rightarrow K^+ + \Sigma^0$. The coefficients are defined in Eq. (4). The solid vertical lines mark the well-known N^* resonances $S_{11}(1650)$, $P_{11}(1710)$, and $P_{13}(1720)$. The dotted line marks the Σ^0 threshold, and the dashed line marks the $D_{13}(1895)$ position.

B. *W* dependence

Resonance structure in the *s*-channel should appear most clearly in the *W* dependence of the cross sections. In Fig. 18 we show the $K^+\Lambda$ cross section at selected angles. The corresponding information for the $K^+\Sigma^0$ channel is shown in Fig. 19. We discuss these results in the next section.

The full set of numerical results from this experiment are available from various archival sources, including a Ph.D. thesis [26], the CLAS database [27], Durham database [28], or private communication [29].

VI. DISCUSSION

A. Comparison to previous data

Figures 14–17 show a sample of the differential cross section for Λ and Σ^0 hyperon photoproduction as a function of angle for a set of *W* values. For comparison, we can examine the previous large-acceptance experiment from SAPHIR at Bonn [8,18]. There is also a set of measurements that was accumulated from the late 1950s to the early 1970s using small-aperture magnetic spectrometers at CalTech [30–33], Cornell [34,35], Bonn [36,37], Orsay [38], DESY [39], and Tokyo [40]. These results are compiled, for example, in Ref. [41].

The agreement with data from SAPHIR is fair or good, but there are some discrepancies. The CLAS results are generally more precise, having statistical uncertainties that are about one-quarter as large, with about twice as many energy bins. The SAPHIR experiment had better backward-angular coverage at low energies as well as coverage at extreme forward angles where CLAS has an acceptance hole. The measurements agree within the estimated uncertainties at some angles and generally near threshold energies, but CLAS measures consistently larger $K^+\Lambda$ cross sections at most kaon angles and for $W > 1.75$ GeV. This is discussed in more detail in the following in the context of the total cross sections, where it appears that there is an energy-independent scale factor of about 3/4 in going from the CLAS to the SAPHIR $K^+\Lambda$ results. The data for the $K^+\Sigma^0$ channel are generally in better agreement overall: The two experiments agree within their stated systematic uncertainties.

We collected the historic (pre-1973) results from different measurements and plotted them together. The error bars are taken as the quoted random uncertainties, with no consideration of the quoted systematic uncertainties. Although these early experiments did not span the large *W* and angular range of the recent experiments, they did make high-precision measurements at selected kinematics. There are 144 $K^+\Lambda$ points and 57 $K^+\Sigma^0$ points that, overall, are in fair agreement with the CLAS results. At backward angles the historic data are in very good agreement with the present results from CLAS; at forward angles the agreement is fair or good. In the mid range of angles, the historic results are lower than our results, being more similar to the SAPHIR data.

The fit coefficients presented in Figs. 9 and 12 are in good qualitative agreement with results published by SAPHIR, apart from an arbitrary overall change in sign. The CLAS results generally have finer binning and smaller estimated uncertainties away from threshold. However, our vertical scales do not agree with SAPHIR, though it is clear their units are incorrect as given, since they should be $\sqrt{\mu\text{b}}$.

Total cross sections σ_{tot} for $\gamma + p \rightarrow K^+ + \Lambda$ and $\gamma + p \rightarrow K^+ + \Sigma^0$ can be calculated from the integrated angular distributions. There is some danger in the integration procedure since (i) it requires some model of the reactions, which may bias the resulting fit, and (ii) in the absence of complete angular coverage there is also the problem of extrapolating the fit into the unmeasured section of phase space. Our procedure for extracting and calculating the total cross sections was based on fitting $d\sigma/d\cos(\theta_{K^+}^{\text{c.m.}})$ in two ways: Using Eq. (4) to fit the magnitude directly and using Eq. (3) to fit the partial wave amplitudes. In the magnitude fit, one of the coefficients directly

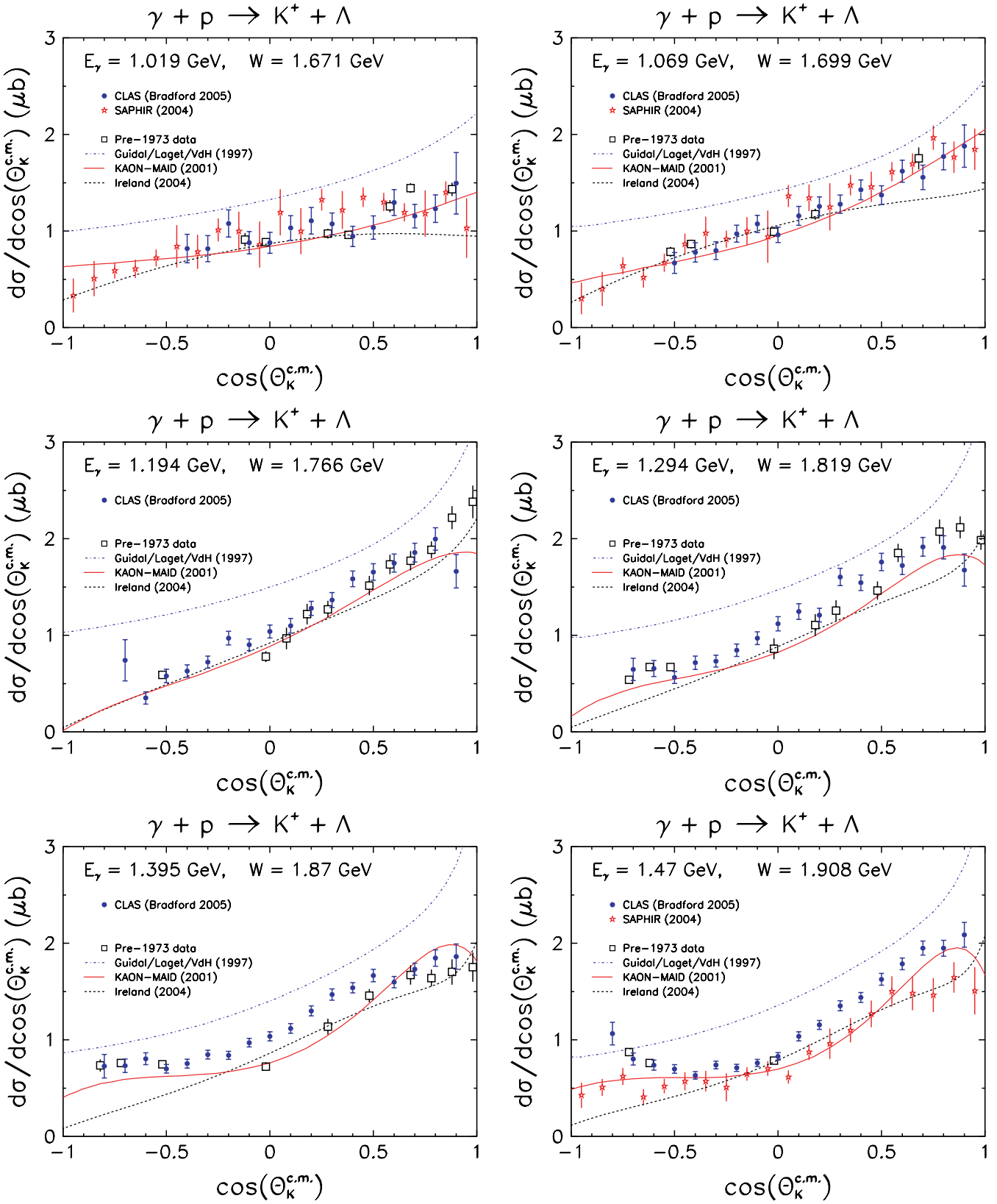

FIG. 14. (Color online) Angular distributions for $\gamma + p \rightarrow K^+ + \Lambda$ for selected bins of total energy W. The present CLAS results (blue circles) are shown with statistical and yield-fit uncertainties. Data from SAPHIR [18] (open red stars) and from older experiments [41] (black squares) are also shown. The curves are for effective Lagrangian calculations computed by KAON-MAID [5] (solid red) and Ireland *et al.* [12] (dashed black) and for a Regge-model calculation of Guidal *et al.* [20,21] (dot-dashed blue).

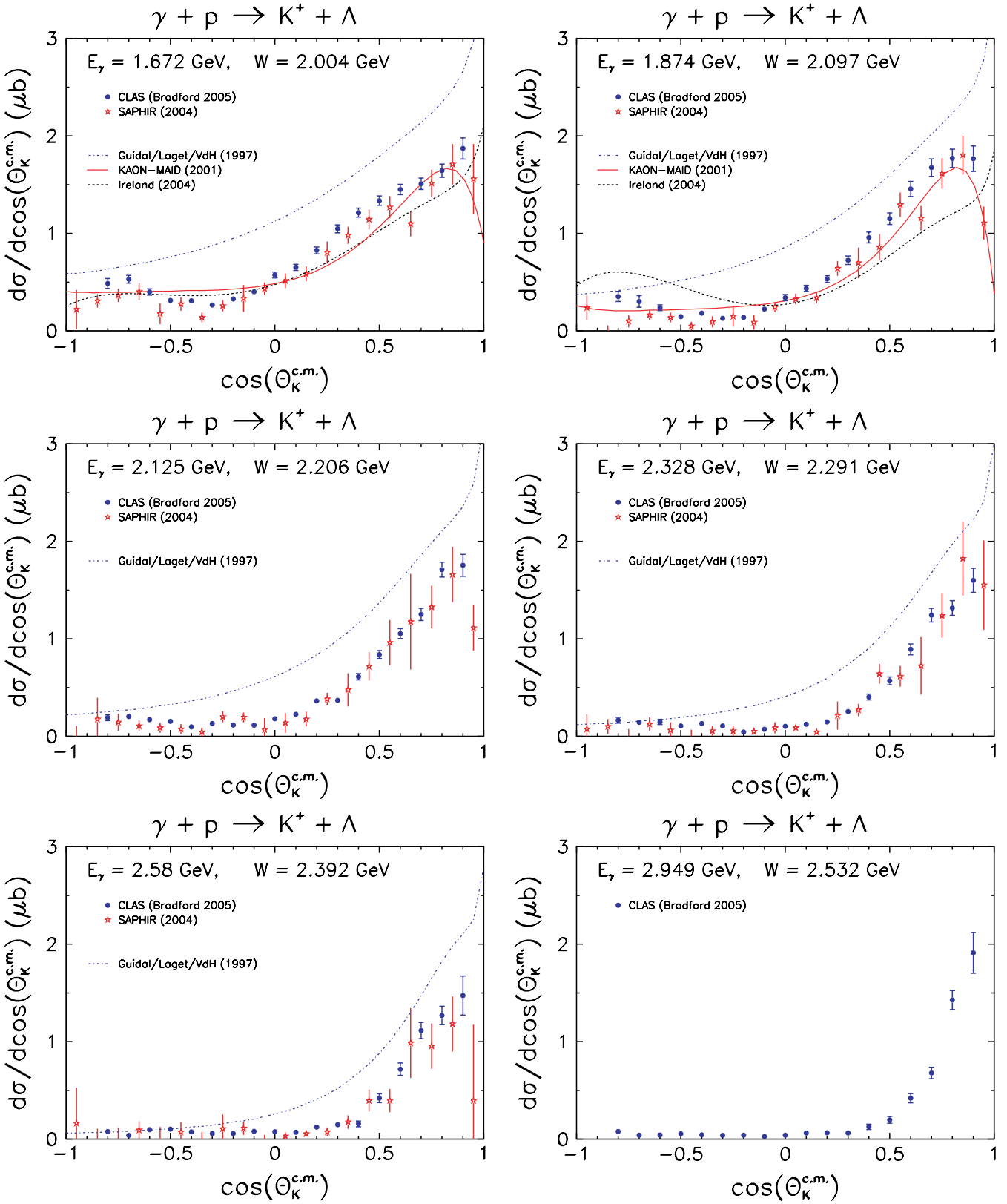

FIG. 15. (Color online) Angular distributions for $\gamma + p \rightarrow K^+ + \Lambda$ for selected bins of total energy W. The present CLAS results (blue circles) are shown with statistical and yield-fit uncertainties. Data from SAPHIR [18] (open stars) and from older experiments [41] (black squares) are also shown. The curves are for effective Lagrangian calculations computed by KAON-MAID [5] (solid red) and Ireland *et al.* [12] (dashed black) and for a Regge-model calculation of Guidal *et al.* [20,21] (dot-dashed blue).

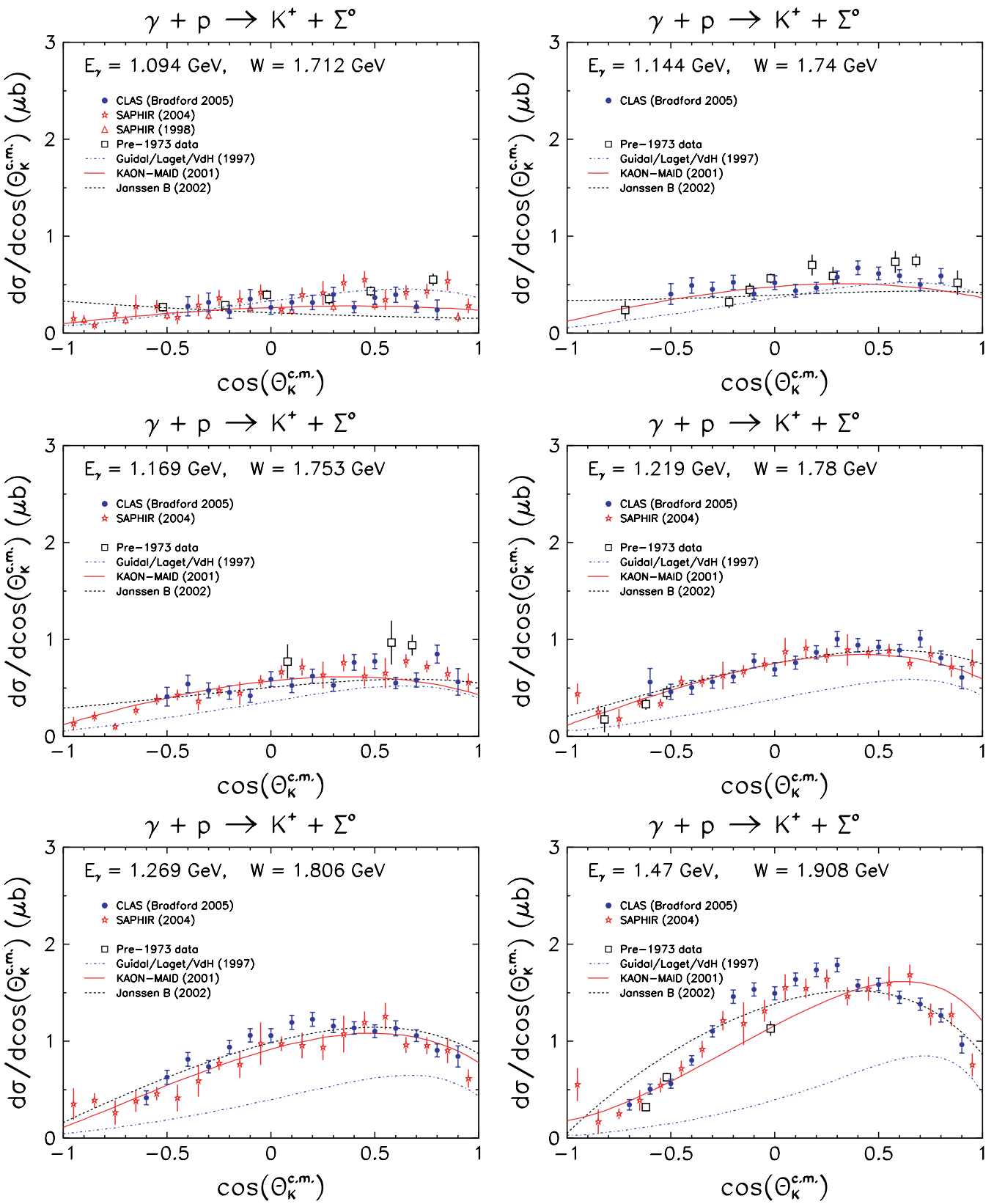

FIG. 16. (Color online) Angular distributions for $\gamma + p \rightarrow K^+ + \Sigma^0$ for selected bins of total energy W. The present CLAS results (blue circles) are shown with statistical and yield-fit uncertainties. Data from SAPHIR (open stars [18] and triangles [8]) and from older experiments [41] (black squares) are also shown. The curves are for effective Lagrangian calculations computed by KAON-MAID [5] (solid red) and Janssen *et al.* [10] (dashed black) and for a Regge-model calculation of Guidal *et al.* [20,21] (dot-dashed blue).

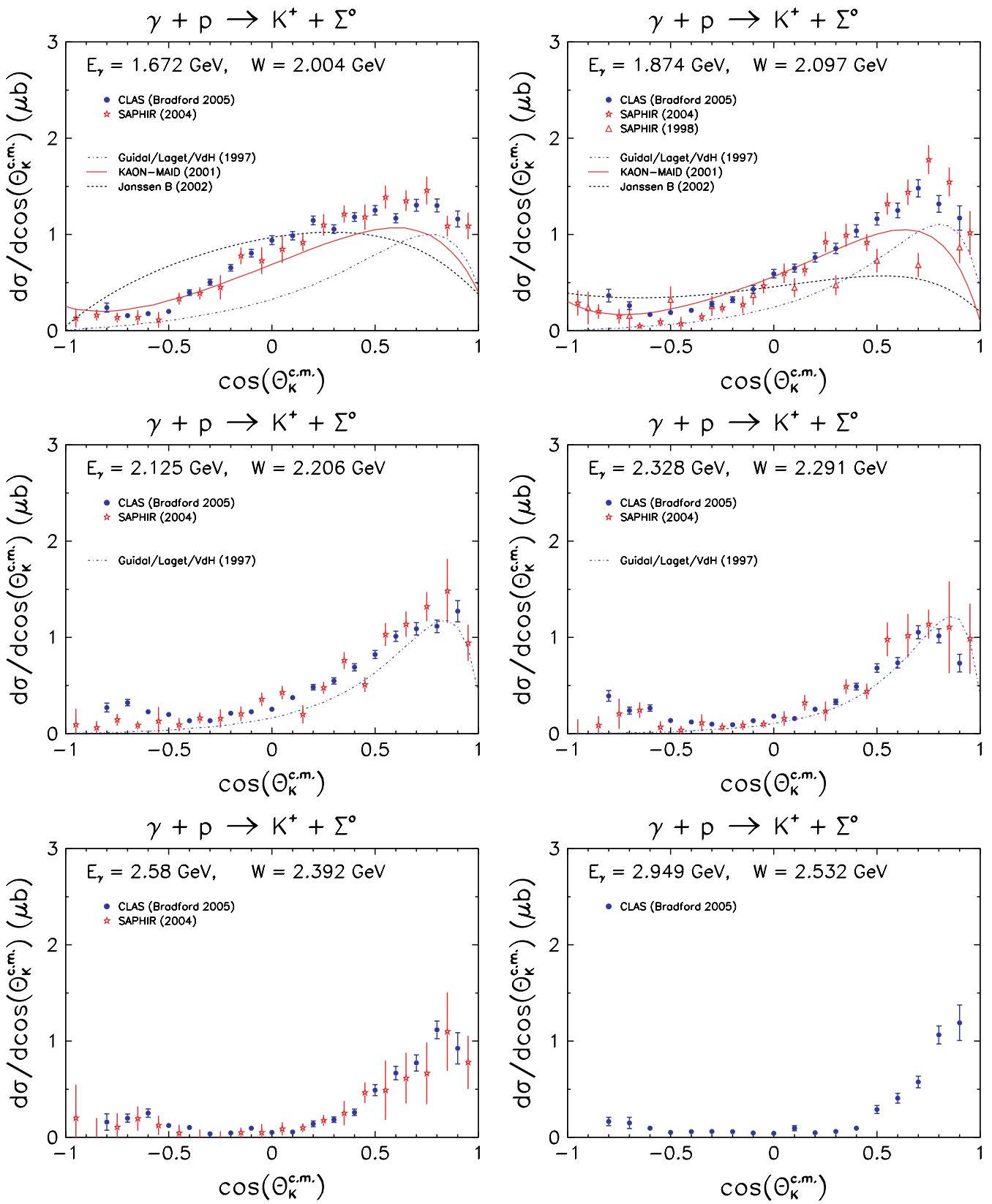

FIG. 17. (Color online) Angular distributions for $\gamma + p \rightarrow K^+ + \Sigma^0$ for selected bins of total energy W. The present CLAS results (blue circles) are shown with statistical and yield-fit uncertainties. Data from SAPHIR (open stars [18] and triangles [8]) and from older experiments [41] (black squares) are also shown. The curves are for effective Lagrangian calculations computed by KAON-MAID [5] (solid red) and Janssen *et al.* [10] (dashed black) and for a Regge-model calculation of Guidal *et al.* [20,21] (dot-dashed blue).

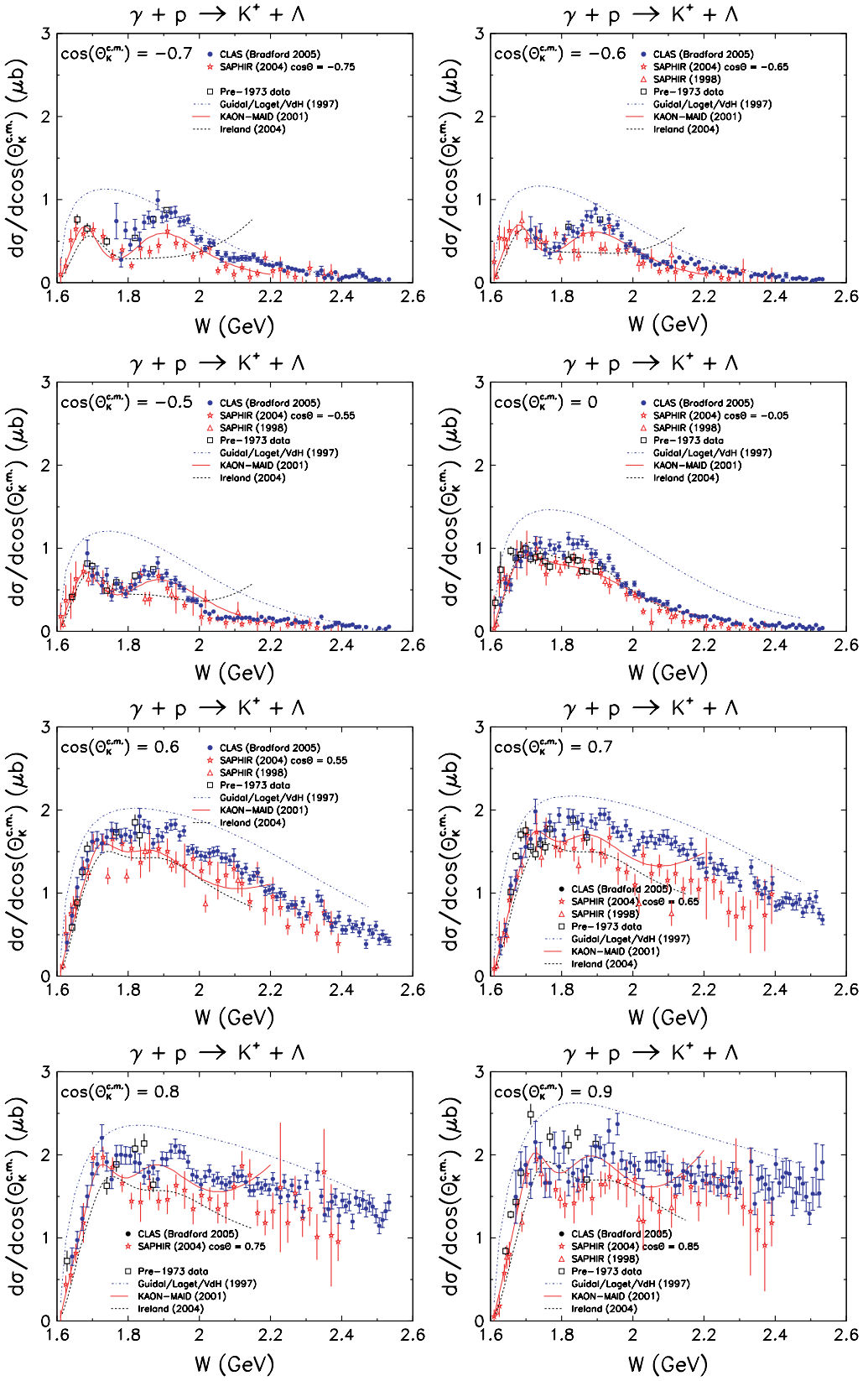

FIG. 18. (Color online) Energy distributions for $\gamma + p \rightarrow K^+ + \Lambda$ for selected c.m. kaon angles. CLAS results (blue circles) are shown with statistical and yield-fit uncertainties. Data from SAPHIR (open stars [18] and triangles [8]) and older experiments [41] (black squares) are also shown. The curves are for effective Lagrangian calculations computed by KAON-MAID [5] (solid red) and Ireland *et al.* [12] (dashed black) and for a Regge-model calculation of Guidal *et al.* [20,21] (dot-dashed blue).

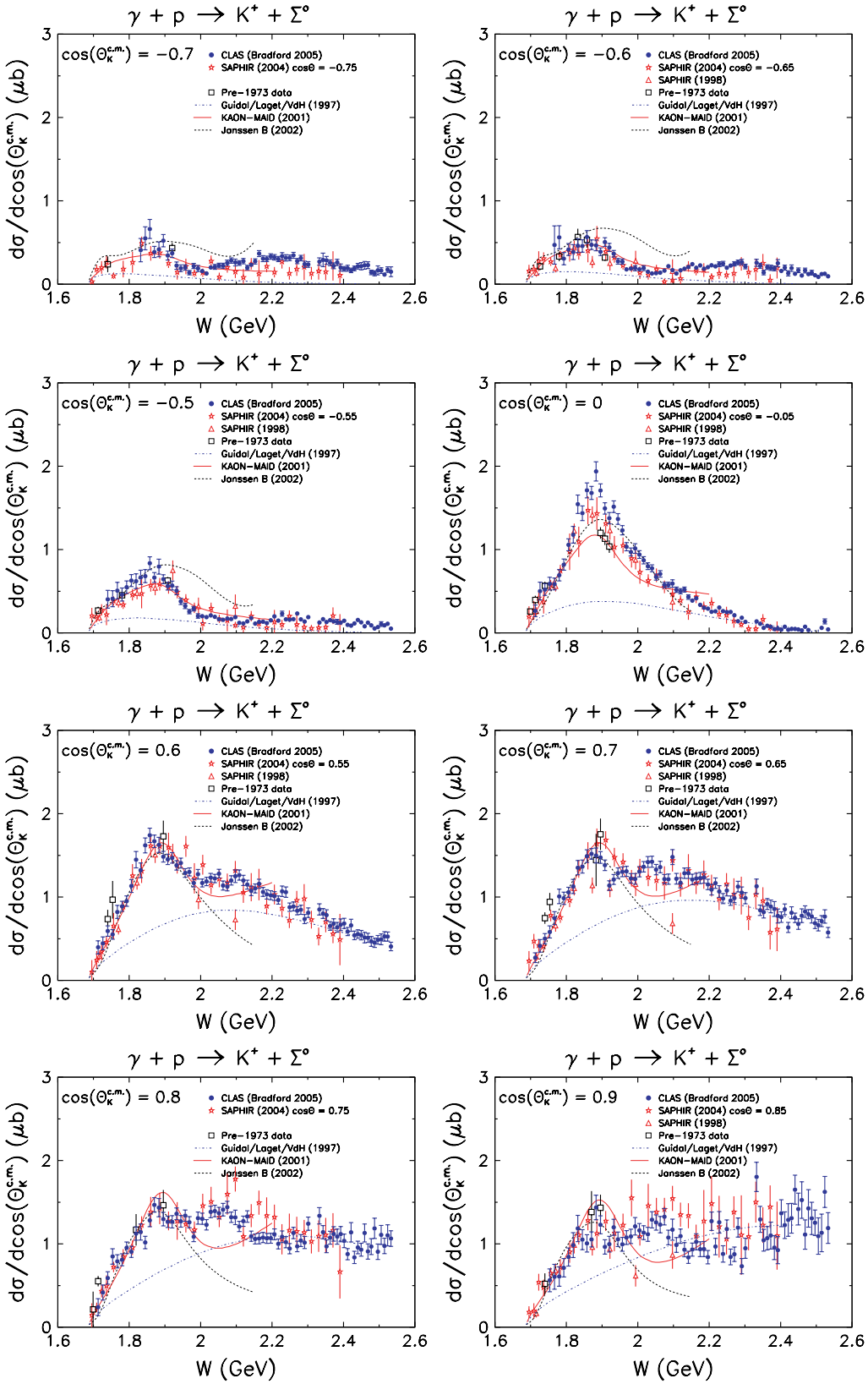

FIG. 19. (Color online) Energy distributions for $\gamma + p \rightarrow K^+ + \Sigma^0$ for selected c.m. kaon angles. CLAS results (blue circles) are shown with statistical and yield-fit uncertainties. Data from SAPHIR (open stars [18] and triangles [8]) and older experiments [41] (black squares) are also shown. The curves are for effective Lagrangian calculations computed by KAON-MAID [5] (solid red) and Janssen *et al.* [10] (dashed black) and for a Regge-model calculation of Guidal *et al.* [20,21] (dot-dashed blue).

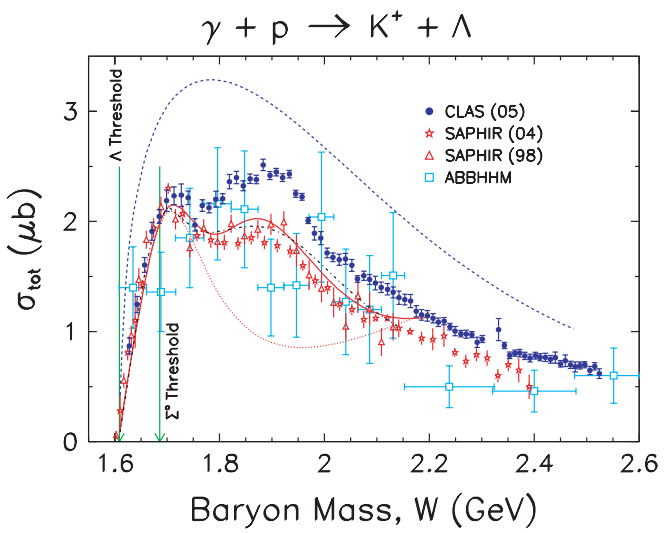

FIG. 20. (Color online) Total cross section for $\gamma + p \to K^+ + \Lambda$. The data from CLAS (blue circles) are shown with combined statistical and fitting uncertainties. Also shown are results from two publications from SAPHIR (red stars (2004) [18] and red triangles (1998) [8]) and the ABBHHM Collaboration (light blue squares) [43]. The curves are from a Regge model (dashed blue) [20,21], KAON-MAID (solid red) [5], KAON-MAID with the $D_{13}(1895)$ turned off (dotted red), and Saghai *et al.* (dot-dashed black) [9].

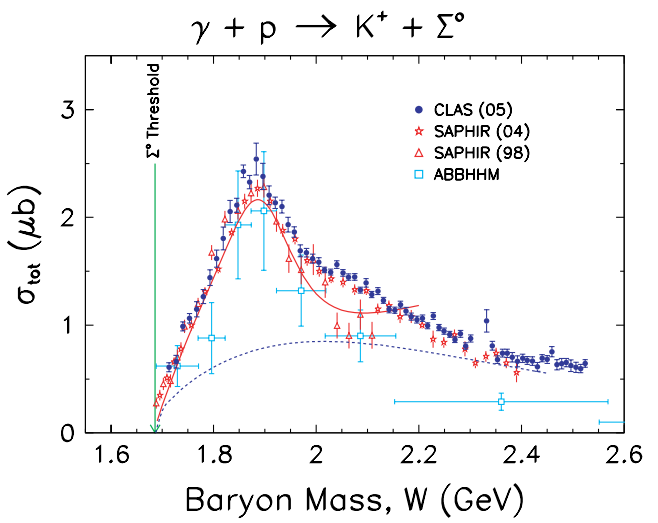

FIG. 21. (Color online) Total cross section for $\gamma + p \to K^+ + \Sigma^0$. The data from CLAS (blue circles) are shown with combined statistical and fitting uncertainties. Also shown are results from two publications from SAPHIR (red stars (2004) [18] and red triangles (1998) [8]) and the ABBHHM Collaboration (light blue squares) [43]. The curves are from a Regge model (dashed blue) [20,21] and from KAON-MAID (solid red) [5].

gives $\sigma_{\rm tot}$ and its associated error. In the amplitude fit $\sigma_{\rm tot}$ is easily computed from the set of fit parameters, but the error is difficult to extract since the fit parameters and their errors are correlated. We estimated the systematic bias in our integrations by taking the standard deviation of the two resultant values as an additional uncertainty, and this was added in quadrature to the other estimated uncertainties.

The total cross section results are shown in Figs. 20 and 21. The error bars combine statistical and estimated systematic uncertainty from the fitting procedure. The gaps in the spectra at $W = 2.312$ and 2.322 GeV stem from photon tagger failures at those energies. For comparison we show two previously published data sets from Bonn [8,18,42]. Also, bubble chamber data for the total cross sections came from Erbe *et al.* (ABBHHM) [43]. Also shown are model curves for two calculations, the effective Lagrangian model embodied in KAON-MAID [5] and the Regge model of Guidal, Laget, and Vanderhaeghen [20,21]. The CLAS results for $\sigma_{\rm tot}$ differ from the Bonn results in an unexpected way; namely, the Bonn $K^+\Lambda$ cross section is smaller than the CLAS result by a factor of close to 3/4. This is in contrast to the $K^+\Sigma^0$ results, where the CLAS and the Bonn results are in good agreement: The values of $\sigma_{\rm tot}$ agree well within their quoted systematic uncertainties. We note that the CLAS results for the two hyperons used exactly the same photon normalizations and that the hyperon yield extractions for both cases were made together, as previously discussed. The acceptance calculations for the CLAS results used the same software as well, differing only in the input events used for the calculations. In short, we have not found any reason within the CLAS analysis for one channel agreeing well with previous work and the other not. Both results are consistent with the ABBHHM data [43].

The CLAS $\sigma_{\rm tot}$ results for $K^+\Lambda$ show a prominent peak centered near 1.9 GeV. It does not resemble a simple single Lorentzian, reflective of the expectation that several resonant structures are present in this mass range. The peak near 1.7 GeV is consistent with contributions from the $P_{11}(1710)$ and $P_{13}(1720)$. In the case of $K^+\Sigma^0$, the $\sigma_{\rm tot}$ curve shows the previously seen strong peak centered at 1.88 GeV, and in addition there is a slight shoulder at about 2.05 GeV. The location of the strong peak is consistent with the mass of several well-established Δ resonances that may contribute to an isospin 3/2 final state.

B. Comparison to reaction models

The model calculations shown in this paper were not fitted to the present results. The effective Lagrangian calculations, in particular, were fitted to the previous data shown in this paper and have, therefore, at least fair agreement with those earlier results. However, since in the case of $K^+\Lambda$ production we have some disagreement with the SAPHIR data in the mid range of angles, we cannot expect these calculations to be in quantitative agreement with ours. It is nevertheless interesting to see what the more copious CLAS results seem to indicate in comparison to a few of these previous models.

The Regge-model calculation [20,21] shown in the preceding figures uses only K and K^* exchanges, with no s-channel resonances. The model was constructed to fit high-energy kaon photoproduction data [44], for W between 5 and 16 GeV, and may be expected to reproduce the average behavior of the cross section in the nucleon-resonance region. However, extrapolated down to the resonance region, the model overpredicts the size of the Λ cross section and underpredicts that of the Σ^0. This is evident in all the graphs, but it is especially easily seen in the total cross sections (Figs. 20

and 21). Since it is a pure t-channel reaction model, it cannot produce a rise at back angles as seen for the Λ and illustrates the need for s- and u-channel contributions to understand that feature.

Two hadrodynamic models [6,10] based on similar effective Lagrangian approaches are also shown. Both emphasize the addition of a small set of s-channel resonances to the nonresonant Born terms; they differ in their treatment of hadronic form factors and gauge invariance restoration. As both were fitted to the previous data from SAPHIR [18], they are expected to be in somewhat poorer agreement with our $K^+\Lambda$ data than our with $K^+\Sigma^0$ data.

Both models contain a set of known s-channel N^* resonances: $S_{11}(1650)$, $P_{11}(1710)$, and $P_{13}(1720)$. The model of Mart and co-workers [6] used in the KAON-MAID calculations contains an additional $D_{13}(1895)$ resonance in its $K^+\Lambda$ description. In the $K^+\Lambda$ case, the calculations of Ireland *et al.* [12] are shown since they represent an update of the earlier work of Janssen *et al.* [10]. These calculations included photon beam asymmetry [13] and electroproduction [14] data points in the data set used for fitting. The curves displayed in Figs. 14, 15, and 18 contain the set of known resonances plus an additional $P_{11}(1895)$ resonance. This combination was found to give the best quantitative agreement with the data set used for fitting. The analysis of Ref. [12] was restricted to a study of the $K^+\Lambda$ channel, so for comparison with the present $K^+\Sigma^0$ data, we use slightly older calculations [10], which contain an additional $D_{13}(1895)$.

The CLAS $K^+\Lambda$ results, which show a structure that varies in width and position with kaon angle, suggest an interference phenomenon between several resonant states in this mass range, rather than a single, well-separated resonance. This should be expected, since several N^* resonances with one- and two-star PDG ratings occupy this mass range. From Fig. 18, the best qualitative modeling of the structure near 1.9 GeV at backward angles is given by KAON-MAID [5], but the model seems to diverge from the trends of the data at forward angles. The calculation of Ref. [12] gives a poor description of the data in the 1.9-GeV region at backward angles, but at forward angles it is similar to the KAON-MAID calculation. Using the model curves as a guide, we see that a fixed position for a single isolated resonance near 1.9 GeV is not consistent with the small (~50 MeV) variation with angle of the feature seen in the cross sections.

In the Σ^0 case there is some indication of a structure above the large peak at 1.9 GeV between 2.0 and 2.1 GeV. This shoulder or small bump in the cross section, seen in Fig. 19 and in the total cross section Fig. (21), is not reproduced by either of the hadrodynamic reaction models.

C. Phenomenological *t* scaling

The forward peaking of the $K^+\Lambda$ cross section suggests that there is substantial contribution to the reaction mechanism by t-channel exchange, even in the nucleon-resonance region. To test this idea, the data can be cast into the form of $d\sigma/dt$ versus $-t$, where t is the Mandelstam invariant that gives the 4-momentum squared of the kaonic exchange particle(s).

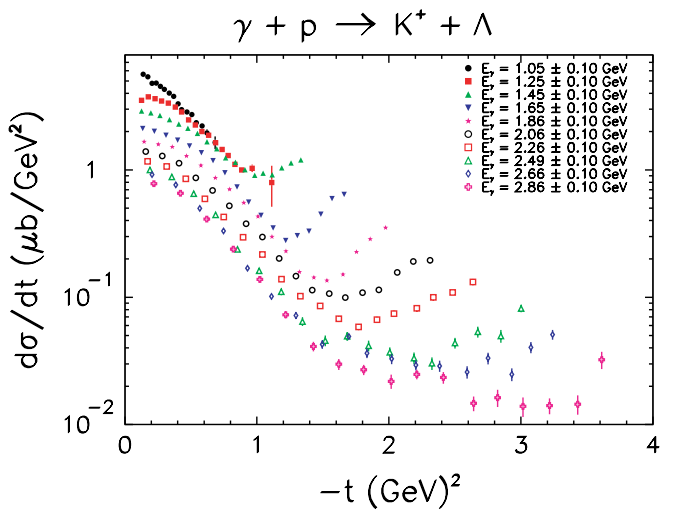

FIG. 22. (Color online) The entire $\gamma + p \to K^+ + \Lambda$ data set shown as $d\sigma/dt$ vs $-t$, for 10 bands of photon energy with $\Delta E_\gamma = 0.20$ GeV. No scaling was applied.

The conversion of the cross section was done using

$$\frac{d\sigma}{dt} = \frac{d\sigma}{d\cos\theta^{\text{c.m.}}_{K^+}} \times \frac{1}{2kq}, \tag{5}$$

where k is the c.m. momentum of the incoming photon and q is the c.m. momentum of the produced kaon. In the simplest Regge picture involving the exchange of a single trajectory, the cross section can be written as [45]

$$\frac{d\sigma}{dt} = D(t)\left(\frac{s}{s_0}\right)^{2\alpha(t)-2}, \tag{6}$$

where $D(t)$ is a function of t only, s_0 is a baryonic scale factor taken to be 1 GeV^2, and $\alpha(t)$ is the Regge trajectory itself that describes how the angular momentum of the exchange varies with t. At our kinematics for small $|t|$ we find $\alpha(t) \approx 0$, so the leading behavior of the cross section is that it approximately scales with s^2.

The cross section $d\sigma/dt$ for $K^+\Lambda$ production is plotted in Fig. 22. To obtain sufficient statistical precision, bands of width 200 MeV were combined as weighted averages (amounting to groups of eight of our actual bins). The lowest band, for $E_\gamma = 1.05 \pm 0.10$ GeV, starts 40 MeV above the reaction threshold. We observe in the figure how the cross section values fall on smoothly varying contours as a function of $-t$. There is an inflected falloff from the minimum $-t$ that is similar for all photon energy bands, but as $|-t|$ increases the falloff flattens and then the curve begins to rise. Figure 23 shows the cross sections scaled by s^2, and it is seen that there is a clear indication of a locus $D(t)$ describing the data over a range of $-t$. We interpret the departures from this locus as the onset of the s- and u-channel contributions to the reaction mechanism. At a given value of $-t$ the residual spread of the points can be used to determine $\alpha(t)$ for this reaction; this work is in progress and will be published separately.

Examination of Figs. 22 and 23 shows a progressive flattening of the slope in the cross section as $|-t| \to 0$. This same "plateau" phenomenon was seen in data from SLAC [44]

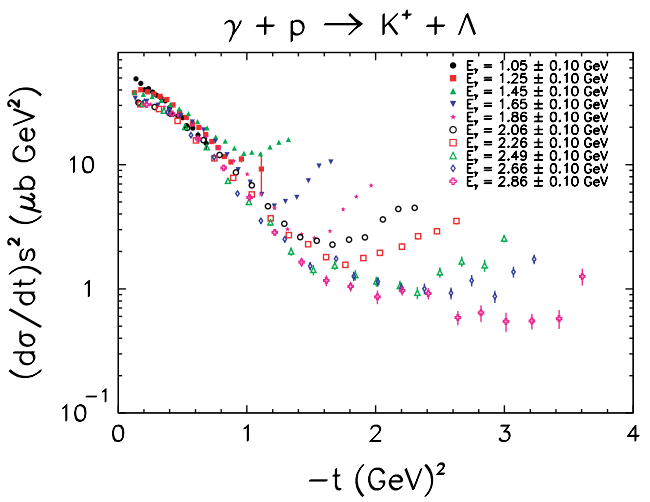

FIG. 23. (Color online) The entire $\gamma + p \to K^+ + \Lambda$ data set shown as $d\sigma/dt$ vs $-t$, for 10 bands of photon energy with $\Delta E_\gamma = 0.20$ GeV. The cross sections were scaled by $s^2 = W^4$, resulting in a well-defined band of data for low $-t$ values.

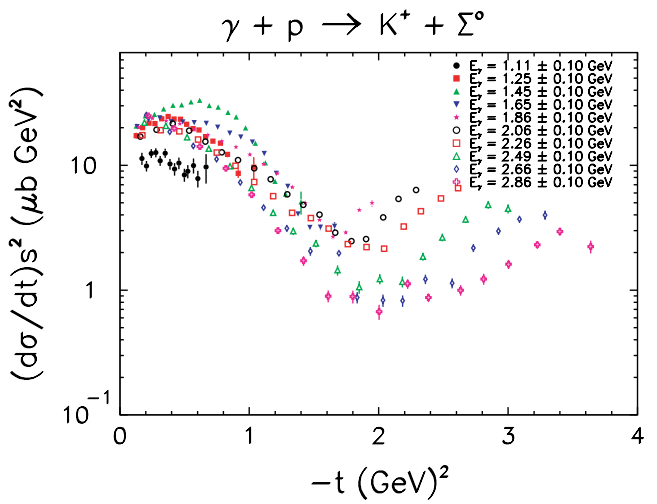

FIG. 25. (Color online) The entire $\gamma + p \to K^+ + \Sigma^0$ data set shown as $d\sigma/dt$ vs $-t$, for 10 bands of photon energy with $\Delta E_\gamma = 0.20$ GeV. The cross sections were scaled by $s^2 = W^4$, showing a less well defined band of points than in the $K^+\Lambda$ case.

taken at $E_\gamma = 5, 8, 11$, and 16 GeV, that is, well above the energies of the present results. In the model of Guidal, Laget, and Vanderhaeghen [20], this effect arose from the interplay of degenerate K and K^* Regge trajectories and the requirements imposed by gauge invariance in the model. The intercepts of these trajectories are at $\alpha(0) = -0.20$ and $+0.25$, respectively, so their average is indeed at about 0, leading to the observed s^2 scaling. We note that this plateau effect persists well into the nucleon-resonance region, which suggests the importance of K and K^* exchange throughout this kinematic region.

The cross section $d\sigma/dt$ for the Σ^0 channel is shown in Fig. 24. In this case, the data do not fall in monotonically shifting contours as E_γ increases, as was the case for the Λ in Fig. 22. Instead, a more nucleon-resonance-dominated picture is suggested by the crossing of the bands of data points. This is emphasized again in Fig. 25, which shows the s^2 scaled cross sections that in this case do not form a tight band of points. There is no consistent trend toward a flattening of the slope, as was the case in $K^+\Lambda$ production; in the previously cited theory [20] this is because in $K^+\Sigma^0$ production the K plays little role compared to K^* since $g_{K\Sigma N} < g_{K\Lambda N}$. Furthermore, the large "resonant" rise in the Σ^0 cross section near $W = 1.90$ GeV is serving to cover up any simple t-channel behavior for this hyperon.

At high enough energies, it is expected, however, that the Σ^0 cross section should also behave as expected by t-channel dominance. In Fig. 26 we show the subset of the data from the previous figure for $E_\gamma > 2.39$ GeV, where the scaling by s^2 does seem to work. We note that this is well above the large "Δ" peak in the total cross section (Fig. 21) and spans the range where the Regge calculation [20,21] is successful in explaining these data.

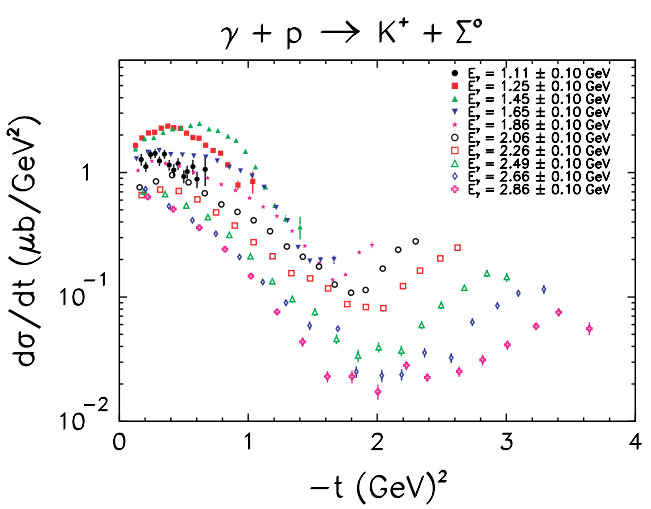

FIG. 24. (Color online) The entire $\gamma + p \to K^+ + \Sigma^0$ data set shown as $d\sigma/dt$ vs $-t$, for 10 bands of photon energy with $\Delta E_\gamma = 0.20$ GeV. No scaling was applied.

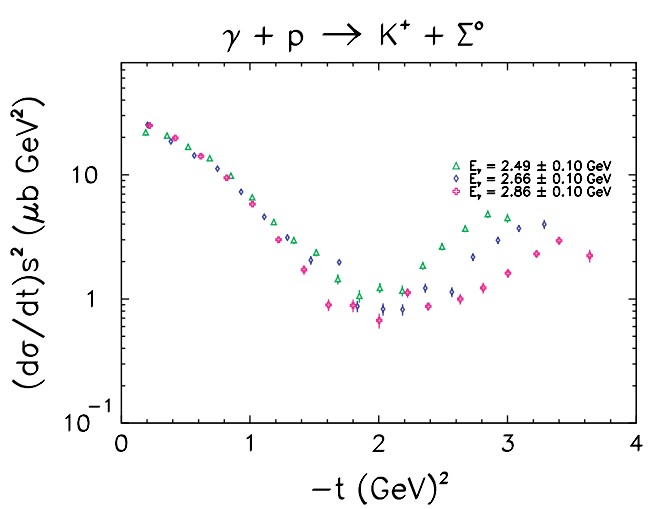

FIG. 26. (Color online) The $\gamma + p \to K^+ + \Sigma^0$ data shown as $d\sigma/dt$ vs $-t$, for the top three bands of photon energy with $\Delta E_\gamma = 0.20$ GeV. The cross sections were scaled by $s^2 = W^4$, showing that for the highest energies the same scaling phenomenon is apparent.

VII. CONCLUSIONS

In summary, we present results from an experimental investigation of Λ and Σ^0 hyperon photoproduction from the proton in the energy range where nucleon-resonance physics should dominate. We provide the to-date largest body of data for these reactions in coverage over energy and meson angle. Our $K^+\Lambda$ cross section results reveal an interesting W dependence: Double-peaked at forward and backward angles, but not at central angles. We see that the structure near $W = 1.9$ GeV shifts in position and shape from forward to backward angles. This finding cannot be explained by a t-channel Regge-based model or by the addition of a single new resonance in the s or u channel. The Σ^0 results confirm a single large maximum in the cross section near 1.9 GeV, with weak indications of more structure between 2.0 and 2.1 GeV. The results are in fair or good agreement with several older experiments. For the $K^+\Lambda$ case we see that a phenomenological scaling of the t dependence of the cross section by s^2 is quite successful in describing the full range of forward-angle data and that this scaling does not work as well for the $K^+\Sigma^0$ data. Our results show that hyperon photoproduction can reveal resonance structure previously "hidden" from view, thereby improving our understanding of nucleonic excitations in the higher mass region where data are sparse. Comprehensive partial wave analysis and amplitude modeling for these results can therefore be hoped to firmly establish the mass and possibly the quantum numbers of these states.

ACKNOWLEDGMENTS

We thank the staff of the Accelerator and the Physics Divisions at Thomas Jefferson National Accelerator Facility who made this experiment possible. We thank D. Seymour for help with the angular distribution fits. Major support came from the U.S. Department of Energy and National Science Foundation, the Italian Instituto Nazionale di Fisica Nucleare, the French Centre National de la Recherche Scientifique, the French Commissariat à l'Energie Atomique, the Deutsche Forschungsgemeinschaft, and the Korean Science and Engineering Foundation. The Southeastern Universities Research Association (SURA) operates Jefferson Lab under United States DOE Contract No. DE-AC05-84ER40150.

APPENDIX: NUMERICAL DATA

The differential cross section results from the present work are given in Table I. Each row corresponds to a given photon energy and gives the result for the $K^+\Lambda$ and $K^+\Sigma^0$ cross sections in the form $d\sigma/d\cos\theta_{K^+}^{\text{c.m.}}$, where $\theta_{K^+}^{\text{c.m.}}$ is the center-of-mass scattering angle of the kaon. The quoted uncertainties are the statistical errors resulting from the yield fitting, acceptance calculations, and photon normalizations. Systematic uncertainties were discussed in the main text. A zero value for a cross section means no data point was extracted at that energy and angle. Electronic tabulations of the results are available from several archival sources [26–29].

TABLE I. Results of CLAS measurements of $\gamma + p \to K^+\Lambda$ and $\gamma + p \to K^+ + \Sigma^0$. The columns marked σ are the differential cross sections $d\sigma/d\cos\theta_{K^+}^{\text{c.m.}}$ for the Λ and Σ^0, respectively; the columns marked $\delta\sigma$ are the associated standard statistical uncertainties.

Index	E_γ (GeV)	W (GeV)	$\cos\theta_K^{\text{c.m.}}$	$\sigma(\Lambda)$ (μb)	$\delta\sigma(\Lambda)$ (μb)	$\sigma(\Sigma^0)$ (μb)	$\delta\sigma(\Sigma^0)$ (μb)
1)	0.944	1.628	−0.80	0.000	0.000	0.000	0.000
2)	0.944	1.628	−0.70	0.000	0.000	0.000	0.000
3)	0.944	1.628	−0.60	0.000	0.000	0.000	0.000
4)	0.944	1.628	−0.50	0.000	0.000	0.000	0.000
5)	0.944	1.628	−0.40	0.000	0.000	0.000	0.000
6)	0.944	1.628	−0.30	0.000	0.000	0.000	0.000
7)	0.944	1.628	−0.20	0.544	0.147	0.000	0.000
8)	0.944	1.628	−0.10	0.348	0.101	0.000	0.000
9)	0.944	1.628	0.00	0.320	0.093	0.000	0.000
10)	0.944	1.628	0.10	0.393	0.097	0.000	0.000
11)	0.944	1.628	0.20	0.636	0.144	0.000	0.000
12)	0.944	1.628	0.30	0.547	0.130	0.000	0.000
13)	0.944	1.628	0.40	0.532	0.134	0.000	0.000
14)	0.944	1.628	0.50	0.593	0.137	0.000	0.000
15)	0.944	1.628	0.60	0.406	0.101	0.000	0.000
16)	0.944	1.628	0.70	0.364	0.107	0.000	0.000
17)	0.944	1.628	0.80	0.000	0.000	0.000	0.000
18)	0.944	1.628	0.90	0.000	0.000	0.000	0.000
19)	0.969	1.643	−0.80	0.000	0.000	0.000	0.000
20)	0.969	1.643	−0.70	0.000	0.000	0.000	0.000
21)	0.969	1.643	−0.60	0.000	0.000	0.000	0.000
22)	0.969	1.643	−0.50	0.000	0.000	0.000	0.000
23)	0.969	1.643	−0.40	0.000	0.000	0.000	0.000
24)	0.969	1.643	−0.30	0.460	0.096	0.000	0.000
25)	0.969	1.643	−0.20	0.818	0.124	0.000	0.000
26)	0.969	1.643	−0.10	0.596	0.105	0.000	0.000
27)	0.969	1.643	0.00	0.582	0.088	0.000	0.000
28)	0.969	1.643	0.10	0.608	0.100	0.000	0.000
29)	0.969	1.643	0.20	0.797	0.122	0.000	0.000
30)	0.969	1.643	0.30	0.688	0.162	0.000	0.000
31)	0.969	1.643	0.40	0.721	0.093	0.000	0.000
32)	0.969	1.643	0.50	0.692	0.093	0.000	0.000
33)	0.969	1.643	0.60	0.728	0.097	0.000	0.000
34)	0.969	1.643	0.70	0.555	0.079	0.000	0.000
35)	0.969	1.643	0.80	0.775	0.105	0.000	0.000
36)	0.969	1.643	0.90	0.000	0.000	0.000	0.000
37)	0.994	1.657	−0.80	0.000	0.000	0.000	0.000
38)	0.994	1.657	−0.70	0.000	0.000	0.000	0.000
39)	0.994	1.657	−0.60	0.000	0.000	0.000	0.000
40)	0.994	1.657	−0.50	0.000	0.000	0.000	0.000
41)	0.994	1.657	−0.40	0.990	0.173	0.000	0.000
42)	0.994	1.657	−0.30	0.675	0.096	0.000	0.000
43)	0.994	1.657	−0.20	0.879	0.114	0.000	0.000
44)	0.994	1.657	−0.10	0.857	0.104	0.000	0.000
45)	0.994	1.657	0.00	0.561	0.073	0.000	0.000
46)	0.994	1.657	0.10	0.966	0.118	0.000	0.000
47)	0.994	1.657	0.20	0.882	0.114	0.000	0.000
48)	0.994	1.657	0.30	1.057	0.106	0.000	0.000
49)	0.994	1.657	0.40	0.804	0.084	0.000	0.000
50)	0.994	1.657	0.50	0.909	0.098	0.000	0.000
51)	0.994	1.657	0.60	1.071	0.116	0.000	0.000
52)	0.994	1.657	0.70	1.091	0.106	0.000	0.000

TABLE I. (*Continued.*)

Index	E_γ (GeV)	W (GeV)	$\cos\theta_K^{\text{c.m.}}$	$\sigma(\Lambda)$ (μb)	$\delta\sigma(\Lambda)$ (μb)	$\sigma(\Sigma^0)$ (μb)	$\delta\sigma(\Sigma^0)$ (μb)
53)	0.994	1.657	0.80	0.974	0.104	0.000	0.000
54)	0.994	1.657	0.90	0.000	0.000	0.000	0.000
55)	1.019	1.671	−0.80	0.000	0.000	0.000	0.000
56)	1.019	1.671	−0.70	0.000	0.000	0.000	0.000
57)	1.019	1.671	−0.60	0.000	0.000	0.000	0.000
58)	1.019	1.671	−0.50	0.000	0.000	0.000	0.000
59)	1.019	1.671	−0.40	0.819	0.148	0.000	0.000
60)	1.019	1.671	−0.30	0.818	0.135	0.000	0.000
61)	1.019	1.671	−0.20	1.079	0.141	0.000	0.000
62)	1.019	1.671	−0.10	0.880	0.115	0.000	0.000
63)	1.019	1.671	0.00	0.879	0.109	0.000	0.000
64)	1.019	1.671	0.10	1.032	0.128	0.000	0.000
65)	1.019	1.671	0.20	1.106	0.138	0.000	0.000
66)	1.019	1.671	0.30	1.074	0.113	0.000	0.000
67)	1.019	1.671	0.40	0.945	0.105	0.000	0.000
68)	1.019	1.671	0.50	1.037	0.121	0.000	0.000
69)	1.019	1.671	0.60	1.295	0.134	0.000	0.000
70)	1.019	1.671	0.70	1.155	0.122	0.000	0.000
71)	1.019	1.671	0.80	1.232	0.143	0.000	0.000
72)	1.019	1.671	0.90	1.495	0.318	0.000	0.000
73)	1.044	1.685	−0.80	0.000	0.000	0.000	0.000
74)	1.044	1.685	−0.70	0.000	0.000	0.000	0.000
75)	1.044	1.685	−0.60	0.000	0.000	0.000	0.000
76)	1.044	1.685	−0.50	0.941	0.158	0.000	0.000
77)	1.044	1.685	−0.40	0.789	0.101	0.000	0.000
78)	1.044	1.685	−0.30	0.860	0.092	0.000	0.000
79)	1.044	1.685	−0.20	0.846	0.085	0.000	0.000
80)	1.044	1.685	−0.10	0.971	0.086	0.000	0.000
81)	1.044	1.685	0.00	0.843	0.076	0.000	0.000
82)	1.044	1.685	0.10	1.099	0.095	0.000	0.000
83)	1.044	1.685	0.20	1.093	0.093	0.000	0.000
84)	1.044	1.685	0.30	1.269	0.092	0.000	0.000
85)	1.044	1.685	0.40	1.245	0.095	0.000	0.000
86)	1.044	1.685	0.50	1.470	0.109	0.000	0.000
87)	1.044	1.685	0.60	1.396	0.105	0.000	0.000
88)	1.044	1.685	0.70	1.429	0.111	0.000	0.000
89)	1.044	1.685	0.80	1.501	0.130	0.000	0.000
90)	1.044	1.685	0.90	1.822	0.214	0.000	0.000
91)	1.069	1.699	−0.80	0.000	0.000	0.000	0.000
92)	1.069	1.699	−0.70	0.000	0.000	0.000	0.000
93)	1.069	1.699	−0.60	0.000	0.000	0.000	0.000
94)	1.069	1.699	−0.50	0.670	0.108	0.000	0.000
95)	1.069	1.699	−0.40	0.780	0.100	0.000	0.000
96)	1.069	1.699	−0.30	0.798	0.092	0.000	0.000
97)	1.069	1.699	−0.20	0.973	0.088	0.000	0.000
98)	1.069	1.699	−0.10	1.074	0.089	0.000	0.000
99)	1.069	1.699	0.00	0.961	0.079	0.000	0.000
100)	1.069	1.699	0.10	1.158	0.098	0.000	0.000
101)	1.069	1.699	0.20	1.256	0.098	0.000	0.000
102)	1.069	1.699	0.30	1.278	0.094	0.000	0.000
103)	1.069	1.699	0.40	1.427	0.103	0.000	0.000
104)	1.069	1.699	0.50	1.372	0.098	0.000	0.000
105)	1.069	1.699	0.60	1.620	0.114	0.000	0.000
106)	1.069	1.699	0.70	1.556	0.126	0.000	0.000
107)	1.069	1.699	0.80	1.772	0.138	0.000	0.000
108)	1.069	1.699	0.90	1.879	0.219	0.000	0.000

TABLE I. (*Continued.*)

Index	E_γ (GeV)	W (GeV)	$\cos\theta_K^{\text{c.m.}}$	$\sigma(\Lambda)$ (μb)	$\delta\sigma(\Lambda)$ (μb)	$\sigma(\Sigma^0)$ (μb)	$\delta\sigma(\Sigma^0)$ (μb)
109)	1.094	1.713	−0.80	0.000	0.000	0.000	0.000
110)	1.094	1.713	−0.70	0.000	0.000	0.000	0.000
111)	1.094	1.713	−0.60	0.635	0.159	0.000	0.000
112)	1.094	1.713	−0.50	0.697	0.090	0.000	0.000
113)	1.094	1.713	−0.40	0.857	0.090	0.278	0.099
114)	1.094	1.713	−0.30	0.936	0.082	0.318	0.097
115)	1.094	1.713	−0.20	0.982	0.078	0.221	0.067
116)	1.094	1.713	−0.10	0.821	0.066	0.353	0.098
117)	1.094	1.713	0.00	0.936	0.068	0.265	0.070
118)	1.094	1.713	0.10	1.164	0.086	0.318	0.078
119)	1.094	1.713	0.20	1.237	0.086	0.317	0.075
120)	1.094	1.713	0.30	1.416	0.088	0.400	0.074
121)	1.094	1.713	0.40	1.410	0.088	0.268	0.058
122)	1.094	1.713	0.50	1.497	0.089	0.367	0.069
123)	1.094	1.713	0.60	1.641	0.100	0.397	0.079
124)	1.094	1.713	0.70	1.653	0.108	0.273	0.059
125)	1.094	1.713	0.80	1.889	0.127	0.241	0.101
126)	1.094	1.713	0.90	1.652	0.177	0.000	0.000
127)	1.119	1.727	−0.80	0.000	0.000	0.000	0.000
128)	1.119	1.727	−0.70	0.000	0.000	0.000	0.000
129)	1.119	1.727	−0.60	0.539	0.138	0.000	0.000
130)	1.119	1.727	−0.50	0.550	0.098	0.000	0.000
131)	1.119	1.727	−0.40	0.716	0.091	0.161	0.077
132)	1.119	1.727	−0.30	0.795	0.084	0.371	0.155
133)	1.119	1.727	−0.20	0.794	0.082	0.324	0.085
134)	1.119	1.727	−0.10	0.904	0.085	0.214	0.073
135)	1.119	1.727	0.00	1.054	0.089	0.502	0.107
136)	1.119	1.727	0.10	0.999	0.089	0.329	0.088
137)	1.119	1.727	0.20	1.209	0.099	0.407	0.087
138)	1.119	1.727	0.30	1.313	0.095	0.480	0.089
139)	1.119	1.727	0.40	1.419	0.104	0.407	0.078
140)	1.119	1.727	0.50	1.594	0.106	0.517	0.089
141)	1.119	1.727	0.60	1.598	0.113	0.445	0.078
142)	1.119	1.727	0.70	1.983	0.147	0.415	0.076
143)	1.119	1.727	0.80	2.205	0.159	0.416	0.091
144)	1.119	1.727	0.90	2.154	0.248	0.000	0.000
145)	1.144	1.740	−0.80	0.000	0.000	0.000	0.000
146)	1.144	1.740	−0.70	0.000	0.000	0.000	0.000
147)	1.144	1.740	−0.60	0.618	0.091	0.000	0.000
148)	1.144	1.740	−0.50	0.680	0.080	0.404	0.107
149)	1.144	1.740	−0.40	0.675	0.061	0.492	0.079
150)	1.144	1.740	−0.30	0.681	0.057	0.453	0.074
151)	1.144	1.740	−0.20	0.850	0.060	0.525	0.073
152)	1.144	1.740	−0.10	0.957	0.063	0.406	0.056
153)	1.144	1.740	0.00	1.068	0.066	0.521	0.071
154)	1.144	1.740	0.10	1.070	0.068	0.438	0.066
155)	1.144	1.740	0.20	1.336	0.076	0.467	0.058
156)	1.144	1.740	0.30	1.327	0.073	0.579	0.062
157)	1.144	1.740	0.40	1.659	0.085	0.674	0.071
158)	1.144	1.740	0.50	1.664	0.083	0.616	0.066
159)	1.144	1.740	0.60	1.674	0.091	0.592	0.062
160)	1.144	1.740	0.70	1.654	0.092	0.501	0.062
161)	1.144	1.740	0.80	1.913	0.110	0.591	0.075
162)	1.144	1.740	0.90	1.971	0.179	0.000	0.000
163)	1.169	1.753	−0.80	0.000	0.000	0.000	0.000
164)	1.169	1.753	−0.70	0.000	0.000	0.000	0.000

TABLE I. (*Continued.*)

Index	E_γ (GeV)	W (GeV)	$\cos\theta_K^{\text{c.m.}}$	$\sigma(\Lambda)$ (μb)	$\delta\sigma(\Lambda)$ (μb)	$\sigma(\Sigma^0)$ (μb)	$\delta\sigma(\Sigma^0)$ (μb)
165)	1.169	1.753	−0.60	0.395	0.071	0.000	0.000
166)	1.169	1.753	−0.50	0.426	0.061	0.411	0.096
167)	1.169	1.753	−0.40	0.504	0.060	0.542	0.091
168)	1.169	1.753	−0.30	0.683	0.065	0.475	0.078
169)	1.169	1.753	−0.20	0.789	0.062	0.454	0.069
170)	1.169	1.753	−0.10	0.913	0.063	0.420	0.068
171)	1.169	1.753	0.00	0.938	0.063	0.591	0.077
172)	1.169	1.753	0.10	1.066	0.076	0.527	0.075
173)	1.169	1.753	0.20	1.137	0.074	0.622	0.072
174)	1.169	1.753	0.30	1.295	0.075	0.528	0.062
175)	1.169	1.753	0.40	1.599	0.089	0.765	0.081
176)	1.169	1.753	0.50	1.618	0.086	0.776	0.075
177)	1.169	1.753	0.60	1.755	0.098	0.552	0.057
178)	1.169	1.753	0.70	1.753	0.099	0.582	0.072
179)	1.169	1.753	0.80	1.703	0.108	0.849	0.093
180)	1.169	1.753	0.90	1.662	0.175	0.564	0.137
181)	1.194	1.767	−0.80	0.000	0.000	0.000	0.000
182)	1.194	1.767	−0.70	0.742	0.214	0.000	0.000
183)	1.194	1.767	−0.60	0.352	0.063	0.471	0.230
184)	1.194	1.767	−0.50	0.579	0.070	0.508	0.100
185)	1.194	1.767	−0.40	0.630	0.064	0.633	0.090
186)	1.194	1.767	−0.30	0.723	0.062	0.477	0.071
187)	1.194	1.767	−0.20	0.971	0.071	0.434	0.059
188)	1.194	1.767	−0.10	0.902	0.061	0.514	0.065
189)	1.194	1.767	0.00	1.040	0.067	0.587	0.071
190)	1.194	1.767	0.10	1.099	0.075	0.674	0.073
191)	1.194	1.767	0.20	1.280	0.073	0.746	0.070
192)	1.194	1.767	0.30	1.365	0.077	0.868	0.080
193)	1.194	1.767	0.40	1.584	0.081	0.782	0.071
194)	1.194	1.767	0.50	1.655	0.086	0.955	0.078
195)	1.194	1.767	0.60	1.748	0.094	0.822	0.078
196)	1.194	1.767	0.70	1.856	0.098	0.747	0.077
197)	1.194	1.767	0.80	1.997	0.116	0.791	0.079
198)	1.194	1.767	0.90	1.663	0.173	0.605	0.149
199)	1.219	1.780	−0.80	0.000	0.000	0.000	0.000
200)	1.219	1.780	−0.70	0.276	0.086	0.000	0.000
201)	1.219	1.780	−0.60	0.427	0.060	0.563	0.139
202)	1.219	1.780	−0.50	0.529	0.057	0.461	0.078
203)	1.219	1.780	−0.40	0.605	0.055	0.505	0.072
204)	1.219	1.780	−0.30	0.664	0.051	0.564	0.066
205)	1.219	1.780	−0.20	0.797	0.056	0.617	0.062
206)	1.219	1.780	−0.10	0.985	0.060	0.779	0.072
207)	1.219	1.780	0.00	0.992	0.060	0.692	0.068
208)	1.219	1.780	0.10	1.079	0.068	0.761	0.067
209)	1.219	1.780	0.20	1.164	0.063	0.869	0.068
210)	1.219	1.780	0.30	1.344	0.069	1.005	0.076
211)	1.219	1.780	0.40	1.574	0.077	0.942	0.069
212)	1.219	1.780	0.50	1.705	0.081	0.923	0.069
213)	1.219	1.780	0.60	1.685	0.086	0.889	0.061
214)	1.219	1.780	0.70	1.761	0.085	1.009	0.087
215)	1.219	1.780	0.80	2.002	0.113	0.809	0.072
216)	1.219	1.780	0.90	2.084	0.190	0.609	0.116
217)	1.244	1.793	−0.80	0.000	0.000	0.000	0.000
218)	1.244	1.793	−0.70	0.629	0.099	0.000	0.000
219)	1.244	1.793	−0.60	0.429	0.053	0.307	0.074
220)	1.244	1.793	−0.50	0.453	0.047	0.549	0.075
221)	1.244	1.793	−0.40	0.678	0.054	0.625	0.067
222)	1.244	1.793	−0.30	0.687	0.048	0.758	0.067
223)	1.244	1.793	−0.20	0.715	0.047	0.857	0.071
224)	1.244	1.793	−0.10	0.899	0.051	0.871	0.066
225)	1.244	1.793	0.00	1.020	0.057	0.820	0.067
226)	1.244	1.793	0.10	1.090	0.062	0.979	0.071
227)	1.244	1.793	0.20	1.243	0.061	1.131	0.076
228)	1.244	1.793	0.30	1.377	0.068	1.140	0.077
229)	1.244	1.793	0.40	1.621	0.071	1.188	0.065
230)	1.244	1.793	0.50	1.672	0.076	1.003	0.062
231)	1.244	1.793	0.60	1.704	0.077	0.952	0.062
232)	1.244	1.793	0.70	1.939	0.087	0.986	0.074
233)	1.244	1.793	0.80	1.993	0.106	0.954	0.070
234)	1.244	1.793	0.90	1.861	0.161	0.714	0.111
235)	1.269	1.806	−0.80	0.000	0.000	0.000	0.000
236)	1.269	1.806	−0.70	0.456	0.070	0.000	0.000
237)	1.269	1.806	−0.60	0.522	0.055	0.417	0.072
238)	1.269	1.806	−0.50	0.529	0.047	0.629	0.072
239)	1.269	1.806	−0.40	0.617	0.047	0.813	0.071
240)	1.269	1.806	−0.30	0.747	0.049	0.737	0.063
241)	1.269	1.806	−0.20	0.895	0.054	0.939	0.069
242)	1.269	1.806	−0.10	0.927	0.050	1.060	0.069
243)	1.269	1.806	0.00	0.914	0.048	1.058	0.072
244)	1.269	1.806	0.10	1.188	0.061	1.194	0.073
245)	1.269	1.806	0.20	1.256	0.058	1.226	0.072
246)	1.269	1.806	0.30	1.617	0.072	1.156	0.067
247)	1.269	1.806	0.40	1.656	0.070	1.137	0.064
248)	1.269	1.806	0.50	1.560	0.068	1.103	0.066
249)	1.269	1.806	0.60	1.679	0.078	1.133	0.077
250)	1.269	1.806	0.70	1.699	0.070	1.057	0.061
251)	1.269	1.806	0.80	1.989	0.102	0.906	0.067
252)	1.269	1.806	0.90	2.093	0.194	0.843	0.108
253)	1.294	1.819	−0.80	0.000	0.000	0.000	0.000
254)	1.294	1.819	−0.70	0.647	0.116	0.000	0.000
255)	1.294	1.819	−0.60	0.657	0.083	0.386	0.090
256)	1.294	1.819	−0.50	0.564	0.062	0.621	0.089
257)	1.294	1.819	−0.40	0.717	0.069	0.765	0.088
258)	1.294	1.819	−0.30	0.733	0.062	0.901	0.086
259)	1.294	1.819	−0.20	0.846	0.064	1.024	0.092
260)	1.294	1.819	−0.10	0.971	0.066	1.203	0.095
261)	1.294	1.819	0.00	1.120	0.074	1.178	0.100
262)	1.294	1.819	0.10	1.246	0.081	1.312	0.103
263)	1.294	1.819	0.20	1.209	0.071	1.471	0.100
264)	1.294	1.819	0.30	1.604	0.090	1.442	0.100
265)	1.294	1.819	0.40	1.544	0.081	1.500	0.097
266)	1.294	1.819	0.50	1.759	0.090	1.174	0.084
267)	1.294	1.819	0.60	1.722	0.092	1.448	0.098
268)	1.294	1.819	0.70	1.916	0.097	1.127	0.085
269)	1.294	1.819	0.80	1.910	0.120	1.124	0.080
270)	1.294	1.819	0.90	1.675	0.166	0.986	0.149
271)	1.320	1.832	−0.80	0.000	0.000	0.000	0.000
272)	1.320	1.832	−0.70	0.521	0.086	0.409	0.139
273)	1.320	1.832	−0.60	0.618	0.071	0.462	0.083
274)	1.320	1.832	−0.50	0.654	0.065	0.667	0.086
275)	1.320	1.832	−0.40	0.705	0.064	1.000	0.096
276)	1.320	1.832	−0.30	0.722	0.056	1.135	0.097

TABLE I. (*Continued.*)

Index	E_γ (GeV)	W (GeV)	$\cos\theta_K^{\text{c.m.}}$	$\sigma(\Lambda)$ (μb)	$\delta\sigma(\Lambda)$ (μb)	$\sigma(\Sigma^0)$ (μb)	$\delta\sigma(\Sigma^0)$ (μb)
277)	1.320	1.832	−0.20	0.828	0.058	1.203	0.087
278)	1.320	1.832	−0.10	0.999	0.064	1.473	0.103
279)	1.320	1.832	0.00	1.049	0.066	1.544	0.110
280)	1.320	1.832	0.10	1.235	0.079	1.406	0.099
281)	1.320	1.832	0.20	1.286	0.070	1.474	0.093
282)	1.320	1.832	0.30	1.464	0.080	1.746	0.112
283)	1.320	1.832	0.40	1.739	0.088	1.482	0.089
284)	1.320	1.832	0.50	1.806	0.094	1.569	0.099
285)	1.320	1.832	0.60	1.925	0.095	1.321	0.087
286)	1.320	1.832	0.70	1.918	0.088	1.353	0.086
287)	1.320	1.832	0.80	1.898	0.116	1.142	0.096
288)	1.320	1.832	0.90	1.777	0.163	1.185	0.158
289)	1.345	1.845	−0.80	0.463	0.164	0.000	0.000
290)	1.345	1.845	−0.70	0.727	0.086	0.551	0.138
291)	1.345	1.845	−0.60	0.601	0.059	0.459	0.075
292)	1.345	1.845	−0.50	0.732	0.061	0.682	0.078
293)	1.345	1.845	−0.40	0.725	0.059	0.826	0.073
294)	1.345	1.845	−0.30	0.842	0.055	0.995	0.075
295)	1.345	1.845	−0.20	0.853	0.055	1.270	0.082
296)	1.345	1.845	−0.10	0.945	0.054	1.485	0.090
297)	1.345	1.845	0.00	1.054	0.058	1.437	0.088
298)	1.345	1.845	0.10	1.072	0.063	1.564	0.093
299)	1.345	1.845	0.20	1.327	0.064	1.607	0.086
300)	1.345	1.845	0.30	1.381	0.067	1.583	0.087
301)	1.345	1.845	0.40	1.431	0.065	1.651	0.083
302)	1.345	1.845	0.50	1.696	0.078	1.631	0.084
303)	1.345	1.845	0.60	1.807	0.080	1.620	0.090
304)	1.345	1.845	0.70	1.849	0.083	1.366	0.079
305)	1.345	1.845	0.80	1.742	0.094	1.017	0.075
306)	1.345	1.845	0.90	1.694	0.142	1.051	0.120
307)	1.370	1.858	−0.80	0.625	0.131	0.000	0.000
308)	1.370	1.858	−0.70	0.784	0.077	0.663	0.114
309)	1.370	1.858	−0.60	0.692	0.063	0.566	0.078
310)	1.370	1.858	−0.50	0.677	0.050	0.836	0.078
311)	1.370	1.858	−0.40	0.663	0.049	0.917	0.069
312)	1.370	1.858	−0.30	0.762	0.046	1.203	0.075
313)	1.370	1.858	−0.20	0.913	0.051	1.361	0.075
314)	1.370	1.858	−0.10	1.063	0.055	1.591	0.084
315)	1.370	1.858	0.00	1.096	0.053	1.711	0.090
316)	1.370	1.858	0.10	1.236	0.063	1.733	0.091
317)	1.370	1.858	0.20	1.375	0.061	1.947	0.090
318)	1.370	1.858	0.30	1.423	0.066	1.858	0.089
319)	1.370	1.858	0.40	1.566	0.061	1.736	0.074
320)	1.370	1.858	0.50	1.576	0.066	1.847	0.083
321)	1.370	1.858	0.60	1.789	0.073	1.741	0.086
322)	1.370	1.858	0.70	1.883	0.077	1.491	0.076
323)	1.370	1.858	0.80	1.792	0.087	1.282	0.076
324)	1.370	1.858	0.90	1.807	0.135	1.007	0.104
325)	1.395	1.870	−0.80	0.728	0.122	0.000	0.000
326)	1.395	1.870	−0.70	0.732	0.070	0.387	0.067
327)	1.395	1.870	−0.60	0.805	0.062	0.474	0.057
328)	1.395	1.870	−0.50	0.701	0.045	0.665	0.060
329)	1.395	1.870	−0.40	0.754	0.047	0.983	0.064
330)	1.395	1.870	−0.30	0.847	0.045	1.097	0.061
331)	1.395	1.870	−0.20	0.840	0.042	1.371	0.068
332)	1.395	1.870	−0.10	0.971	0.045	1.647	0.075
333)	1.395	1.870	0.00	1.036	0.047	1.680	0.079
334)	1.395	1.870	0.10	1.118	0.050	1.739	0.077
335)	1.395	1.870	0.20	1.300	0.052	1.773	0.072
336)	1.395	1.870	0.30	1.469	0.058	1.823	0.078
337)	1.395	1.870	0.40	1.540	0.053	1.789	0.066
338)	1.395	1.870	0.50	1.666	0.065	1.829	0.081
339)	1.395	1.870	0.60	1.598	0.059	1.669	0.074
340)	1.395	1.870	0.70	1.732	0.063	1.519	0.064
341)	1.395	1.870	0.80	1.847	0.085	1.468	0.087
342)	1.395	1.870	0.90	1.862	0.130	1.053	0.091
343)	1.421	1.883	−0.80	0.875	0.176	0.000	0.000
344)	1.421	1.883	−0.70	0.993	0.113	0.418	0.089
345)	1.421	1.883	−0.60	0.794	0.073	0.466	0.064
346)	1.421	1.883	−0.50	0.825	0.071	0.796	0.090
347)	1.421	1.883	−0.40	0.835	0.067	0.888	0.077
348)	1.421	1.883	−0.30	0.789	0.057	1.130	0.082
349)	1.421	1.883	−0.20	0.775	0.056	1.546	0.099
350)	1.421	1.883	−0.10	1.030	0.061	1.761	0.104
351)	1.421	1.883	0.00	0.937	0.060	1.938	0.115
352)	1.421	1.883	0.10	1.288	0.074	1.651	0.089
353)	1.421	1.883	0.20	1.379	0.072	2.096	0.108
354)	1.421	1.883	0.30	1.396	0.073	1.961	0.105
355)	1.421	1.883	0.40	1.563	0.077	1.729	0.091
356)	1.421	1.883	0.50	1.632	0.077	1.996	0.101
357)	1.421	1.883	0.60	1.694	0.083	1.626	0.091
358)	1.421	1.883	0.70	1.867	0.087	1.498	0.090
359)	1.421	1.883	0.80	1.707	0.099	1.435	0.110
360)	1.421	1.883	0.90	1.938	0.168	1.437	0.148
361)	1.446	1.896	−0.80	0.842	0.104	0.000	0.000
362)	1.446	1.896	−0.70	0.789	0.069	0.523	0.074
363)	1.446	1.896	−0.60	0.887	0.062	0.390	0.045
364)	1.446	1.896	−0.50	0.644	0.044	0.645	0.054
365)	1.446	1.896	−0.40	0.752	0.047	0.949	0.057
366)	1.446	1.896	−0.30	0.750	0.042	1.204	0.064
367)	1.446	1.896	−0.20	0.797	0.042	1.386	0.066
368)	1.446	1.896	−0.10	0.851	0.041	1.502	0.068
369)	1.446	1.896	0.00	0.934	0.045	1.710	0.078
370)	1.446	1.896	0.10	1.117	0.053	1.747	0.077
371)	1.446	1.896	0.20	1.115	0.047	1.770	0.072
372)	1.446	1.896	0.30	1.308	0.053	1.833	0.075
373)	1.446	1.896	0.40	1.461	0.057	1.763	0.072
374)	1.446	1.896	0.50	1.670	0.061	1.859	0.073
375)	1.446	1.896	0.60	1.678	0.062	1.484	0.064
376)	1.446	1.896	0.70	1.834	0.072	1.475	0.069
377)	1.446	1.896	0.80	1.953	0.083	1.298	0.081
378)	1.446	1.896	0.90	2.105	0.137	1.229	0.108
379)	1.471	1.908	−0.80	1.065	0.118	0.000	0.000
380)	1.471	1.908	−0.70	0.802	0.063	0.344	0.054
381)	1.471	1.908	−0.60	0.738	0.052	0.506	0.052
382)	1.471	1.908	−0.50	0.699	0.045	0.562	0.047
383)	1.471	1.908	−0.40	0.633	0.039	0.802	0.049
384)	1.471	1.908	−0.30	0.740	0.040	1.102	0.057
385)	1.471	1.908	−0.20	0.711	0.037	1.459	0.069
386)	1.471	1.908	−0.10	0.761	0.037	1.533	0.068
387)	1.471	1.908	0.00	0.829	0.039	1.493	0.068
388)	1.471	1.908	0.10	1.037	0.047	1.638	0.066

TABLE I. (*Continued.*)

Index	E_γ (GeV)	W (GeV)	$\cos\theta_K^{\text{c.m.}}$	$\sigma(\Lambda)$ (μb)	$\delta\sigma(\Lambda)$ (μb)	$\sigma(\Sigma^0)$ (μb)	$\delta\sigma(\Sigma^0)$ (μb)
389)	1.471	1.908	0.20	1.155	0.046	1.736	0.070
390)	1.471	1.908	0.30	1.353	0.052	1.785	0.070
391)	1.471	1.908	0.40	1.440	0.051	1.574	0.062
392)	1.471	1.908	0.50	1.627	0.062	1.584	0.064
393)	1.471	1.908	0.60	1.787	0.060	1.452	0.062
394)	1.471	1.908	0.70	1.950	0.073	1.382	0.063
395)	1.471	1.908	0.80	1.949	0.082	1.265	0.068
396)	1.471	1.908	0.90	2.087	0.129	0.964	0.086
397)	1.496	1.920	−0.80	0.808	0.098	0.225	0.101
398)	1.496	1.920	−0.70	0.841	0.068	0.371	0.051
399)	1.496	1.920	−0.60	0.650	0.051	0.442	0.049
400)	1.496	1.920	−0.50	0.582	0.042	0.568	0.054
401)	1.496	1.920	−0.40	0.714	0.046	0.811	0.053
402)	1.496	1.920	−0.30	0.613	0.037	1.058	0.060
403)	1.496	1.920	−0.20	0.649	0.038	1.196	0.060
404)	1.496	1.920	−0.10	0.795	0.041	1.401	0.067
405)	1.496	1.920	0.00	0.770	0.042	1.377	0.068
406)	1.496	1.920	0.10	1.058	0.051	1.582	0.069
407)	1.496	1.920	0.20	1.112	0.047	1.705	0.071
408)	1.496	1.920	0.30	1.375	0.056	1.698	0.071
409)	1.496	1.920	0.40	1.521	0.058	1.582	0.066
410)	1.496	1.920	0.50	1.623	0.063	1.557	0.060
411)	1.496	1.920	0.60	1.821	0.064	1.470	0.063
412)	1.496	1.920	0.70	1.948	0.073	1.138	0.058
413)	1.496	1.920	0.80	2.043	0.088	1.265	0.073
414)	1.496	1.920	0.90	1.995	0.129	0.997	0.094
415)	1.521	1.933	−0.80	0.832	0.096	0.263	0.094
416)	1.521	1.933	−0.70	0.852	0.067	0.223	0.045
417)	1.521	1.933	−0.60	0.767	0.054	0.365	0.040
418)	1.521	1.933	−0.50	0.621	0.042	0.507	0.048
419)	1.521	1.933	−0.40	0.617	0.041	0.751	0.049
420)	1.521	1.933	−0.30	0.583	0.035	0.953	0.053
421)	1.521	1.933	−0.20	0.675	0.037	1.158	0.058
422)	1.521	1.933	−0.10	0.760	0.038	1.340	0.060
423)	1.521	1.933	0.00	0.883	0.044	1.514	0.070
424)	1.521	1.933	0.10	0.985	0.044	1.521	0.063
425)	1.521	1.933	0.20	1.101	0.046	1.649	0.067
426)	1.521	1.933	0.30	1.369	0.054	1.543	0.064
427)	1.521	1.933	0.40	1.463	0.056	1.525	0.063
428)	1.521	1.933	0.50	1.604	0.059	1.437	0.059
429)	1.521	1.933	0.60	1.829	0.062	1.381	0.057
430)	1.521	1.933	0.70	1.901	0.074	1.211	0.059
431)	1.521	1.933	0.80	2.104	0.085	1.361	0.070
432)	1.521	1.933	0.90	2.287	0.144	1.199	0.096
433)	1.546	1.945	−0.80	0.923	0.100	0.332	0.102
434)	1.546	1.945	−0.70	0.734	0.058	0.192	0.039
435)	1.546	1.945	−0.60	0.634	0.049	0.274	0.034
436)	1.546	1.945	−0.50	0.553	0.041	0.379	0.038
437)	1.546	1.945	−0.40	0.545	0.038	0.593	0.042
438)	1.546	1.945	−0.30	0.464	0.030	0.877	0.051
439)	1.546	1.945	−0.20	0.586	0.033	1.125	0.057
440)	1.546	1.945	−0.10	0.663	0.035	1.093	0.050
441)	1.546	1.945	0.00	0.753	0.039	1.367	0.064
442)	1.546	1.945	0.10	0.846	0.041	1.383	0.059
443)	1.546	1.945	0.20	1.085	0.047	1.624	0.067
444)	1.546	1.945	0.30	1.266	0.051	1.480	0.060
445)	1.546	1.945	0.40	1.409	0.051	1.405	0.055
446)	1.546	1.945	0.50	1.489	0.055	1.319	0.057
447)	1.546	1.945	0.60	1.688	0.060	1.408	0.060
448)	1.546	1.945	0.70	1.789	0.069	1.288	0.062
449)	1.546	1.945	0.80	2.040	0.084	1.271	0.070
450)	1.546	1.945	0.90	2.022	0.121	1.055	0.087
451)	1.571	1.957	−0.80	0.762	0.076	0.207	0.061
452)	1.571	1.957	−0.70	0.742	0.056	0.202	0.032
453)	1.571	1.957	−0.60	0.697	0.048	0.272	0.031
454)	1.571	1.957	−0.50	0.512	0.036	0.324	0.032
455)	1.571	1.957	−0.40	0.464	0.032	0.569	0.038
456)	1.571	1.957	−0.30	0.457	0.028	0.720	0.041
457)	1.571	1.957	−0.20	0.532	0.030	0.982	0.047
458)	1.571	1.957	−0.10	0.613	0.032	1.111	0.050
459)	1.571	1.957	0.00	0.671	0.033	1.232	0.055
460)	1.571	1.957	0.10	0.870	0.039	1.364	0.056
461)	1.571	1.957	0.20	0.998	0.040	1.366	0.055
462)	1.571	1.957	0.30	1.217	0.047	1.553	0.061
463)	1.571	1.957	0.40	1.341	0.051	1.400	0.057
464)	1.571	1.957	0.50	1.546	0.054	1.372	0.053
465)	1.571	1.957	0.60	1.749	0.061	1.289	0.052
466)	1.571	1.957	0.70	1.735	0.065	1.303	0.059
467)	1.571	1.957	0.80	2.030	0.080	1.339	0.068
468)	1.571	1.957	0.90	2.370	0.130	0.995	0.083
469)	1.596	1.969	−0.80	0.674	0.070	0.155	0.050
470)	1.596	1.969	−0.70	0.762	0.053	0.139	0.027
471)	1.596	1.969	−0.60	0.566	0.040	0.178	0.023
472)	1.596	1.969	−0.50	0.389	0.031	0.256	0.027
473)	1.596	1.969	−0.40	0.381	0.028	0.473	0.034
474)	1.596	1.969	−0.30	0.406	0.026	0.713	0.040
475)	1.596	1.969	−0.20	0.426	0.025	0.846	0.042
476)	1.596	1.969	−0.10	0.526	0.028	1.044	0.047
477)	1.596	1.969	0.00	0.552	0.031	1.035	0.049
478)	1.596	1.969	0.10	0.758	0.034	1.212	0.051
479)	1.596	1.969	0.20	0.912	0.037	1.260	0.051
480)	1.596	1.969	0.30	1.085	0.042	1.310	0.053
481)	1.596	1.969	0.40	1.294	0.047	1.212	0.045
482)	1.596	1.969	0.50	1.404	0.050	1.220	0.050
483)	1.596	1.969	0.60	1.511	0.052	1.302	0.049
484)	1.596	1.969	0.70	1.683	0.062	1.309	0.060
485)	1.596	1.969	0.80	1.915	0.078	1.260	0.067
486)	1.596	1.969	0.90	1.935	0.111	1.076	0.083
487)	1.621	1.981	−0.80	0.574	0.061	0.230	0.054
488)	1.621	1.981	−0.70	0.617	0.045	0.219	0.031
489)	1.621	1.981	−0.60	0.444	0.036	0.188	0.025
490)	1.621	1.981	−0.50	0.381	0.029	0.291	0.027
491)	1.621	1.981	−0.40	0.373	0.026	0.433	0.030
492)	1.621	1.981	−0.30	0.352	0.023	0.601	0.036
493)	1.621	1.981	−0.20	0.367	0.022	0.789	0.039
494)	1.621	1.981	−0.10	0.455	0.027	0.924	0.045
495)	1.621	1.981	0.00	0.568	0.031	0.971	0.048
496)	1.621	1.981	0.10	0.761	0.035	1.130	0.047
497)	1.621	1.981	0.20	0.950	0.040	1.263	0.051
498)	1.621	1.981	0.30	1.084	0.042	1.368	0.053
499)	1.621	1.981	0.40	1.353	0.049	1.324	0.049
500)	1.621	1.981	0.50	1.413	0.053	1.237	0.053

TABLE I. (*Continued.*)

Index	E_γ (GeV)	W (GeV)	$\cos\theta_K^{\text{c.m.}}$	$\sigma(\Lambda)$ (μb)	$\delta\sigma(\Lambda)$ (μb)	$\sigma(\Sigma^0)$ (μb)	$\delta\sigma(\Sigma^0)$ (μb)
501)	1.621	1.981	0.60	1.532	0.053	1.169	0.047
502)	1.621	1.981	0.70	1.812	0.071	1.224	0.058
503)	1.621	1.981	0.80	1.761	0.072	1.085	0.057
504)	1.621	1.981	0.90	1.832	0.104	1.090	0.086
505)	1.647	1.993	−0.80	0.697	0.081	0.133	0.046
506)	1.647	1.993	−0.70	0.514	0.048	0.189	0.036
507)	1.647	1.993	−0.60	0.470	0.041	0.193	0.031
508)	1.647	1.993	−0.50	0.368	0.032	0.204	0.028
509)	1.647	1.993	−0.40	0.280	0.026	0.401	0.035
510)	1.647	1.993	−0.30	0.293	0.026	0.510	0.036
511)	1.647	1.993	−0.20	0.334	0.025	0.756	0.044
512)	1.647	1.993	−0.10	0.425	0.028	1.011	0.050
513)	1.647	1.993	0.00	0.470	0.035	1.013	0.057
514)	1.647	1.993	0.10	0.650	0.036	0.995	0.048
515)	1.647	1.993	0.20	0.926	0.044	1.038	0.050
516)	1.647	1.993	0.30	1.063	0.047	1.233	0.055
517)	1.647	1.993	0.40	1.231	0.053	1.188	0.056
518)	1.647	1.993	0.50	1.417	0.058	1.148	0.054
519)	1.647	1.993	0.60	1.494	0.058	1.274	0.058
520)	1.647	1.993	0.70	1.704	0.072	1.218	0.065
521)	1.647	1.993	0.80	1.737	0.075	1.309	0.073
522)	1.647	1.993	0.90	1.905	0.116	1.211	0.105
523)	1.672	2.005	−0.80	0.487	0.051	0.241	0.048
524)	1.672	2.005	−0.70	0.530	0.040	0.157	0.024
525)	1.672	2.005	−0.60	0.400	0.032	0.178	0.021
526)	1.672	2.005	−0.50	0.313	0.025	0.202	0.021
527)	1.672	2.005	−0.40	0.309	0.024	0.397	0.030
528)	1.672	2.005	−0.30	0.266	0.019	0.504	0.031
529)	1.672	2.005	−0.20	0.327	0.022	0.655	0.034
530)	1.672	2.005	−0.10	0.402	0.023	0.806	0.039
531)	1.672	2.005	0.00	0.573	0.030	0.941	0.046
532)	1.672	2.005	0.10	0.652	0.031	0.987	0.043
533)	1.672	2.005	0.20	0.826	0.035	1.146	0.046
534)	1.672	2.005	0.30	1.047	0.040	1.056	0.044
535)	1.672	2.005	0.40	1.213	0.046	1.182	0.046
536)	1.672	2.005	0.50	1.336	0.048	1.252	0.050
537)	1.672	2.005	0.60	1.451	0.053	1.169	0.048
538)	1.672	2.005	0.70	1.509	0.059	1.304	0.061
539)	1.672	2.005	0.80	1.644	0.068	1.302	0.067
540)	1.672	2.005	0.90	1.871	0.108	1.162	0.083
541)	1.698	2.016	−0.80	0.573	0.041	0.148	0.020
542)	1.698	2.016	−0.70	0.413	0.035	0.130	0.024
543)	1.698	2.016	−0.60	0.373	0.033	0.193	0.029
544)	1.698	2.016	−0.50	0.236	0.022	0.189	0.022
545)	1.698	2.016	−0.40	0.252	0.022	0.330	0.027
546)	1.698	2.016	−0.30	0.213	0.018	0.439	0.030
547)	1.698	2.016	−0.20	0.250	0.019	0.628	0.036
548)	1.698	2.016	−0.10	0.351	0.023	0.790	0.040
549)	1.698	2.016	0.00	0.456	0.028	0.872	0.043
550)	1.698	2.016	0.10	0.612	0.030	0.981	0.042
551)	1.698	2.016	0.20	0.792	0.036	1.063	0.046
552)	1.698	2.016	0.30	0.955	0.039	1.075	0.044
553)	1.698	2.016	0.40	1.211	0.049	1.120	0.050
554)	1.698	2.016	0.50	1.314	0.048	1.214	0.050
555)	1.698	2.016	0.60	1.439	0.054	1.187	0.050
556)	1.698	2.016	0.70	1.583	0.064	1.364	0.062

TABLE I. (*Continued.*)

Index	E_γ (GeV)	W (GeV)	$\cos\theta_K^{\text{c.m.}}$	$\sigma(\Lambda)$ (μb)	$\delta\sigma(\Lambda)$ (μb)	$\sigma(\Sigma^0)$ (μb)	$\delta\sigma(\Sigma^0)$ (μb)
557)	1.698	2.016	0.80	1.738	0.071	1.229	0.063
558)	1.698	2.016	0.90	1.818	0.103	1.135	0.083
559)	1.723	2.028	−0.80	0.542	0.053	0.196	0.037
560)	1.723	2.028	−0.70	0.483	0.043	0.201	0.024
561)	1.723	2.028	−0.60	0.315	0.027	0.150	0.020
562)	1.723	2.028	−0.50	0.210	0.022	0.210	0.023
563)	1.723	2.028	−0.40	0.233	0.021	0.345	0.026
564)	1.723	2.028	−0.30	0.179	0.016	0.317	0.024
565)	1.723	2.028	−0.20	0.258	0.019	0.571	0.032
566)	1.723	2.028	−0.10	0.318	0.021	0.642	0.035
567)	1.723	2.028	0.00	0.437	0.027	0.801	0.040
568)	1.723	2.028	0.10	0.566	0.028	0.824	0.036
569)	1.723	2.028	0.20	0.760	0.034	0.996	0.044
570)	1.723	2.028	0.30	0.993	0.040	1.155	0.047
571)	1.723	2.028	0.40	1.042	0.040	1.108	0.044
572)	1.723	2.028	0.50	1.303	0.048	1.180	0.048
573)	1.723	2.028	0.60	1.480	0.054	1.233	0.052
574)	1.723	2.028	0.70	1.674	0.067	1.421	0.065
575)	1.723	2.028	0.80	1.807	0.073	1.384	0.069
576)	1.723	2.028	0.90	1.617	0.097	1.115	0.085
577)	1.748	2.040	−0.80	0.529	0.055	0.300	0.052
578)	1.748	2.040	−0.70	0.477	0.038	0.208	0.029
579)	1.748	2.040	−0.60	0.314	0.029	0.130	0.020
580)	1.748	2.040	−0.50	0.239	0.023	0.193	0.024
581)	1.748	2.040	−0.40	0.166	0.018	0.251	0.023
582)	1.748	2.040	−0.30	0.167	0.017	0.383	0.027
583)	1.748	2.040	−0.20	0.243	0.019	0.549	0.031
584)	1.748	2.040	−0.10	0.296	0.022	0.738	0.039
585)	1.748	2.040	0.00	0.377	0.026	0.776	0.041
586)	1.748	2.040	0.10	0.572	0.029	0.834	0.037
587)	1.748	2.040	0.20	0.745	0.033	0.923	0.041
588)	1.748	2.040	0.30	1.005	0.041	1.061	0.045
589)	1.748	2.040	0.40	1.116	0.047	1.181	0.051
590)	1.748	2.040	0.50	1.295	0.047	1.192	0.048
591)	1.748	2.040	0.60	1.497	0.056	1.223	0.050
592)	1.748	2.040	0.70	1.610	0.065	1.424	0.066
593)	1.748	2.040	0.80	1.693	0.071	1.394	0.069
594)	1.748	2.040	0.90	1.917	0.108	1.289	0.098
595)	1.774	2.052	−0.80	0.455	0.046	0.236	0.044
596)	1.774	2.052	−0.70	0.358	0.030	0.224	0.028
597)	1.774	2.052	−0.60	0.262	0.026	0.133	0.019
598)	1.774	2.052	−0.50	0.155	0.022	0.166	0.019
599)	1.774	2.052	−0.40	0.194	0.020	0.253	0.022
600)	1.774	2.052	−0.30	0.170	0.015	0.346	0.025
601)	1.774	2.052	−0.20	0.166	0.015	0.494	0.030
602)	1.774	2.052	−0.10	0.296	0.022	0.657	0.036
603)	1.774	2.052	0.00	0.391	0.026	0.671	0.037
604)	1.774	2.052	0.10	0.543	0.028	0.830	0.040
605)	1.774	2.052	0.20	0.737	0.034	0.905	0.041
606)	1.774	2.052	0.30	0.922	0.039	1.020	0.044
607)	1.774	2.052	0.40	1.188	0.049	1.026	0.046
608)	1.774	2.052	0.50	1.310	0.051	1.193	0.050
609)	1.774	2.052	0.60	1.507	0.056	1.281	0.052
610)	1.774	2.052	0.70	1.685	0.068	1.329	0.062
611)	1.774	2.052	0.80	1.720	0.070	1.370	0.069
612)	1.774	2.052	0.90	1.921	0.106	1.257	0.092

TABLE I. (*Continued.*)

Index	E_γ (GeV)	W (GeV)	$\cos\theta_K^{\text{c.m.}}$	$\sigma(\Lambda)$ (μb)	$\delta\sigma(\Lambda)$ (μb)	$\sigma(\Sigma^0)$ (μb)	$\delta\sigma(\Sigma^0)$ (μb)
613)	1.799	2.063	−0.80	0.351	0.045	0.208	0.043
614)	1.799	2.063	−0.70	0.284	0.035	0.222	0.030
615)	1.799	2.063	−0.60	0.217	0.025	0.139	0.026
616)	1.799	2.063	−0.50	0.154	0.021	0.158	0.023
617)	1.799	2.063	−0.40	0.100	0.013	0.243	0.026
618)	1.799	2.063	−0.30	0.187	0.017	0.299	0.025
619)	1.799	2.063	−0.20	0.184	0.017	0.527	0.032
620)	1.799	2.063	−0.10	0.277	0.021	0.574	0.034
621)	1.799	2.063	0.00	0.381	0.027	0.708	0.039
622)	1.799	2.063	0.10	0.549	0.029	0.782	0.039
623)	1.799	2.063	0.20	0.679	0.035	0.909	0.043
624)	1.799	2.063	0.30	0.824	0.038	0.916	0.043
625)	1.799	2.063	0.40	0.996	0.046	1.031	0.049
626)	1.799	2.063	0.50	1.185	0.048	1.094	0.049
627)	1.799	2.063	0.60	1.424	0.059	1.139	0.055
628)	1.799	2.063	0.70	1.599	0.069	1.360	0.069
629)	1.799	2.063	0.80	1.664	0.074	1.411	0.075
630)	1.799	2.063	0.90	1.919	0.115	1.231	0.098
631)	1.824	2.075	−0.80	0.416	0.048	0.290	0.047
632)	1.824	2.075	−0.70	0.343	0.032	0.258	0.032
633)	1.824	2.075	−0.60	0.223	0.026	0.164	0.023
634)	1.824	2.075	−0.50	0.175	0.019	0.172	0.021
635)	1.824	2.075	−0.40	0.134	0.017	0.238	0.022
636)	1.824	2.075	−0.30	0.131	0.015	0.289	0.024
637)	1.824	2.075	−0.20	0.169	0.017	0.475	0.030
638)	1.824	2.075	−0.10	0.268	0.021	0.512	0.031
639)	1.824	2.075	0.00	0.363	0.026	0.575	0.033
640)	1.824	2.075	0.10	0.507	0.028	0.765	0.036
641)	1.824	2.075	0.20	0.643	0.033	0.818	0.040
642)	1.824	2.075	0.30	0.905	0.040	0.946	0.043
643)	1.824	2.075	0.40	1.005	0.042	1.022	0.046
644)	1.824	2.075	0.50	1.205	0.047	1.168	0.050
645)	1.824	2.075	0.60	1.422	0.059	1.126	0.052
646)	1.824	2.075	0.70	1.643	0.064	1.216	0.055
647)	1.824	2.075	0.80	1.640	0.069	1.441	0.070
648)	1.824	2.075	0.90	1.868	0.109	1.326	0.099
649)	1.849	2.086	−0.80	0.388	0.046	0.214	0.042
650)	1.849	2.086	−0.70	0.284	0.029	0.284	0.032
651)	1.849	2.086	−0.60	0.254	0.024	0.216	0.023
652)	1.849	2.086	−0.50	0.167	0.018	0.167	0.021
653)	1.849	2.086	−0.40	0.146	0.016	0.219	0.020
654)	1.849	2.086	−0.30	0.168	0.015	0.301	0.023
655)	1.849	2.086	−0.20	0.182	0.017	0.404	0.030
656)	1.849	2.086	−0.10	0.246	0.019	0.435	0.029
657)	1.849	2.086	0.00	0.326	0.023	0.578	0.032
658)	1.849	2.086	0.10	0.491	0.026	0.683	0.034
659)	1.849	2.086	0.20	0.602	0.031	0.779	0.038
660)	1.849	2.086	0.30	0.732	0.034	0.871	0.040
661)	1.849	2.086	0.40	0.930	0.042	1.033	0.047
662)	1.849	2.086	0.50	1.220	0.045	1.050	0.044
663)	1.849	2.086	0.60	1.391	0.058	1.200	0.055
664)	1.849	2.086	0.70	1.690	0.070	1.215	0.061
665)	1.849	2.086	0.80	1.670	0.066	1.320	0.062
666)	1.849	2.086	0.90	1.925	0.119	1.077	0.088
667)	1.875	2.097	−0.80	0.353	0.052	0.365	0.066
668)	1.875	2.097	−0.70	0.302	0.059	0.261	0.040

TABLE I. (*Continued.*)

Index	E_γ (GeV)	W (GeV)	$\cos\theta_K^{\text{c.m.}}$	$\sigma(\Lambda)$ (μb)	$\delta\sigma(\Lambda)$ (μb)	$\sigma(\Sigma^0)$ (μb)	$\delta\sigma(\Sigma^0)$ (μb)
669)	1.875	2.097	−0.60	0.238	0.029	0.169	0.025
670)	1.875	2.097	−0.50	0.146	0.021	0.189	0.026
671)	1.875	2.097	−0.40	0.183	0.023	0.213	0.026
672)	1.875	2.097	−0.30	0.130	0.018	0.276	0.028
673)	1.875	2.097	−0.20	0.138	0.018	0.323	0.030
674)	1.875	2.097	−0.10	0.224	0.025	0.431	0.041
675)	1.875	2.097	0.00	0.341	0.032	0.593	0.044
676)	1.875	2.097	0.10	0.436	0.031	0.651	0.041
677)	1.875	2.097	0.20	0.531	0.035	0.762	0.048
678)	1.875	2.097	0.30	0.725	0.044	0.856	0.053
679)	1.875	2.097	0.40	0.958	0.056	1.038	0.063
680)	1.875	2.097	0.50	1.151	0.059	1.163	0.064
681)	1.875	2.097	0.60	1.456	0.078	1.250	0.076
682)	1.875	2.097	0.70	1.675	0.090	1.480	0.090
683)	1.875	2.097	0.80	1.770	0.095	1.319	0.087
684)	1.875	2.097	0.90	1.766	0.131	1.171	0.127
685)	1.900	2.108	−0.80	0.364	0.045	0.310	0.046
686)	1.900	2.108	−0.70	0.287	0.027	0.254	0.029
687)	1.900	2.108	−0.60	0.190	0.024	0.129	0.020
688)	1.900	2.108	−0.50	0.167	0.020	0.121	0.018
689)	1.900	2.108	−0.40	0.169	0.019	0.170	0.020
690)	1.900	2.108	−0.30	0.148	0.015	0.248	0.021
691)	1.900	2.108	−0.20	0.170	0.016	0.347	0.024
692)	1.900	2.108	−0.10	0.226	0.019	0.417	0.029
693)	1.900	2.108	0.00	0.260	0.022	0.519	0.032
694)	1.900	2.108	0.10	0.450	0.026	0.601	0.032
695)	1.900	2.108	0.20	0.565	0.031	0.808	0.041
696)	1.900	2.108	0.30	0.718	0.035	0.812	0.040
697)	1.900	2.108	0.40	0.866	0.041	0.992	0.048
698)	1.900	2.108	0.50	1.095	0.047	1.035	0.046
699)	1.900	2.108	0.60	1.325	0.059	1.264	0.061
700)	1.900	2.108	0.70	1.590	0.070	1.220	0.064
701)	1.900	2.108	0.80	1.739	0.074	1.209	0.061
702)	1.900	2.108	0.90	1.777	0.108	0.988	0.089
703)	1.925	2.120	−0.80	0.351	0.042	0.368	0.054
704)	1.925	2.120	−0.70	0.297	0.030	0.277	0.032
705)	1.925	2.120	−0.60	0.252	0.023	0.167	0.020
706)	1.925	2.120	−0.50	0.157	0.019	0.114	0.019
707)	1.925	2.120	−0.40	0.138	0.017	0.179	0.019
708)	1.925	2.120	−0.30	0.147	0.015	0.252	0.023
709)	1.925	2.120	−0.20	0.168	0.016	0.312	0.023
710)	1.925	2.120	−0.10	0.228	0.019	0.464	0.030
711)	1.925	2.120	0.00	0.266	0.023	0.500	0.031
712)	1.925	2.120	0.10	0.415	0.024	0.623	0.032
713)	1.925	2.120	0.20	0.570	0.031	0.708	0.036
714)	1.925	2.120	0.30	0.736	0.036	0.807	0.040
715)	1.925	2.120	0.40	0.895	0.041	0.884	0.042
716)	1.925	2.120	0.50	1.075	0.044	1.002	0.045
717)	1.925	2.120	0.60	1.238	0.058	1.200	0.061
718)	1.925	2.120	0.70	1.615	0.069	1.171	0.060
719)	1.925	2.120	0.80	1.747	0.070	1.272	0.062
720)	1.925	2.120	0.90	1.628	0.098	1.093	0.086
721)	1.950	2.131	−0.80	0.357	0.040	0.318	0.044
722)	1.950	2.131	−0.70	0.296	0.034	0.200	0.027
723)	1.950	2.131	−0.60	0.303	0.025	0.187	0.022
724)	1.950	2.131	−0.50	0.166	0.017	0.138	0.017

TABLE I. (*Continued.*)

Index	E_γ (GeV)	W (GeV)	$\cos\theta_K^{\text{c.m.}}$	$\sigma(\Lambda)$ (μb)	$\delta\sigma(\Lambda)$ (μb)	$\sigma(\Sigma^0)$ (μb)	$\delta\sigma(\Sigma^0)$ (μb)
725)	1.950	2.131	−0.40	0.151	0.018	0.158	0.018
726)	1.950	2.131	−0.30	0.146	0.015	0.241	0.020
727)	1.950	2.131	−0.20	0.168	0.017	0.258	0.022
728)	1.950	2.131	−0.10	0.223	0.020	0.418	0.030
729)	1.950	2.131	0.00	0.302	0.023	0.520	0.030
730)	1.950	2.131	0.10	0.394	0.023	0.589	0.030
731)	1.950	2.131	0.20	0.511	0.027	0.645	0.032
732)	1.950	2.131	0.30	0.627	0.031	0.759	0.037
733)	1.950	2.131	0.40	0.781	0.037	0.857	0.040
734)	1.950	2.131	0.50	1.105	0.044	1.015	0.043
735)	1.950	2.131	0.60	1.302	0.055	1.149	0.054
736)	1.950	2.131	0.70	1.510	0.066	1.286	0.062
737)	1.950	2.131	0.80	1.674	0.069	1.329	0.069
738)	1.950	2.131	0.90	1.633	0.098	0.931	0.085
739)	1.975	2.142	−0.80	0.348	0.040	0.372	0.049
740)	1.975	2.142	−0.70	0.290	0.027	0.233	0.026
741)	1.975	2.142	−0.60	0.252	0.023	0.206	0.021
742)	1.975	2.142	−0.50	0.166	0.019	0.178	0.021
743)	1.975	2.142	−0.40	0.169	0.018	0.168	0.019
744)	1.975	2.142	−0.30	0.179	0.015	0.201	0.015
745)	1.975	2.142	−0.20	0.171	0.017	0.300	0.023
746)	1.975	2.142	−0.10	0.185	0.017	0.319	0.025
747)	1.975	2.142	0.00	0.225	0.020	0.431	0.028
748)	1.975	2.142	0.10	0.297	0.020	0.525	0.028
749)	1.975	2.142	0.20	0.472	0.026	0.645	0.033
750)	1.975	2.142	0.30	0.650	0.032	0.764	0.037
751)	1.975	2.142	0.40	0.793	0.036	0.764	0.037
752)	1.975	2.142	0.50	1.014	0.043	0.977	0.043
753)	1.975	2.142	0.60	1.163	0.055	1.075	0.057
754)	1.975	2.142	0.70	1.528	0.066	1.287	0.064
755)	1.975	2.142	0.80	1.568	0.067	1.092	0.062
756)	1.975	2.142	0.90	1.805	0.101	0.839	0.072
757)	2.001	2.153	−0.80	0.323	0.044	0.292	0.045
758)	2.001	2.153	−0.70	0.325	0.033	0.274	0.031
759)	2.001	2.153	−0.60	0.237	0.023	0.241	0.024
760)	2.001	2.153	−0.50	0.142	0.017	0.112	0.016
761)	2.001	2.153	−0.40	0.155	0.017	0.142	0.017
762)	2.001	2.153	−0.30	0.139	0.014	0.196	0.017
763)	2.001	2.153	−0.20	0.153	0.015	0.283	0.021
764)	2.001	2.153	−0.10	0.194	0.018	0.341	0.025
765)	2.001	2.153	0.00	0.242	0.020	0.389	0.025
766)	2.001	2.153	0.10	0.322	0.021	0.556	0.030
767)	2.001	2.153	0.20	0.433	0.025	0.601	0.031
768)	2.001	2.153	0.30	0.542	0.028	0.719	0.035
769)	2.001	2.153	0.40	0.745	0.035	0.766	0.038
770)	2.001	2.153	0.50	1.021	0.045	0.845	0.041
771)	2.001	2.153	0.60	1.207	0.054	1.104	0.054
772)	2.001	2.153	0.70	1.462	0.066	1.211	0.063
773)	2.001	2.153	0.80	1.570	0.070	1.059	0.061
774)	2.001	2.153	0.90	1.789	0.102	0.932	0.078
775)	2.026	2.164	−0.80	0.287	0.036	0.428	0.053
776)	2.026	2.164	−0.70	0.276	0.028	0.367	0.036
777)	2.026	2.164	−0.60	0.287	0.024	0.198	0.023
778)	2.026	2.164	−0.50	0.140	0.018	0.133	0.018
779)	2.026	2.164	−0.40	0.165	0.018	0.164	0.018
780)	2.026	2.164	−0.30	0.112	0.015	0.176	0.018

TABLE I. (*Continued.*)

Index	E_γ (GeV)	W (GeV)	$\cos\theta_K^{\text{c.m.}}$	$\sigma(\Lambda)$ (μb)	$\delta\sigma(\Lambda)$ (μb)	$\sigma(\Sigma^0)$ (μb)	$\delta\sigma(\Sigma^0)$ (μb)
781)	2.026	2.164	−0.20	0.162	0.016	0.260	0.022
782)	2.026	2.164	−0.10	0.185	0.017	0.340	0.027
783)	2.026	2.164	0.00	0.190	0.018	0.417	0.026
784)	2.026	2.164	0.10	0.264	0.020	0.425	0.025
785)	2.026	2.164	0.20	0.436	0.025	0.574	0.030
786)	2.026	2.164	0.30	0.571	0.029	0.629	0.032
787)	2.026	2.164	0.40	0.755	0.035	0.771	0.038
788)	2.026	2.164	0.50	0.881	0.041	0.843	0.041
789)	2.026	2.164	0.60	1.249	0.054	1.159	0.055
790)	2.026	2.164	0.70	1.592	0.071	1.224	0.062
791)	2.026	2.164	0.80	1.654	0.073	1.065	0.064
792)	2.026	2.164	0.90	1.761	0.105	1.025	0.096
793)	2.051	2.175	−0.80	0.239	0.029	0.400	0.057
794)	2.051	2.175	−0.70	0.249	0.028	0.307	0.036
795)	2.051	2.175	−0.60	0.222	0.024	0.225	0.025
796)	2.051	2.175	−0.50	0.174	0.022	0.136	0.019
797)	2.051	2.175	−0.40	0.139	0.016	0.140	0.017
798)	2.051	2.175	−0.30	0.116	0.014	0.141	0.017
799)	2.051	2.175	−0.20	0.136	0.016	0.232	0.021
800)	2.051	2.175	−0.10	0.141	0.016	0.283	0.023
801)	2.051	2.175	0.00	0.189	0.019	0.338	0.025
802)	2.051	2.175	0.10	0.321	0.023	0.461	0.028
803)	2.051	2.175	0.20	0.358	0.023	0.536	0.029
804)	2.051	2.175	0.30	0.473	0.028	0.593	0.033
805)	2.051	2.175	0.40	0.687	0.034	0.864	0.041
806)	2.051	2.175	0.50	0.893	0.040	0.848	0.042
807)	2.051	2.175	0.60	1.138	0.052	1.062	0.054
808)	2.051	2.175	0.70	1.459	0.068	1.228	0.067
809)	2.051	2.175	0.80	1.600	0.073	1.077	0.062
810)	2.051	2.175	0.90	1.665	0.109	0.937	0.089
811)	2.076	2.185	−0.80	0.174	0.031	0.345	0.051
812)	2.076	2.185	−0.70	0.218	0.025	0.304	0.033
813)	2.076	2.185	−0.60	0.248	0.025	0.186	0.021
814)	2.076	2.185	−0.50	0.128	0.018	0.118	0.019
815)	2.076	2.185	−0.40	0.117	0.017	0.100	0.016
816)	2.076	2.185	−0.30	0.117	0.015	0.145	0.017
817)	2.076	2.185	−0.20	0.116	0.014	0.209	0.022
818)	2.076	2.185	−0.10	0.130	0.016	0.229	0.024
819)	2.076	2.185	0.00	0.174	0.018	0.304	0.023
820)	2.076	2.185	0.10	0.274	0.021	0.440	0.028
821)	2.076	2.185	0.20	0.368	0.025	0.517	0.031
822)	2.076	2.185	0.30	0.499	0.030	0.610	0.035
823)	2.076	2.185	0.40	0.678	0.036	0.672	0.036
824)	2.076	2.185	0.50	0.834	0.035	0.875	0.040
825)	2.076	2.185	0.60	1.022	0.049	1.032	0.055
826)	2.076	2.185	0.70	1.354	0.067	1.235	0.068
827)	2.076	2.185	0.80	1.636	0.070	1.066	0.060
828)	2.076	2.185	0.90	1.859	0.113	0.938	0.091
829)	2.101	2.196	−0.80	0.322	0.042	0.364	0.052
830)	2.101	2.196	−0.70	0.214	0.026	0.333	0.033
831)	2.101	2.196	−0.60	0.168	0.022	0.205	0.025
832)	2.101	2.196	−0.50	0.163	0.020	0.152	0.020
833)	2.101	2.196	−0.40	0.160	0.017	0.137	0.016
834)	2.101	2.196	−0.30	0.102	0.013	0.174	0.017
835)	2.101	2.196	−0.20	0.134	0.014	0.167	0.019
836)	2.101	2.196	−0.10	0.118	0.015	0.230	0.020

TABLE I. (*Continued.*)

Index	E_γ (GeV)	W (GeV)	$\cos\theta_K^{\text{c.m.}}$	$\sigma(\Lambda)$ (μb)	$\delta\sigma(\Lambda)$ (μb)	$\sigma(\Sigma^0)$ (μb)	$\delta\sigma(\Sigma^0)$ (μb)
837)	2.101	2.196	0.00	0.178	0.017	0.292	0.023
838)	2.101	2.196	0.10	0.239	0.020	0.454	0.028
839)	2.101	2.196	0.20	0.322	0.022	0.496	0.029
840)	2.101	2.196	0.30	0.463	0.027	0.591	0.033
841)	2.101	2.196	0.40	0.585	0.032	0.653	0.035
842)	2.101	2.196	0.50	0.823	0.037	0.897	0.042
843)	2.101	2.196	0.60	1.039	0.049	1.022	0.054
844)	2.101	2.196	0.70	1.362	0.065	1.152	0.063
845)	2.101	2.196	0.80	1.581	0.069	1.068	0.059
846)	2.101	2.196	0.90	1.693	0.101	0.841	0.080
847)	2.126	2.207	−0.80	0.191	0.030	0.272	0.046
848)	2.126	2.207	−0.70	0.204	0.023	0.323	0.033
849)	2.126	2.207	−0.60	0.171	0.019	0.227	0.023
850)	2.126	2.207	−0.50	0.154	0.022	0.199	0.024
851)	2.126	2.207	−0.40	0.097	0.015	0.136	0.018
852)	2.126	2.207	−0.30	0.132	0.015	0.136	0.016
853)	2.126	2.207	−0.20	0.116	0.014	0.213	0.020
854)	2.126	2.207	−0.10	0.115	0.017	0.227	0.023
855)	2.126	2.207	0.00	0.180	0.018	0.255	0.022
856)	2.126	2.207	0.10	0.225	0.020	0.376	0.026
857)	2.126	2.207	0.20	0.364	0.025	0.483	0.029
858)	2.126	2.207	0.30	0.369	0.025	0.548	0.034
859)	2.126	2.207	0.40	0.611	0.032	0.690	0.037
860)	2.126	2.207	0.50	0.839	0.040	0.823	0.041
861)	2.126	2.207	0.60	1.053	0.051	1.012	0.053
862)	2.126	2.207	0.70	1.250	0.063	1.090	0.064
863)	2.126	2.207	0.80	1.710	0.076	1.115	0.065
864)	2.126	2.207	0.90	1.754	0.112	1.272	0.111
865)	2.151	2.217	−0.80	0.230	0.029	0.380	0.045
866)	2.151	2.217	−0.70	0.225	0.023	0.302	0.031
867)	2.151	2.217	−0.60	0.129	0.016	0.214	0.022
868)	2.151	2.217	−0.50	0.120	0.014	0.149	0.019
869)	2.151	2.217	−0.40	0.121	0.015	0.123	0.016
870)	2.151	2.217	−0.30	0.117	0.013	0.119	0.014
871)	2.151	2.217	−0.20	0.114	0.014	0.169	0.018
872)	2.151	2.217	−0.10	0.112	0.015	0.226	0.021
873)	2.151	2.217	0.00	0.138	0.016	0.259	0.020
874)	2.151	2.217	0.10	0.166	0.017	0.292	0.022
875)	2.151	2.217	0.20	0.306	0.022	0.401	0.026
876)	2.151	2.217	0.30	0.384	0.024	0.501	0.029
877)	2.151	2.217	0.40	0.533	0.029	0.563	0.030
878)	2.151	2.217	0.50	0.778	0.036	0.770	0.038
879)	2.151	2.217	0.60	0.958	0.047	0.965	0.049
880)	2.151	2.217	0.70	1.421	0.065	1.167	0.063
881)	2.151	2.217	0.80	1.589	0.071	1.000	0.060
882)	2.151	2.217	0.90	1.664	0.104	0.969	0.098
883)	2.177	2.228	−0.80	0.273	0.035	0.419	0.051
884)	2.177	2.228	−0.70	0.221	0.029	0.337	0.041
885)	2.177	2.228	−0.60	0.183	0.024	0.240	0.029
886)	2.177	2.228	−0.50	0.132	0.024	0.232	0.030
887)	2.177	2.228	−0.40	0.114	0.018	0.168	0.020
888)	2.177	2.228	−0.30	0.118	0.016	0.162	0.020
889)	2.177	2.228	−0.20	0.118	0.015	0.231	0.024
890)	2.177	2.228	−0.10	0.143	0.019	0.214	0.026
891)	2.177	2.228	0.00	0.180	0.020	0.305	0.026
892)	2.177	2.228	0.10	0.172	0.021	0.318	0.028

TABLE I. (*Continued.*)

Index	E_γ (GeV)	W (GeV)	$\cos\theta_K^{\text{c.m.}}$	$\sigma(\Lambda)$ (μb)	$\delta\sigma(\Lambda)$ (μb)	$\sigma(\Sigma^0)$ (μb)	$\delta\sigma(\Sigma^0)$ (μb)
893)	2.177	2.228	0.20	0.295	0.025	0.412	0.031
894)	2.177	2.228	0.30	0.380	0.029	0.515	0.037
895)	2.177	2.228	0.40	0.494	0.033	0.610	0.037
896)	2.177	2.228	0.50	0.741	0.042	0.789	0.044
897)	2.177	2.228	0.60	1.003	0.056	1.069	0.063
898)	2.177	2.228	0.70	1.298	0.071	1.066	0.070
899)	2.177	2.228	0.80	1.491	0.078	1.085	0.070
900)	2.177	2.228	0.90	1.767	0.128	1.259	0.130
901)	2.202	2.239	−0.80	0.246	0.034	0.388	0.052
902)	2.202	2.239	−0.70	0.145	0.026	0.317	0.038
903)	2.202	2.239	−0.60	0.129	0.019	0.246	0.028
904)	2.202	2.239	−0.50	0.142	0.026	0.163	0.025
905)	2.202	2.239	−0.40	0.101	0.016	0.129	0.020
906)	2.202	2.239	−0.30	0.093	0.014	0.148	0.018
907)	2.202	2.239	−0.20	0.105	0.016	0.171	0.020
908)	2.202	2.239	−0.10	0.133	0.016	0.203	0.017
909)	2.202	2.239	0.00	0.161	0.017	0.261	0.022
910)	2.202	2.239	0.10	0.152	0.019	0.316	0.026
911)	2.202	2.239	0.20	0.273	0.024	0.400	0.029
912)	2.202	2.239	0.30	0.385	0.029	0.461	0.031
913)	2.202	2.239	0.40	0.486	0.029	0.617	0.036
914)	2.202	2.239	0.50	0.659	0.040	0.735	0.044
915)	2.202	2.239	0.60	0.968	0.051	1.059	0.062
916)	2.202	2.239	0.70	1.279	0.067	0.982	0.061
917)	2.202	2.239	0.80	1.680	0.083	1.021	0.067
918)	2.202	2.239	0.90	1.617	0.110	0.880	0.098
919)	2.227	2.249	−0.80	0.180	0.033	0.321	0.049
920)	2.227	2.249	−0.70	0.185	0.014	0.317	0.034
921)	2.227	2.249	−0.60	0.185	0.026	0.198	0.025
922)	2.227	2.249	−0.50	0.152	0.021	0.159	0.021
923)	2.227	2.249	−0.40	0.102	0.014	0.121	0.016
924)	2.227	2.249	−0.30	0.111	0.014	0.121	0.015
925)	2.227	2.249	−0.20	0.076	0.013	0.111	0.014
926)	2.227	2.249	−0.10	0.106	0.014	0.177	0.020
927)	2.227	2.249	0.00	0.149	0.016	0.250	0.021
928)	2.227	2.249	0.10	0.165	0.018	0.260	0.022
929)	2.227	2.249	0.20	0.196	0.020	0.350	0.025
930)	2.227	2.249	0.30	0.369	0.026	0.441	0.029
931)	2.227	2.249	0.40	0.464	0.028	0.580	0.033
932)	2.227	2.249	0.50	0.683	0.036	0.761	0.039
933)	2.227	2.249	0.60	0.830	0.046	0.878	0.050
934)	2.227	2.249	0.70	1.347	0.067	1.079	0.066
935)	2.227	2.249	0.80	1.508	0.072	0.943	0.061
936)	2.227	2.249	0.90	1.645	0.107	1.178	0.109
937)	2.253	2.260	−0.80	0.131	0.026	0.307	0.051
938)	2.253	2.260	−0.70	0.170	0.024	0.346	0.036
939)	2.253	2.260	−0.60	0.183	0.023	0.223	0.025
940)	2.253	2.260	−0.50	0.091	0.017	0.165	0.023
941)	2.253	2.260	−0.40	0.094	0.013	0.133	0.016
942)	2.253	2.260	−0.30	0.100	0.013	0.131	0.016
943)	2.253	2.260	−0.20	0.091	0.013	0.134	0.016
944)	2.253	2.260	−0.10	0.113	0.016	0.208	0.024
945)	2.253	2.260	0.00	0.131	0.015	0.252	0.021
946)	2.253	2.260	0.10	0.175	0.019	0.222	0.021
947)	2.253	2.260	0.20	0.207	0.020	0.345	0.027
948)	2.253	2.260	0.30	0.320	0.025	0.413	0.030

TABLE I. (*Continued.*)

Index	E_γ (GeV)	W (GeV)	$\cos\theta_K^{\text{c.m.}}$	$\sigma(\Lambda)$ (μb)	$\delta\sigma(\Lambda)$ (μb)	$\sigma(\Sigma^0)$ (μb)	$\delta\sigma(\Sigma^0)$ (μb)
949)	2.253	2.260	0.40	0.398	0.027	0.597	0.033
950)	2.253	2.260	0.50	0.559	0.033	0.671	0.039
951)	2.253	2.260	0.60	0.858	0.051	0.888	0.054
952)	2.253	2.260	0.70	1.272	0.060	0.957	0.057
953)	2.253	2.260	0.80	1.633	0.075	1.131	0.068
954)	2.253	2.260	0.90	1.620	0.115	0.844	0.094
955)	2.278	2.270	−0.80	0.233	0.033	0.360	0.048
956)	2.278	2.270	−0.70	0.160	0.024	0.278	0.031
957)	2.278	2.270	−0.60	0.134	0.020	0.245	0.027
958)	2.278	2.270	−0.50	0.136	0.018	0.234	0.025
959)	2.278	2.270	−0.40	0.100	0.015	0.093	0.014
960)	2.278	2.270	−0.30	0.111	0.014	0.117	0.014
961)	2.278	2.270	−0.20	0.076	0.012	0.104	0.017
962)	2.278	2.270	−0.10	0.070	0.012	0.140	0.019
963)	2.278	2.270	0.00	0.144	0.016	0.212	0.019
964)	2.278	2.270	0.10	0.134	0.015	0.230	0.020
965)	2.278	2.270	0.20	0.211	0.021	0.280	0.023
966)	2.278	2.270	0.30	0.321	0.027	0.386	0.032
967)	2.278	2.270	0.40	0.404	0.027	0.524	0.030
968)	2.278	2.270	0.50	0.635	0.036	0.660	0.039
969)	2.278	2.270	0.60	0.860	0.047	0.836	0.049
970)	2.278	2.270	0.70	1.181	0.057	0.988	0.056
971)	2.278	2.270	0.80	1.438	0.071	0.970	0.063
972)	2.278	2.270	0.90	1.734	0.114	0.876	0.087
973)	2.303	2.281	−0.80	0.237	0.033	0.326	0.050
974)	2.303	2.281	−0.70	0.145	0.021	0.313	0.033
975)	2.303	2.281	−0.60	0.123	0.019	0.262	0.028
976)	2.303	2.281	−0.50	0.108	0.020	0.164	0.024
977)	2.303	2.281	−0.40	0.131	0.019	0.093	0.017
978)	2.303	2.281	−0.30	0.061	0.011	0.107	0.016
979)	2.303	2.281	−0.20	0.114	0.014	0.146	0.017
980)	2.303	2.281	−0.10	0.076	0.015	0.126	0.019
981)	2.303	2.281	0.00	0.088	0.014	0.140	0.017
982)	2.303	2.281	0.10	0.131	0.017	0.210	0.020
983)	2.303	2.281	0.20	0.158	0.021	0.256	0.026
984)	2.303	2.281	0.30	0.263	0.024	0.366	0.030
985)	2.303	2.281	0.40	0.409	0.028	0.489	0.031
986)	2.303	2.281	0.50	0.534	0.035	0.669	0.041
987)	2.303	2.281	0.60	0.753	0.049	0.848	0.055
988)	2.303	2.281	0.70	1.185	0.061	1.126	0.064
989)	2.303	2.281	0.80	1.610	0.086	1.040	0.072
990)	2.303	2.281	0.90	1.788	0.121	1.196	0.115
991)	2.328	2.291	−0.80	0.165	0.030	0.393	0.055
992)	2.328	2.291	−0.70	0.144	0.026	0.240	0.037
993)	2.328	2.291	−0.60	0.148	0.027	0.266	0.033
994)	2.328	2.291	−0.50	0.106	0.021	0.137	0.023
995)	2.328	2.291	−0.40	0.131	0.019	0.122	0.019
996)	2.328	2.291	−0.30	0.107	0.015	0.099	0.016
997)	2.328	2.291	−0.20	0.044	0.011	0.094	0.015
998)	2.328	2.291	−0.10	0.073	0.015	0.135	0.020
999)	2.328	2.291	0.00	0.103	0.016	0.183	0.020
1000)	2.328	2.291	0.10	0.124	0.017	0.158	0.020
1001)	2.328	2.291	0.20	0.149	0.020	0.254	0.026
1002)	2.328	2.291	0.30	0.255	0.025	0.331	0.028
1003)	2.328	2.291	0.40	0.403	0.030	0.490	0.035
1004)	2.328	2.291	0.50	0.569	0.040	0.682	0.044

TABLE I. (*Continued.*)

Index	E_γ (GeV)	W (GeV)	$\cos\theta_K^{\text{c.m.}}$	$\sigma(\Lambda)$ (μb)	$\delta\sigma(\Lambda)$ (μb)	$\sigma(\Sigma^0)$ (μb)	$\delta\sigma(\Sigma^0)$ (μb)
1005)	2.328	2.291	0.60	0.892	0.056	0.736	0.054
1006)	2.328	2.291	0.70	1.243	0.070	1.053	0.068
1007)	2.328	2.291	0.80	1.316	0.076	1.016	0.073
1008)	2.328	2.291	0.90	1.600	0.124	0.733	0.091
1009)	2.353	2.301	−0.80	0.146	0.027	0.362	0.053
1010)	2.353	2.301	−0.70	0.101	0.019	0.238	0.034
1011)	2.353	2.301	−0.60	0.109	0.022	0.213	0.028
1012)	2.353	2.301	−0.50	0.114	0.015	0.189	0.022
1013)	2.353	2.301	−0.40	0.102	0.019	0.102	0.021
1014)	2.353	2.301	−0.30	0.099	0.013	0.104	0.015
1015)	2.353	2.301	−0.20	0.092	0.012	0.108	0.017
1016)	2.353	2.301	−0.10	0.110	0.015	0.182	0.020
1017)	2.353	2.301	0.00	0.088	0.014	0.134	0.019
1018)	2.353	2.301	0.10	0.149	0.020	0.181	0.021
1019)	2.353	2.301	0.20	0.178	0.020	0.239	0.024
1020)	2.353	2.301	0.30	0.259	0.027	0.343	0.029
1021)	2.353	2.301	0.40	0.382	0.029	0.459	0.033
1022)	2.353	2.301	0.50	0.580	0.042	0.564	0.042
1023)	2.353	2.301	0.60	0.725	0.050	0.812	0.058
1024)	2.353	2.301	0.70	1.087	0.066	0.987	0.067
1025)	2.353	2.301	0.80	1.672	0.087	1.242	0.079
1026)	2.353	2.301	0.90	1.665	0.141	0.947	0.121
1027)	2.378	2.312	−0.80	0.000	0.000	0.000	0.000
1028)	2.378	2.312	−0.70	0.000	0.000	0.000	0.000
1029)	2.378	2.312	−0.60	0.000	0.000	0.000	0.000
1030)	2.378	2.312	−0.50	0.000	0.000	0.000	0.000
1031)	2.378	2.312	−0.40	0.000	0.000	0.000	0.000
1032)	2.378	2.312	−0.30	0.000	0.000	0.000	0.000
1033)	2.378	2.312	−0.20	0.000	0.000	0.000	0.000
1034)	2.378	2.312	−0.10	0.000	0.000	0.000	0.000
1035)	2.378	2.312	0.00	0.000	0.000	0.000	0.000
1036)	2.378	2.312	0.10	0.000	0.000	0.000	0.000
1037)	2.378	2.312	0.20	0.000	0.000	0.000	0.000
1038)	2.378	2.312	0.30	0.000	0.000	0.000	0.000
1039)	2.378	2.312	0.40	0.000	0.000	0.000	0.000
1040)	2.378	2.312	0.50	0.000	0.000	0.000	0.000
1041)	2.378	2.312	0.60	0.000	0.000	0.000	0.000
1042)	2.378	2.312	0.70	0.000	0.000	0.000	0.000
1043)	2.378	2.312	0.80	0.000	0.000	0.000	0.000
1044)	2.378	2.312	0.90	0.000	0.000	0.000	0.000
1045)	2.405	2.322	−0.80	0.000	0.000	0.000	0.000
1046)	2.405	2.322	−0.70	0.000	0.000	0.000	0.000
1047)	2.405	2.322	−0.60	0.000	0.000	0.000	0.000
1048)	2.405	2.322	−0.50	0.000	0.000	0.000	0.000
1049)	2.405	2.322	−0.40	0.000	0.000	0.000	0.000
1050)	2.405	2.322	−0.30	0.000	0.000	0.000	0.000
1051)	2.405	2.322	−0.20	0.000	0.000	0.000	0.000
1052)	2.405	2.322	−0.10	0.000	0.000	0.000	0.000
1053)	2.405	2.322	0.00	0.000	0.000	0.000	0.000
1054)	2.405	2.322	0.10	0.000	0.000	0.000	0.000
1055)	2.405	2.322	0.20	0.000	0.000	0.000	0.000
1056)	2.405	2.322	0.30	0.000	0.000	0.000	0.000
1057)	2.405	2.322	0.40	0.000	0.000	0.000	0.000
1058)	2.405	2.322	0.50	0.000	0.000	0.000	0.000
1059)	2.405	2.322	0.60	0.000	0.000	0.000	0.000
1060)	2.405	2.322	0.70	0.000	0.000	0.000	0.000

TABLE I. (*Continued.*)

Index	E_γ (GeV)	W (GeV)	$\cos\theta_K^{\text{c.m.}}$	$\sigma(\Lambda)$ (μb)	$\delta\sigma(\Lambda)$ (μb)	$\sigma(\Sigma^0)$ (μb)	$\delta\sigma(\Sigma^0)$ (μb)
1061)	2.405	2.322	0.80	0.000	0.000	0.000	0.000
1062)	2.405	2.322	0.90	0.000	0.000	0.000	0.000
1063)	2.430	2.332	−0.80	0.232	0.097	0.417	0.075
1064)	2.430	2.332	−0.70	0.107	0.031	0.272	0.044
1065)	2.430	2.332	−0.60	0.077	0.025	0.257	0.043
1066)	2.430	2.332	−0.50	0.103	0.020	0.126	0.022
1067)	2.430	2.332	−0.40	0.053	0.014	0.171	0.026
1068)	2.430	2.332	−0.30	0.078	0.019	0.097	0.021
1069)	2.430	2.332	−0.20	0.072	0.016	0.060	0.017
1070)	2.430	2.332	−0.10	0.060	0.023	0.181	0.052
1071)	2.430	2.332	0.00	0.139	0.023	0.139	0.024
1072)	2.430	2.332	0.10	0.104	0.027	0.196	0.028
1073)	2.430	2.332	0.20	0.170	0.023	0.190	0.025
1074)	2.430	2.332	0.30	0.226	0.034	0.372	0.039
1075)	2.430	2.332	0.40	0.325	0.032	0.385	0.036
1076)	2.430	2.332	0.50	0.511	0.052	0.639	0.056
1077)	2.430	2.332	0.60	0.965	0.070	0.852	0.067
1078)	2.430	2.332	0.70	1.315	0.085	1.129	0.088
1079)	2.430	2.332	0.80	1.794	0.107	1.337	0.098
1080)	2.430	2.332	0.90	1.919	0.162	1.804	0.175
1081)	2.455	2.343	−0.80	0.171	0.015	0.278	0.050
1082)	2.455	2.343	−0.70	0.147	0.051	0.292	0.081
1083)	2.455	2.343	−0.60	0.102	0.019	0.222	0.030
1084)	2.455	2.343	−0.50	0.176	0.026	0.166	0.026
1085)	2.455	2.343	−0.40	0.091	0.017	0.093	0.017
1086)	2.455	2.343	−0.30	0.109	0.019	0.063	0.013
1087)	2.455	2.343	−0.20	0.061	0.013	0.092	0.017
1088)	2.455	2.343	−0.10	0.086	0.014	0.051	0.012
1089)	2.455	2.343	0.00	0.084	0.018	0.110	0.019
1090)	2.455	2.343	0.10	0.097	0.021	0.155	0.021
1091)	2.455	2.343	0.20	0.092	0.017	0.138	0.020
1092)	2.455	2.343	0.30	0.221	0.028	0.266	0.030
1093)	2.455	2.343	0.40	0.315	0.027	0.393	0.032
1094)	2.455	2.343	0.50	0.455	0.038	0.546	0.043
1095)	2.455	2.343	0.60	0.908	0.066	0.803	0.060
1096)	2.455	2.343	0.70	1.125	0.072	0.842	0.063
1097)	2.455	2.343	0.80	1.502	0.084	1.140	0.079
1098)	2.455	2.343	0.90	1.410	0.129	1.294	0.156
1099)	2.480	2.353	−0.80	0.064	0.027	0.154	0.044
1100)	2.480	2.353	−0.70	0.057	0.020	0.286	0.048
1101)	2.480	2.353	−0.60	0.096	0.024	0.141	0.029
1102)	2.480	2.353	−0.50	0.046	0.014	0.132	0.023
1103)	2.480	2.353	−0.40	0.019	0.009	0.100	0.017
1104)	2.480	2.353	−0.30	0.099	0.016	0.088	0.016
1105)	2.480	2.353	−0.20	0.093	0.014	0.078	0.013
1106)	2.480	2.353	−0.10	0.076	0.017	0.076	0.021
1107)	2.480	2.353	0.00	0.057	0.014	0.062	0.015
1108)	2.480	2.353	0.10	0.071	0.015	0.117	0.020
1109)	2.480	2.353	0.20	0.118	0.022	0.176	0.024
1110)	2.480	2.353	0.30	0.170	0.025	0.161	0.028
1111)	2.480	2.353	0.40	0.263	0.030	0.410	0.033
1112)	2.480	2.353	0.50	0.365	0.037	0.612	0.048
1113)	2.480	2.353	0.60	0.740	0.056	0.783	0.064
1114)	2.480	2.353	0.70	1.088	0.070	0.819	0.070
1115)	2.480	2.353	0.80	1.279	0.081	0.971	0.076
1116)	2.480	2.353	0.90	1.707	0.154	1.044	0.131

TABLE I. (*Continued.*)

Index	E_γ (GeV)	W (GeV)	$\cos\theta_K^{\text{c.m.}}$	$\sigma(\Lambda)$ (μb)	$\delta\sigma(\Lambda)$ (μb)	$\sigma(\Sigma^0)$ (μb)	$\delta\sigma(\Sigma^0)$ (μb)
1117)	2.505	2.363	−0.80	0.114	0.023	0.229	0.038
1118)	2.505	2.363	−0.70	0.092	0.019	0.257	0.035
1119)	2.505	2.363	−0.60	0.085	0.020	0.205	0.028
1120)	2.505	2.363	−0.50	0.056	0.013	0.154	0.023
1121)	2.505	2.363	−0.40	0.082	0.015	0.116	0.016
1122)	2.505	2.363	−0.30	0.030	0.012	0.116	0.028
1123)	2.505	2.363	−0.20	0.053	0.011	0.066	0.015
1124)	2.505	2.363	−0.10	0.067	0.016	0.077	0.019
1125)	2.505	2.363	0.00	0.102	0.015	0.086	0.018
1126)	2.505	2.363	0.10	0.085	0.019	0.135	0.022
1127)	2.505	2.363	0.20	0.106	0.020	0.180	0.027
1128)	2.505	2.363	0.30	0.157	0.022	0.189	0.024
1129)	2.505	2.363	0.40	0.224	0.029	0.315	0.030
1130)	2.505	2.363	0.50	0.422	0.038	0.496	0.045
1131)	2.505	2.363	0.60	0.709	0.053	0.653	0.052
1132)	2.505	2.363	0.70	0.983	0.062	0.916	0.065
1133)	2.505	2.363	0.80	1.346	0.088	1.074	0.077
1134)	2.505	2.363	0.90	1.728	0.150	1.068	0.140
1135)	2.530	2.372	−0.80	0.144	0.017	0.235	0.045
1136)	2.530	2.372	−0.70	0.057	0.018	0.221	0.035
1137)	2.530	2.372	−0.60	0.117	0.026	0.197	0.032
1138)	2.530	2.372	−0.50	0.064	0.017	0.138	0.023
1139)	2.530	2.372	−0.40	0.065	0.015	0.086	0.016
1140)	2.530	2.372	−0.30	0.089	0.021	0.086	0.019
1141)	2.530	2.372	−0.20	0.053	0.016	0.077	0.019
1142)	2.530	2.372	−0.10	0.065	0.015	0.049	0.013
1143)	2.530	2.372	0.00	0.079	0.015	0.075	0.020
1144)	2.530	2.372	0.10	0.058	0.014	0.106	0.018
1145)	2.530	2.372	0.20	0.107	0.020	0.153	0.025
1146)	2.530	2.372	0.30	0.205	0.025	0.250	0.028
1147)	2.530	2.372	0.40	0.240	0.027	0.326	0.030
1148)	2.530	2.372	0.50	0.332	0.033	0.500	0.042
1149)	2.530	2.372	0.60	0.596	0.054	0.682	0.058
1150)	2.530	2.372	0.70	1.061	0.078	0.888	0.076
1151)	2.530	2.372	0.80	1.438	0.089	1.120	0.087
1152)	2.530	2.372	0.90	1.646	0.190	1.100	0.161
1153)	2.555	2.382	−0.80	0.085	0.029	0.263	0.061
1154)	2.555	2.382	−0.70	0.126	0.026	0.261	0.038
1155)	2.555	2.382	−0.60	0.068	0.018	0.190	0.029
1156)	2.555	2.382	−0.50	0.096	0.027	0.134	0.030
1157)	2.555	2.382	−0.40	0.053	0.021	0.064	0.018
1158)	2.555	2.382	−0.30	0.029	0.010	0.030	0.010
1159)	2.555	2.382	−0.20	0.041	0.014	0.035	0.013
1160)	2.555	2.382	−0.10	0.051	0.016	0.043	0.014
1161)	2.555	2.382	0.00	0.069	0.015	0.046	0.014
1162)	2.555	2.382	0.10	0.076	0.020	0.090	0.020
1163)	2.555	2.382	0.20	0.066	0.021	0.113	0.030
1164)	2.555	2.382	0.30	0.149	0.027	0.188	0.027
1165)	2.555	2.382	0.40	0.243	0.029	0.299	0.032
1166)	2.555	2.382	0.50	0.356	0.040	0.405	0.044
1167)	2.555	2.382	0.60	0.643	0.059	0.638	0.058
1168)	2.555	2.382	0.70	0.945	0.080	0.857	0.088
1169)	2.555	2.382	0.80	1.495	0.098	1.087	0.091
1170)	2.555	2.382	0.90	1.588	0.167	0.955	0.144
1171)	2.580	2.392	−0.80	0.079	0.012	0.159	0.085
1172)	2.580	2.392	−0.70	0.038	0.017	0.200	0.042

TABLE I. (*Continued.*)

Index	E_γ (GeV)	W (GeV)	$\cos\theta_K^{\text{c.m.}}$	$\sigma(\Lambda)$ (μb)	$\delta\sigma(\Lambda)$ (μb)	$\sigma(\Sigma^0)$ (μb)	$\delta\sigma(\Sigma^0)$ (μb)
1173)	2.580	2.392	−0.60	0.098	0.026	0.252	0.043
1174)	2.580	2.392	−0.50	0.102	0.023	0.123	0.024
1175)	2.580	2.392	−0.40	0.074	0.020	0.102	0.023
1176)	2.580	2.392	−0.30	0.058	0.023	0.036	0.015
1177)	2.580	2.392	−0.20	0.057	0.013	0.046	0.011
1178)	2.580	2.392	−0.10	0.080	0.017	0.096	0.020
1179)	2.580	2.392	0.00	0.076	0.016	0.051	0.014
1180)	2.580	2.392	0.10	0.071	0.025	0.056	0.018
1181)	2.580	2.392	0.20	0.124	0.022	0.141	0.030
1182)	2.580	2.392	0.30	0.148	0.026	0.184	0.029
1183)	2.580	2.392	0.40	0.157	0.029	0.260	0.033
1184)	2.580	2.392	0.50	0.420	0.045	0.491	0.057
1185)	2.580	2.392	0.60	0.718	0.064	0.668	0.069
1186)	2.580	2.392	0.70	1.114	0.083	0.773	0.084
1187)	2.580	2.392	0.80	1.269	0.095	1.117	0.092
1188)	2.580	2.392	0.90	1.473	0.201	0.925	0.162
1189)	2.605	2.402	−0.80	0.131	0.035	0.189	0.043
1190)	2.605	2.402	−0.70	0.060	0.018	0.184	0.029
1191)	2.605	2.402	−0.60	0.065	0.015	0.160	0.022
1192)	2.605	2.402	−0.50	0.073	0.017	0.146	0.025
1193)	2.605	2.402	−0.40	0.072	0.015	0.072	0.015
1194)	2.605	2.402	−0.30	0.069	0.018	0.076	0.017
1195)	2.605	2.402	−0.20	0.074	0.018	0.063	0.016
1196)	2.605	2.402	−0.10	0.044	0.015	0.071	0.025
1197)	2.605	2.402	0.00	0.069	0.016	0.040	0.013
1198)	2.605	2.402	0.10	0.103	0.018	0.108	0.017
1199)	2.605	2.402	0.20	0.130	0.024	0.124	0.023
1200)	2.605	2.402	0.30	0.110	0.025	0.141	0.026
1201)	2.605	2.402	0.40	0.235	0.026	0.314	0.038
1202)	2.605	2.402	0.50	0.320	0.036	0.464	0.047
1203)	2.605	2.402	0.60	0.559	0.052	0.684	0.061
1204)	2.605	2.402	0.70	0.844	0.061	0.760	0.063
1205)	2.605	2.402	0.80	1.450	0.089	1.036	0.081
1206)	2.605	2.402	0.90	1.889	0.177	1.368	0.162
1207)	2.630	2.411	−0.80	0.132	0.028	0.212	0.041
1208)	2.630	2.411	−0.70	0.077	0.024	0.191	0.036
1209)	2.630	2.411	−0.60	0.079	0.016	0.200	0.030
1210)	2.630	2.411	−0.50	0.065	0.016	0.098	0.018
1211)	2.630	2.411	−0.40	0.104	0.022	0.052	0.013
1212)	2.630	2.411	−0.30	0.045	0.011	0.056	0.011
1213)	2.630	2.411	−0.20	0.063	0.013	0.091	0.017
1214)	2.630	2.411	−0.10	0.085	0.015	0.074	0.017
1215)	2.630	2.411	0.00	0.100	0.016	0.074	0.016
1216)	2.630	2.411	0.10	0.107	0.022	0.078	0.017
1217)	2.630	2.411	0.20	0.117	0.018	0.103	0.018
1218)	2.630	2.411	0.30	0.154	0.025	0.220	0.027
1219)	2.630	2.411	0.40	0.237	0.027	0.256	0.024
1220)	2.630	2.411	0.50	0.323	0.036	0.385	0.038
1221)	2.630	2.411	0.60	0.556	0.049	0.586	0.049
1222)	2.630	2.411	0.70	0.860	0.059	0.853	0.064
1223)	2.630	2.411	0.80	1.385	0.083	0.877	0.067
1224)	2.630	2.411	0.90	1.662	0.162	1.225	0.160
1225)	2.655	2.421	−0.80	0.093	0.026	0.238	0.048
1226)	2.655	2.421	−0.70	0.069	0.017	0.166	0.028
1227)	2.655	2.421	−0.60	0.028	0.010	0.131	0.031
1228)	2.655	2.421	−0.50	0.071	0.022	0.088	0.022

TABLE I. (*Continued.*)

Index	E_γ (GeV)	W (GeV)	$\cos\theta_K^{\text{c.m.}}$	$\sigma(\Lambda)$ (μb)	$\delta\sigma(\Lambda)$ (μb)	$\sigma(\Sigma^0)$ (μb)	$\delta\sigma(\Sigma^0)$ (μb)
1229)	2.655	2.421	−0.40	0.063	0.020	0.074	0.019
1230)	2.655	2.421	−0.30	0.061	0.012	0.097	0.015
1231)	2.655	2.421	−0.20	0.079	0.016	0.036	0.011
1232)	2.655	2.421	−0.10	0.063	0.017	0.112	0.027
1233)	2.655	2.421	0.00	0.055	0.019	0.039	0.012
1234)	2.655	2.421	0.10	0.065	0.014	0.063	0.015
1235)	2.655	2.421	0.20	0.079	0.022	0.092	0.031
1236)	2.655	2.421	0.30	0.129	0.020	0.141	0.021
1237)	2.655	2.421	0.40	0.175	0.025	0.210	0.028
1238)	2.655	2.421	0.50	0.255	0.035	0.388	0.044
1239)	2.655	2.421	0.60	0.672	0.058	0.661	0.073
1240)	2.655	2.421	0.70	0.889	0.066	0.636	0.060
1241)	2.655	2.421	0.80	1.428	0.101	1.139	0.116
1242)	2.655	2.421	0.90	1.732	0.190	1.287	0.196
1243)	2.680	2.431	−0.80	0.189	0.050	0.167	0.058
1244)	2.680	2.431	−0.70	0.084	0.019	0.190	0.029
1245)	2.680	2.431	−0.60	0.091	0.031	0.193	0.039
1246)	2.680	2.431	−0.50	0.083	0.022	0.115	0.023
1247)	2.680	2.431	−0.40	0.104	0.023	0.054	0.014
1248)	2.680	2.431	−0.30	0.073	0.023	0.068	0.027
1249)	2.680	2.431	−0.20	0.053	0.012	0.018	0.008
1250)	2.680	2.431	−0.10	0.051	0.013	0.018	0.011
1251)	2.680	2.431	0.00	0.047	0.015	0.049	0.016
1252)	2.680	2.431	0.10	0.037	0.011	0.066	0.016
1253)	2.680	2.431	0.20	0.110	0.022	0.154	0.028
1254)	2.680	2.431	0.30	0.129	0.021	0.177	0.027
1255)	2.680	2.431	0.40	0.177	0.024	0.222	0.026
1256)	2.680	2.431	0.50	0.314	0.040	0.441	0.047
1257)	2.680	2.431	0.60	0.581	0.057	0.541	0.052
1258)	2.680	2.431	0.70	0.943	0.070	0.811	0.072
1259)	2.680	2.431	0.80	1.198	0.088	0.838	0.074
1260)	2.680	2.431	0.90	1.784	0.176	1.308	0.179
1261)	2.704	2.440	−0.80	0.108	0.027	0.220	0.053
1262)	2.704	2.440	−0.70	0.092	0.023	0.216	0.034
1263)	2.704	2.440	−0.60	0.025	0.010	0.125	0.026
1264)	2.704	2.440	−0.50	0.050	0.016	0.155	0.025
1265)	2.704	2.440	−0.40	0.025	0.012	0.090	0.022
1266)	2.704	2.440	−0.30	0.025	0.013	0.045	0.016
1267)	2.704	2.440	−0.20	0.073	0.019	0.061	0.021
1268)	2.704	2.440	−0.10	0.062	0.015	0.031	0.008
1269)	2.704	2.440	0.00	0.063	0.013	0.048	0.012
1270)	2.704	2.440	0.10	0.070	0.012	0.088	0.015
1271)	2.704	2.440	0.20	0.093	0.018	0.106	0.031
1272)	2.704	2.440	0.30	0.129	0.018	0.161	0.020
1273)	2.704	2.440	0.40	0.154	0.021	0.220	0.025
1274)	2.704	2.440	0.50	0.248	0.029	0.320	0.034
1275)	2.704	2.440	0.60	0.613	0.052	0.556	0.051
1276)	2.704	2.440	0.70	0.936	0.065	0.751	0.057
1277)	2.704	2.440	0.80	1.485	0.091	0.957	0.076
1278)	2.704	2.440	0.90	1.771	0.159	1.651	0.174
1279)	2.729	2.450	−0.80	0.079	0.025	0.296	0.054
1280)	2.729	2.450	−0.70	0.136	0.034	0.216	0.044
1281)	2.729	2.450	−0.60	0.050	0.016	0.167	0.029
1282)	2.729	2.450	−0.50	0.056	0.016	0.127	0.025
1283)	2.729	2.450	−0.40	0.047	0.012	0.081	0.016
1284)	2.729	2.450	−0.30	0.068	0.016	0.079	0.018

TABLE I. (*Continued.*)

Index	E_γ (GeV)	W (GeV)	$\cos\theta_K^{\text{c.m.}}$	$\sigma(\Lambda)$ (μb)	$\delta\sigma(\Lambda)$ (μb)	$\sigma(\Sigma^0)$ (μb)	$\delta\sigma(\Sigma^0)$ (μb)
1285)	2.729	2.450	−0.20	0.038	0.010	0.080	0.016
1286)	2.729	2.450	−0.10	0.042	0.012	0.036	0.012
1287)	2.729	2.450	0.00	0.082	0.022	0.042	0.013
1288)	2.729	2.450	0.10	0.091	0.017	0.070	0.014
1289)	2.729	2.450	0.20	0.105	0.019	0.093	0.019
1290)	2.729	2.450	0.30	0.119	0.020	0.135	0.021
1291)	2.729	2.450	0.40	0.166	0.027	0.221	0.028
1292)	2.729	2.450	0.50	0.318	0.040	0.337	0.039
1293)	2.729	2.450	0.60	0.530	0.054	0.543	0.057
1294)	2.729	2.450	0.70	0.860	0.064	0.677	0.063
1295)	2.729	2.450	0.80	1.392	0.092	0.931	0.078
1296)	2.729	2.450	0.90	1.437	0.166	1.419	0.191
1297)	2.754	2.459	−0.80	0.054	0.027	0.173	0.044
1298)	2.754	2.459	−0.70	0.098	0.030	0.227	0.046
1299)	2.754	2.459	−0.60	0.049	0.019	0.104	0.025
1300)	2.754	2.459	−0.50	0.020	0.017	0.081	0.024
1301)	2.754	2.459	−0.40	0.016	0.011	0.023	0.012
1302)	2.754	2.459	−0.30	0.053	0.015	0.074	0.019
1303)	2.754	2.459	−0.20	0.023	0.015	0.040	0.019
1304)	2.754	2.459	−0.10	0.075	0.020	0.082	0.024
1305)	2.754	2.459	0.00	0.043	0.017	0.032	0.014
1306)	2.754	2.459	0.10	0.108	0.005	0.122	0.005
1307)	2.754	2.459	0.20	0.032	0.010	0.069	0.025
1308)	2.754	2.459	0.30	0.144	0.029	0.224	0.044
1309)	2.754	2.459	0.40	0.196	0.034	0.263	0.038
1310)	2.754	2.459	0.50	0.349	0.048	0.314	0.054
1311)	2.754	2.459	0.60	0.631	0.071	0.514	0.064
1312)	2.754	2.459	0.70	0.883	0.086	0.776	0.082
1313)	2.754	2.459	0.80	1.456	0.112	1.131	0.107
1314)	2.754	2.459	0.90	1.543	0.188	1.526	0.219
1315)	2.778	2.469	−0.80	0.063	0.028	0.186	0.046
1316)	2.778	2.469	−0.70	0.064	0.019	0.229	0.041
1317)	2.778	2.469	−0.60	0.063	0.019	0.165	0.029
1318)	2.778	2.469	−0.50	0.051	0.014	0.123	0.023
1319)	2.778	2.469	−0.40	0.030	0.015	0.090	0.022
1320)	2.778	2.469	−0.30	0.041	0.015	0.076	0.026
1321)	2.778	2.469	−0.20	0.040	0.012	0.044	0.014
1322)	2.778	2.469	−0.10	0.030	0.010	0.087	0.025
1323)	2.778	2.469	0.00	0.077	0.016	0.074	0.017
1324)	2.778	2.469	0.10	0.046	0.011	0.052	0.016
1325)	2.778	2.469	0.20	0.051	0.016	0.073	0.017
1326)	2.778	2.469	0.30	0.142	0.023	0.088	0.019
1327)	2.778	2.469	0.40	0.147	0.025	0.228	0.031
1328)	2.778	2.469	0.50	0.268	0.045	0.320	0.049
1329)	2.778	2.469	0.60	0.386	0.051	0.511	0.055
1330)	2.778	2.469	0.70	0.925	0.071	0.826	0.069
1331)	2.778	2.469	0.80	1.354	0.101	0.909	0.091
1332)	2.778	2.469	0.90	1.718	0.196	1.112	0.176
1333)	2.803	2.478	−0.80	0.027	0.023	0.158	0.057
1334)	2.803	2.478	−0.70	0.028	0.013	0.142	0.027
1335)	2.803	2.478	−0.60	0.045	0.016	0.122	0.023
1336)	2.803	2.478	−0.50	0.000	0.000	0.091	0.020
1337)	2.803	2.478	−0.40	0.048	0.015	0.068	0.017
1338)	2.803	2.478	−0.30	0.063	0.019	0.054	0.017
1339)	2.803	2.478	−0.20	0.075	0.016	0.047	0.005
1340)	2.803	2.478	−0.10	0.078	0.015	0.094	0.016

TABLE I. (*Continued.*)

Index	E_γ (GeV)	W (GeV)	$\cos\theta_K^{\text{c.m.}}$	$\sigma(\Lambda)$ (μb)	$\delta\sigma(\Lambda)$ (μb)	$\sigma(\Sigma^0)$ (μb)	$\delta\sigma(\Sigma^0)$ (μb)
1341)	2.803	2.478	0.00	0.051	0.018	0.035	0.016
1342)	2.803	2.478	0.10	0.060	0.017	0.026	0.011
1343)	2.803	2.478	0.20	0.065	0.018	0.025	0.010
1344)	2.803	2.478	0.30	0.093	0.020	0.123	0.022
1345)	2.803	2.478	0.40	0.136	0.026	0.145	0.027
1346)	2.803	2.478	0.50	0.340	0.039	0.334	0.043
1347)	2.803	2.478	0.60	0.553	0.060	0.469	0.060
1348)	2.803	2.478	0.70	0.766	0.058	0.795	0.055
1349)	2.803	2.478	0.80	1.418	0.102	0.968	0.095
1350)	2.803	2.478	0.90	1.652	0.201	1.426	0.225
1351)	2.827	2.487	−0.80	0.080	0.027	0.148	0.039
1352)	2.827	2.487	−0.70	0.032	0.016	0.131	0.030
1353)	2.827	2.487	−0.60	0.050	0.017	0.139	0.028
1354)	2.827	2.487	−0.50	0.026	0.016	0.054	0.018
1355)	2.827	2.487	−0.40	0.072	0.026	0.039	0.016
1356)	2.827	2.487	−0.30	0.063	0.015	0.071	0.014
1357)	2.827	2.487	−0.20	0.054	0.013	0.048	0.014
1358)	2.827	2.487	−0.10	0.053	0.013	0.075	0.017
1359)	2.827	2.487	0.00	0.032	0.013	0.017	0.010
1360)	2.827	2.487	0.10	0.039	0.012	0.072	0.017
1361)	2.827	2.487	0.20	0.067	0.019	0.063	0.022
1362)	2.827	2.487	0.30	0.145	0.028	0.166	0.040
1363)	2.827	2.487	0.40	0.136	0.025	0.126	0.031
1364)	2.827	2.487	0.50	0.345	0.042	0.331	0.043
1365)	2.827	2.487	0.60	0.515	0.057	0.452	0.056
1366)	2.827	2.487	0.70	0.836	0.074	0.769	0.081
1367)	2.827	2.487	0.80	1.377	0.103	1.186	0.122
1368)	2.827	2.487	0.90	1.495	0.177	1.306	0.194
1369)	2.852	2.496	−0.80	0.100	0.031	0.139	0.039
1370)	2.852	2.496	−0.70	0.045	0.019	0.167	0.054
1371)	2.852	2.496	−0.60	0.011	0.006	0.108	0.023
1372)	2.852	2.496	−0.50	0.017	0.008	0.071	0.014
1373)	2.852	2.496	−0.40	0.026	0.012	0.104	0.021
1374)	2.852	2.496	−0.30	0.053	0.013	0.085	0.019
1375)	2.852	2.496	−0.20	0.047	0.014	0.073	0.017
1376)	2.852	2.496	−0.10	0.071	0.010	0.059	0.010
1377)	2.852	2.496	0.00	0.057	0.017	0.026	0.008
1378)	2.852	2.496	0.10	0.061	0.016	0.050	0.016
1379)	2.852	2.496	0.20	0.053	0.015	0.046	0.010
1380)	2.852	2.496	0.30	0.112	0.026	0.094	0.023
1381)	2.852	2.496	0.40	0.134	0.021	0.136	0.021
1382)	2.852	2.496	0.50	0.334	0.038	0.282	0.036
1383)	2.852	2.496	0.60	0.605	0.056	0.487	0.052
1384)	2.852	2.496	0.70	0.933	0.066	0.686	0.064
1385)	2.852	2.496	0.80	1.266	0.085	0.906	0.092
1386)	2.852	2.496	0.90	1.294	0.130	1.254	0.153
1387)	2.876	2.506	−0.80	0.000	0.000	0.154	0.049
1388)	2.876	2.506	−0.70	0.035	0.016	0.163	0.034
1389)	2.876	2.506	−0.60	0.028	0.013	0.087	0.024
1390)	2.876	2.506	−0.50	0.039	0.020	0.107	0.029
1391)	2.876	2.506	−0.40	0.051	0.023	0.025	0.018
1392)	2.876	2.506	−0.30	0.015	0.008	0.028	0.018
1393)	2.876	2.506	−0.20	0.052	0.017	0.038	0.015
1394)	2.876	2.506	−0.10	0.028	0.010	0.045	0.018
1395)	2.876	2.506	0.00	0.035	0.015	0.026	0.015
1396)	2.876	2.506	0.10	0.046	0.014	0.029	0.011

TABLE I. (*Continued.*)

Index	E_γ (GeV)	W (GeV)	$\cos\theta_K^{\text{c.m.}}$	$\sigma(\Lambda)$ (μb)	$\delta\sigma(\Lambda)$ (μb)	$\sigma(\Sigma^0)$ (μb)	$\delta\sigma(\Sigma^0)$ (μb)
1397)	2.876	2.506	0.20	0.077	0.020	0.081	0.021
1398)	2.876	2.506	0.30	0.085	0.020	0.060	0.017
1399)	2.876	2.506	0.40	0.154	0.025	0.109	0.026
1400)	2.876	2.506	0.50	0.305	0.042	0.283	0.044
1401)	2.876	2.506	0.60	0.443	0.062	0.493	0.065
1402)	2.876	2.506	0.70	0.834	0.070	0.663	0.069
1403)	2.876	2.506	0.80	1.147	0.096	1.108	0.114
1404)	2.876	2.506	0.90	1.531	0.198	1.094	0.219
1405)	2.901	2.515	−0.80	0.047	0.021	0.159	0.049
1406)	2.901	2.515	−0.70	0.016	0.013	0.117	0.025
1407)	2.901	2.515	−0.60	0.036	0.012	0.122	0.020
1408)	2.901	2.515	−0.50	0.025	0.012	0.092	0.021
1409)	2.901	2.515	−0.40	0.018	0.009	0.058	0.014
1410)	2.901	2.515	−0.30	0.020	0.012	0.024	0.008
1411)	2.901	2.515	−0.20	0.034	0.012	0.022	0.008
1412)	2.901	2.515	−0.10	0.071	0.014	0.038	0.012
1413)	2.901	2.515	0.00	0.077	0.026	0.061	0.025
1414)	2.901	2.515	0.10	0.073	0.013	0.067	0.016
1415)	2.901	2.515	0.20	0.072	0.018	0.094	0.019
1416)	2.901	2.515	0.30	0.063	0.021	0.105	0.038
1417)	2.901	2.515	0.40	0.152	0.025	0.182	0.025
1418)	2.901	2.515	0.50	0.249	0.035	0.306	0.043
1419)	2.901	2.515	0.60	0.499	0.054	0.528	0.056
1420)	2.901	2.515	0.70	0.957	0.072	0.712	0.066
1421)	2.901	2.515	0.80	1.216	0.091	0.976	0.093
1422)	2.901	2.515	0.90	1.827	0.309	1.132	0.225
1423)	2.925	2.524	−0.80	0.114	0.045	0.046	0.021
1424)	2.925	2.524	−0.70	0.020	0.009	0.175	0.033
1425)	2.925	2.524	−0.60	0.047	0.014	0.125	0.021
1426)	2.925	2.524	−0.50	0.029	0.012	0.111	0.022
1427)	2.925	2.524	−0.40	0.040	0.013	0.084	0.018

TABLE I. (*Continued.*)

Index	E_γ (GeV)	W (GeV)	$\cos\theta_K^{\text{c.m.}}$	$\sigma(\Lambda)$ (μb)	$\delta\sigma(\Lambda)$ (μb)	$\sigma(\Sigma^0)$ (μb)	$\delta\sigma(\Sigma^0)$ (μb)
1428)	2.925	2.524	−0.30	0.010	0.009	0.085	0.013
1429)	2.925	2.524	−0.20	0.046	0.017	0.093	0.021
1430)	2.925	2.524	−0.10	0.095	0.020	0.047	0.012
1431)	2.925	2.524	0.00	0.028	0.011	0.139	0.030
1432)	2.925	2.524	0.10	0.053	0.016	0.047	0.024
1433)	2.925	2.524	0.20	0.046	0.013	0.028	0.011
1434)	2.925	2.524	0.30	0.051	0.015	0.117	0.025
1435)	2.925	2.524	0.40	0.169	0.022	0.205	0.022
1436)	2.925	2.524	0.50	0.226	0.035	0.244	0.037
1437)	2.925	2.524	0.60	0.457	0.050	0.527	0.055
1438)	2.925	2.524	0.70	0.755	0.063	0.767	0.080
1439)	2.925	2.524	0.80	1.321	0.101	1.103	0.127
1440)	2.925	2.524	0.90	1.538	0.167	1.624	0.186
1441)	2.950	2.533	−0.80	0.078	0.023	0.165	0.044
1442)	2.950	2.533	−0.70	0.040	0.021	0.150	0.059
1443)	2.950	2.533	−0.60	0.042	0.013	0.095	0.020
1444)	2.950	2.533	−0.50	0.055	0.026	0.052	0.021
1445)	2.950	2.533	−0.40	0.044	0.019	0.059	0.022
1446)	2.950	2.533	−0.30	0.039	0.009	0.061	0.016
1447)	2.950	2.533	−0.20	0.041	0.013	0.059	0.016
1448)	2.950	2.533	−0.10	0.027	0.011	0.047	0.016
1449)	2.950	2.533	0.00	0.041	0.022	0.043	0.015
1450)	2.950	2.533	0.10	0.063	0.017	0.095	0.027
1451)	2.950	2.533	0.20	0.066	0.018	0.048	0.019
1452)	2.950	2.533	0.30	0.063	0.017	0.061	0.016
1453)	2.950	2.533	0.40	0.127	0.027	0.095	0.024
1454)	2.950	2.533	0.50	0.198	0.035	0.290	0.041
1455)	2.950	2.533	0.60	0.421	0.047	0.407	0.051
1456)	2.950	2.533	0.70	0.679	0.059	0.575	0.060
1457)	2.950	2.533	0.80	1.427	0.098	1.064	0.094
1458)	2.950	2.533	0.90	1.911	0.209	1.190	0.184

[1] J. W. C. McNabb *et al.* (CLAS Collaboration), Phys. Rev. C **69**, 042201(R) (2004).

[2] S. Capstick and W. Roberts, Phys. Rev. D **58**, 074011 (1998), and references therein.

[3] S. Eidelman *et al.*, Phys. Lett. **B592**, 1 (2004).

[4] See, for example, E. Klempt, nucl-ex/0203002; Phys. Rev. C **66**, 058201 (2002).

[5] T. Mart, C. Bennhold, H. Haberzettl, and L. Tiator, computer code KAONMAID 2000, available at www.kph.uni-mainz.de/MAID/kaon/kaonmaid.html.

[6] T. Mart and C. Bennhold, Phys. Rev. C **61**, 012201(R) (1999); C. Bennhold, H. Haberzettl, and T. Mart, nucl-th/9909022 and in *Proceedings of the 2nd ICTP International Conference on Perspectives in Hadronic Physics, Trieste, Italy, 10–14 May 1999*, edited by S. Boffi (World Scientific, Singapore, 1999).

[7] U. Löring, B. Ch. Metsch, and H. R. Petry, Eur. Phys. J. A **10**, 395 (2001).

[8] M. Q. Tran *et al.*, Phys. Lett. **B445**, 20 (1998); M. Bockhorst *et al.*, Z. Phys. C **63**, 37 (1994).

[9] B. Saghai, AIP Conf. Proc. **594**, 57 (2001); See also J. C. David, C. Fayard, G. H. Lamot, and B. Saghai, Phys. Rev. C **53**, 2613 (1996); σ_{tot} curve by private communication.

[10] S. Janssen, J. Ryckebusch, D. Debruyne, and T. Van Cauteren, Phys. Rev. C **65**, 015201 (2001); S. Janssen *et al.*, Eur. Phys. J. A **11**, 105 (2001); curves via private communication.

[11] S. Janssen, D. G. Ireland, and J. Ryckebusch, Phys. Lett. **B562**, 51 (2003).

[12] D. G. Ireland, S. Janssen, and J. Ryckebusch, Nucl. Phys. **A740**, 147 (2004).

[13] R. G. T. Zegers *et al.* (LEPS Collaboration), Phys. Rev. Lett. **91**, 092001 (2003).

[14] R. M. Mohring *et al.* (E93018 Collaboration), Phys. Rev. C **67**, 055205 (2003).

[15] G. Penner and U. Mosel, Phys. Rev. C **66**, 055212 (2002).

[16] W. T. Chiang, Ph.D. thesis, University of Pittsburgh, 2000 (unpublished); W.-T. Chiang, B. Saghai, F. Tabakin, and T. S. H. Lee, Phys. Rev. C **69**, 065208 (2004).

[17] V. Shklyar, H. Lenske, and U. Mosel, Phys. Rev. C **72**, 015210 (2005).

[18] K.-H. Glander *et al.*, Eur. Phys. J. **19**, 251 (2004).

[19] A. V. Sarantsev, V. A. Nikonov, A. V. Anisovich, E. Klempt, and U. Thoma, Eur. Phys. J. A **25**, 441 (2005).

[20] M. Guidal, J.-M. Laget, and M. Vanderhaeghen, Nucl. Phys. **A627**, 645 (1997).

[21] M. Guidal, J.-M. Laget, and M. Vanderhaeghen, Phys. Rev. C **61**, 025204 (2000).
[22] D. Sober *et al.*, Nucl. Instrum. Methods A **440**, 263 (2000).
[23] B. Mecking *et al.*, Nucl. Instrum. Methods A **503**, 513 (2003), and references therein.
[24] R. A. Arndt, W. J. Briscoe, I. I. Strakovsky, and R. L. Workman, Phys. Rev. C **66**, 055213 (2002).
[25] J. W. C. McNabb, Ph.D. thesis, Carnegie Mellon University, 2002 (unpublished); available at www.jlab.org/Hall-B/general/clas_thesis.html.
[26] R. K. Bradford, Ph.D. thesis, Carnegie Mellon University, 2005 (unpublished); available at www.jlab.org/Hall-B/general/clas_thesis.html.
[27] The CLAS Database collects all data from CLAS. It is reachable via http://clasweb.jlab.org/physicsdb.
[28] Durham Database Group, Durham University (UK), http://durpdg.dur.ac.uk/HEPDATA/.
[29] Text file available by sending e-mail request to schumacher@cmu.edu.
[30] H. M. Brody, A. M. Wetherell, and R. L. Walker, Phys. Rev. **119**, 1710 (1960).
[31] C. W. Peck, Phys. Rev. **135**, B830 (1964).
[32] D. E. Groom and J. H. Marshall, Phys. Rev. **159**, 1213 (1967).
[33] P. L. Donoho and R. L Walker, Phys. Rev. **112**, 981 (1958); **107**, 1198 (1957).
[34] R. L. Anderson *et al.*, Phys. Rev. Lett. **9**, 131 (1962); also Phys. Rev. **123**, 1003 (1961).
[35] H. Thom, Phys. Rev. **151**, 1322 (1966); Phys. Rev. Lett. **11**, 432 (1963).
[36] A. Bleckmann *et al.*, Z. Phys. **239**, 1 (1970).
[37] P. Feller, D. Menze, U. Opara, W. Schulz, and W. J. Schwille, Nucl. Phys. **B39**, 413 (1972).
[38] D. Decamp *et al.*, Preprint LAL 1236, Orsay, 1970; Th. Fourneron, LAL 1258, Orsay, 1971.
[39] H. Göing, W. Schorsch, J. Tietge, and W. Weilnböck, Nucl. Phys. **B26**, 121 (1971).
[40] T. Fujii *et al.*, Phys. Rev. D **2**, 439 (1970).
[41] H. Genzel, P. Joos, and W. Pfeil, eds., *Photoproduction of Elementary Particles*, Landolt-Börnstein, New Series I/8 (Springer-Verlag, New York, 1973).
[42] The σ_{tot} values were read from the published graphs.
[43] R. Erbe *et al.* (ABBHHM Collaboration), Phys. Rev. **188**, 2060 (1969); data tabulated in *Numerical Data and Functional Relationships in Science and Technology*, edited by H. Schopper, Landolt-Börnstein, New Series I/12b (Springer-Verlag, New York, 1988), p. 355.
[44] A. M. Boyarski *et al.*, Phys. Rev. Lett. **22**, 1131 (1969).
[45] See, for example, D. H. Perkins, *Introduction to High Energy Physics*, 2nd ed. (Addison Wesley, Reading, MA, 1982), p. 166.